Ph.D. thesis

Structural Dynamics and Physiological Processes of Actin Filament Length Regulator Proteins

Dávid Zoltán Szatmári

Supervisors:

Prof. Dr. Miklós Nyitrai

Prof. Dr. Robert C. Robinson

University of Pécs, Medical School

Department of Biophysics

Pécs, 2018

Interdisciplinary Medical Sciences Doctoral School D93

Head of Doctoral School: Prof. Dr. Balázs Sümegi

Program (B-130): Investigating functional protein dynamics using biophysical methods

Program leader: Prof. Dr. Miklós Nyitrai

Supervisors: Prof. Dr. Miklós Nyitrai, Prof. Dr. Robert C. Robinson

“I believe there is another world waiting for us. A better world. And I'll be waiting for you there.”

- David Mitchell, Cloud Atlas

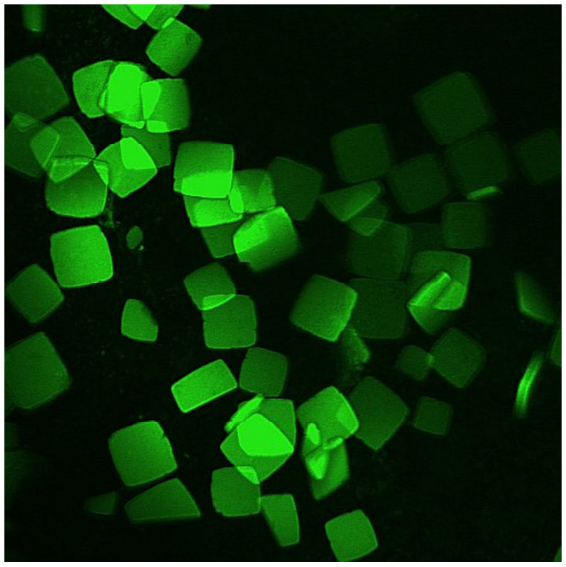

GSN M3-Alexa488 crystals

Acknowledgements

First of all I would like to express my gratitude to Prof. Dr. Miklós Nyitrai and to Prof. Dr. Robert Robinson who established my experience in the world of actin cytoskeleton. I would like to express my sincere appreciation for their guidance and motivation.
I am grateful to all members of the University of Pécs, Department of Biophysics and the A*STAR, Institute of Molecular and Cell Biology, Bob Robinson's Lab who always provided me great help and friendly atmosphere during my Ph.D. work. My faithful pleasure was to obtain a scholarship from the A*STAR, Research Attachment Program for the excellent two years experience in Singapore.

Finally, I would like to express my thanks to my Wife and my Family for their continued patience, submissive support and help.

TABLE OF CONTENT

I. Introduction

Actin is a 42 kDa globular protein. Actin forms microfilaments in eukaryotic cells that are the major component of the cytoskeletal system. In muscle cells, actin filaments are the main component of thin filaments and work as a scaffold of sarcomeres. *In vivo* actin can be presented as monomer G-actin (globular) or polymer F-actin (filamentous). Both of them are essential for important functions of a cell such as mobility, contraction, division, intracellular transport, signaling processes or maintaining the cell junctions and cell shape. A significant aspect of actin activity is that many intracellular processes are mediated by regulated interactions of actin with cellular membranes [1]. In vertebrates there are three main actin isoforms, alpha, beta, and gamma. Alpha actins, found in muscle tissues, are the major mass of the contractile apparatus. Beta and gamma actins are represented together in many cell types as components of cytoskeleton and mediators of internal cell motility.

Nuclear actin may play a role as scaffold and to control of gene expression despite it that it evolved in the cytoplasm as a defining feature of the eukaryotic cell [2]. The amount of actin in nuclei is lower than that in the cytoplasm and it is found in the nuclei of various types of cells [3-6]. With the development of experimental tools, convincing evidence has been obtained that nuclear actin indeed does exist and plays crucial roles in many nuclear processes. For example, actin is found in all types of RNA polymerase complexes [7] and in a number of chromatin remodeling complexes [8, 9]. It also binds to transcription regulators to control their activities [10]. Dynamic changes between globular (G-) and filamentous (F-) forms of nuclear actin affect these nuclear events. Nuclear actin polymerization is regulated by multiple mechanisms; more than 30 of actin-binding proteins that affect its polymerized states have been discovered in nuclei [11-13]. It is of great interest to reveal how these actin-binding proteins orchestrate the balance of monomeric/polymeric actin during the above-mentioned nuclear events. The regulation of the total amount of nuclear actin is another critical factor that affects activities of actin mediated nuclear events. Nuclear actin is actively exported to the cyto-

plasm by exportin-6 as the profilin-actin heterodimer [14]. Conversely, cytoplasmic actin together with cofilin is imported to the nucleus by importin-9 [15].

Cells control the production of F-actin based microfilaments and their dynamical length regulation allows for rapid remodeling of cytoskeletal system, therefore allowing the cell to respond to any external or internal signals [16]. The property of actin that it can be polymerized to long filaments endow an important roles in different cellular processes such as morphogenesis [16, 17], membrane trafficking [18], and cell division [19]. Strong cell adhesions, in order to form tissues [20], or structural proteins in a protrusion of cell membrane, can be anchored to this actin scaffold to allow processes such as endocytosis and cytokinesis [18, 21, 22]. Actin can generate force by its polymerization or by the contribution of motor proteins, therefore actin plays important roles in processes of intracellular transport of vesicles and organelles as well as muscle contraction and cell migration, and is implicated in embryogenesis and invasion of cancer cells [17, 23-27]. To fulfill precisely these versatile functions, the spatial-temporal organization of actin network is controlled by a large number of actin binding proteins [28, 29]. These effectors can disassemble actin structures and assist in the formation of new actin networks with diverse architecture depending on the cellular process in which they are involved. To understand this actin-based machinery, it is necessary to explore the types of conformational and dynamic changes that occur in the filamentous actin due to the interaction with actin-binding proteins.

A huge number of disorders and somatic abnormalities are caused by mutations in the genes of actin or actin-binding proteins. The production of actin is critical for the process of infection for some pathogenic microorganisms [30]. Mutations in the different human genes what regulate actin production thus can cause myopathies [31], different size and functional abnormalities of the heart [32]. The remodeling of the cytoskeleton system can be related to the pathogenicity of intracellular bacteria and viruses, particularly in processes to avoid the actions of the immune system [33].

I.1 Actin

I.1.1. Actin polymerization

The polymerization of monomeric actin into filaments is a thermal diffusion mediated process [34, 35]. The spontaneous association of monomers can be enhanced by high magnesium and potassium concentration [36]. The polymerization starts with the formation of a few monomer based actin nuclei (Fig 1.). The nucleation is proceeds by an imbalanced thermodynamical force where the entropy of dimers and trimers decreases by the local concentration of monomers [35, 37, 38]. Afterward, when the actin seeds are formed the filament elongation is started immediately with different kinetics at the ends [38]. The fast growing end of the filament is the barbed end (+ end), and the pointed end is the slowly elongating end (- end) [36]. The kinetics of the elongation depends on the concentration of the free actin monomers (C_{free}) that are available in the solution and determines the association rate (k_a) of the actin subunits to filaments [37, 39, 40]. Finally, the elongation of filaments reaches a reversible dynamical state where subsequent change in the length of the filaments does not occur. At this stage of the actin polymerization the steady-state equilibrium is maintained between the actin monomers and filaments, resulting in the continuous presence of around 0.1 μM concentration of actin monomers under in vitro conditions [31, 39].

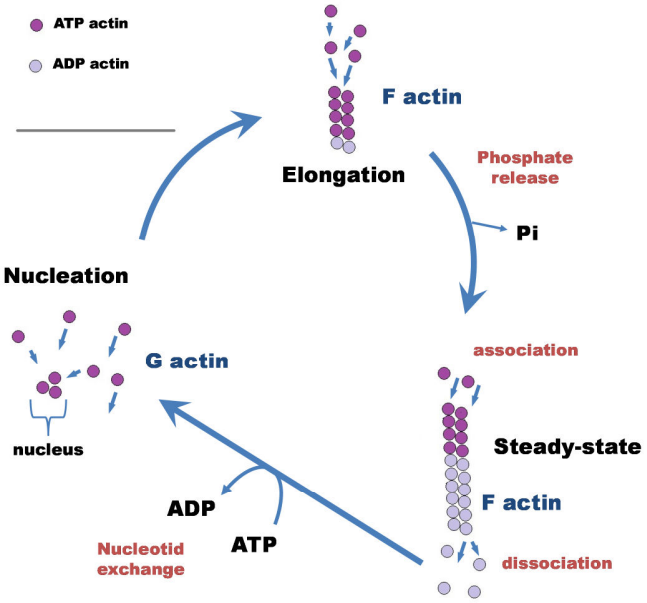

Figure 1. *Polymerization of actin*. Nucleation is the promoting step of polymerization when under polymerizing conditions ATP actin monomers bind together and form nuclei. After several monomers bind and form a nucleus, the elongation of filament proceeds rapidly triggering ATP hydrolysis with a slow release of inorganic phosphate, leaving the older parts of the filament bound to ADP. The steady-state length of filamentous actin is balanced by the continuous association of monomers at the barbed end and dissociation of monomers at the pointed end. Recycling of the released monomers is proceeds by exchanging the bound ADP for ATP, allowing them to participate in further rounds of polymerization.

However the average length of the actin filament does not change, but continuous association and dissociation of the actin subunits take place at the barbed end and the pointed end of the filaments, respectively [40]. The nature of this dynamical growing and shrinking of actin filaments arises from the structural and biochemical dissimilarity of monomers at the pointed end with respect to the barbed end. During the assembly, actins contact each together in a head to tail manner, which results in a structural difference between the two ends of the two filaments [41]. This process is called annealing. The association of actin monomers to the filament is accompanied by the irreversible hydrolysation of the bound ATP that leads to two different forms of actin, a newly incorporated ATP form and the older ADP-bound actin. These structural and biochemical dissimilarities between the barbed end and pointed end of the filament are manifested in different association (k_{ass}) and dissociation (k_{diss}) rates of ATP actin (Fig 2.)[37]. It was

estimated by using electron microscopy that the association and dissociation rate constants of the ATP actin monomer at the barbed end are 11.6 $\mu M^{-1}s^{-1}$ and 1.4 s^{-1}, respectively resulting in an appr. 0.1 μM dissociation constant (*Kd*) [36, 42]. The dissociation equilibrium constant of the barbed end determines the critical concentration (C_c = 0.2 μM) of polymerization, which reflects how easily the actin monomer can join the barbed end [43, 44]. The dissociation rate constant at the pointed end for the ATP actin subunits is 0.8 s^{-1}, but the association rate constant is 1.3 $\mu M^{-1}s^{-1}$ around 10 times lower than at the barbed end. Based on the measured association and dissociation rate constants the critical concentration (C_c) of the actin monomers for the nucleation at the barbed end is around 7 times lower than at the pointed end [44, 45]. Similar data were measured by fluorescence spectroscopy [46]. In the view of these considerations, the steady-state concentration of actin monomers in the solution is around 0.1 μM, which is balanced by the polymerization at the barbed end and the depolymerization from the pointed end [47]. This process of treadmilling is based on three steps: the dissociation of ADP actin monomers at the pointed end; the replacement of ADP to ATP on G-actin; and the subsequent incorporation of the ATP actin monomers at the barbed end. The rate-limiting step of the actin filament treadmilling is the dissociation rate of actin subunits at the pointed end, with in vitro rate constant of 0.2 s^{-1} [47, 48].

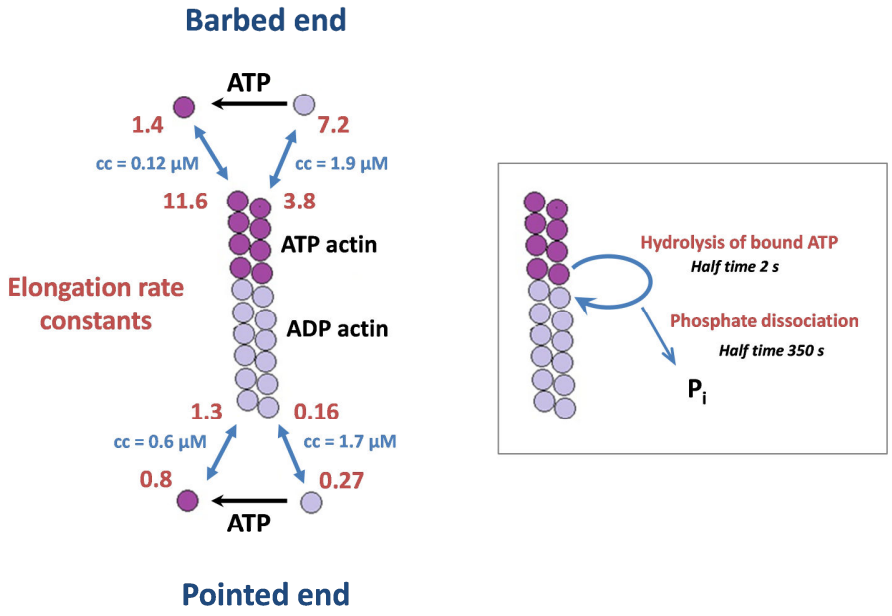

Figure 2. *Actin association and dissociation rates.* The orientation of monomers in the actin filament decorated with myosin led to the naming of the two opposite ends of the actin filament as "barbed" and "pointed" end. The cartoon of the actin filament indicating the association (μM^{-1} s^{-1}) and dissociation (s^{-1}) rates of actin monomer species (ADP or ATP) and critical concentrations at the two ends of the filament expressed as the ratio of dissociation and association rates [49]. The time course for ATP hydrolysis and P_i release from the filament is shown on the right side of the image [50].

Interestingly, the in vitro treadmilling rate is around two times slower than the observed treadmilling rate in vivo [51]. The faster rate of actin filament turnover in cells is probably caused by actin-binding proteins, which can modify the kinetics of each step in the polymerization and treadmilling of actin filaments.

I.1.2. Actin binding proteins and their complexes

Actin-binding proteins (ABPs) are able to bind to actin monomers, polymers, or to both. Not only ABPs but also small molecules can bind to actin, and therefore contribute to the modulation of the dynamics of the actin cytoskeleton, and catalyze actin filament polymerization or depolymerization [28, 52]. This is not only integral to broader cellular processes such as cell migration and mechanosensing, but may also be exploited for

experimental purposes. Proteins that bind to actin filaments affect the location rate and timing of actin filament assembly and disassembly. Actin monomers are polymerized into filaments under physiological conditions, but spontaneous depolymerization is too slow to maintain the fast actin filament dynamics observed in vivo [53]. Gelsolin, actin depolymerizing factor ADF/cofilin, and several other actin severing/depolymerizing proteins can enhance disassembly of actin filaments and promote reorganization of the actin cytoskeleton [54-56]. Many ABPs can regulate G-actin pool sizes through monomer sequestration or promotion/inhibition of nucleotide exchange. Actin-binding proteins also mediate interactions between actin and other cellular components, such as membranes, microtubules and other regulatory proteins [22, 51, 56]. While some actin-binding proteins regulate the actin cytoskeleton, others use the binding of actin monomers or filaments to regulate their own activities or direct their cellular location [56]. There is a great structural diversity in the types of proteins, which bind to actin, but the actin binding domains (ABDs) themselves can be grouped according to the conserved structures they form (Fig 3.)[56-64].

Common types of actin binding domains (ABDs):

- calponin-homology (CH) domain
- leucine rich repeat (LRR) domain
- formin-homology-2 (FH2) domain
- WASp-homology-2 (WH2) domain
- actin-depolymerizing factor/cofilin (ADF/cofilin) domain
- gelsolin-homology domain
- myosin motor domain

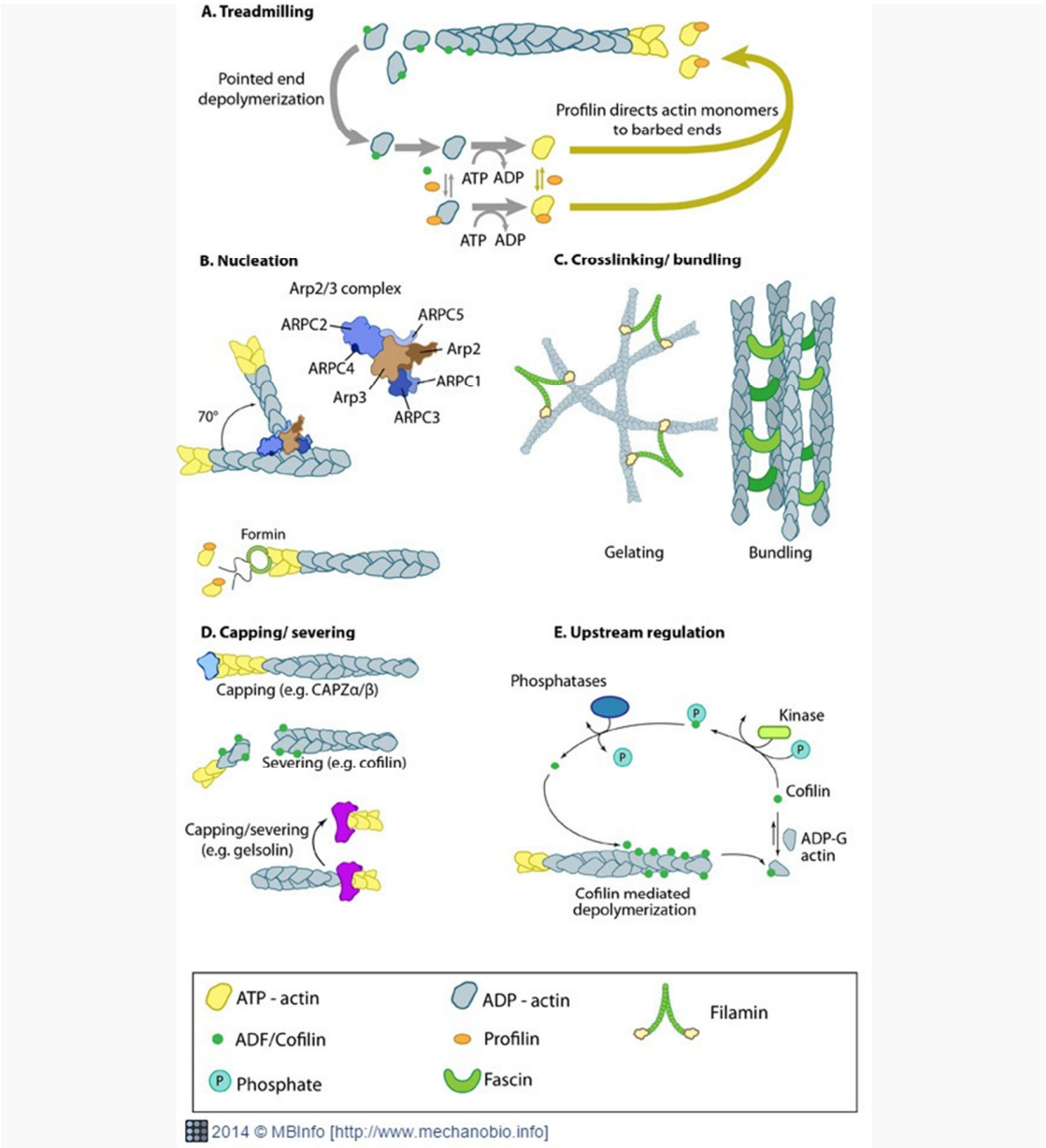

Figure 3. *Actin-binding proteins influence actin dynamics.* (**A)** Treadmilling of actin filaments can be altered by profilin and ADF, which generally increase and decrease the size of actin filaments, respectively. (**B**) New filaments are nucleated by the ARP2/3 complex, which binds both G-actin monomers and the side of actin filaments to nucleate new filaments by branching. Formins nucleate new filaments by binding G-actin and through cooperation with profilin. (**C**) Actin cross-linking proteins influence the packing and organization of actin filaments into secondary structures. (**D**) Capping and severing proteins promote disassembly of actin filaments. (**E**) Actin filament assembly can be modulated by events such as controlled nucleotide hydrolysis (e.g. ATP on actin) and reversible modifications (e.g. phosphorylation) on components that control actin assembly. [www.mechanobio.info]

The function of fascin is an example of how actin-binding proteins can modify the dynamics and structure of the actin filament network by producing actin filament bundles in case of filopodia formation [65]. Generally, different types of crosslinking proteins will give rise to different types of filament-based structures and will also modulate physical dynamics of the network to increase diversity [16, 66, 67]. Other cross-linking proteins can initialize the formation of big networks, or filamentous structures, in different parts of the cell. Basically, proteins with similar functions (e.g. fascin, α-actinin) act cooperatively to enhance the mechanical stability and reactivity of the network [68] [69].

I.1.3. Gelsolin and leiomodin are actin filament length regulator proteins

The intracellular functions of F-actin length regulator proteins are linked to their structural dynamics and physiologically relevant complexes, and through them the whole cytoskeletal system can be remodeled or the length of thin filaments can be optimized [70, 71]. Leiomodin is muscle specific and gelsolin is more common type of actin binding protein [72, 73]. We are interested in their structural changes and the physiological processes, by which are activated for actin binding.

Activated gelsolin binds to the barbed-end, and leiomodin binds the pointed-end, and both can bind to the sides of filaments. These two different F-actin length regulator proteins play different roles to modify the dynamics and kinetics of actin filament polymerization. Gelsolin is severing and capping, and leiomodin is nucleating and elongating actin filaments [70, 71]. Gelsolin is mobilizing short-capped actin polymers, whereas leiomodin is stabilizing the optimal length of filaments for an adequate contractible acto-myosin complex [72, 74], but their simultaneous intra-sarcomere presence and function have not studied yet. However, we can describe their muscle function as the summary of different independent data. Active gelsolin can be localized randomly along the actin filament and reduce the length in sarcomere [75], tropomyosin competes with gelsolin on filaments, thus tropomyosin-gelsolin complex can regulate the length of thin filaments [76]. Gelsolin enhances the ATPase activity of actomyosin is potentiated by tropomyosin which is a Ca^{2+}-insensitive acto-myosin enhancer [73]. Leiomodin can be found near the M-lines and also shows diffuse distribution along the entire length of the

thin filaments [72, 77]. The expression and sarcomeric localization of leiomodins are enhanced during myofibril maturation [78]. Leiomodins bind to different isoforms of tropomyosin and this interaction affects the actin polymerization promoting effect of leiomodins [79-82]. It was suggested that tropomyosin modifies the pointed-end interaction but not the *de novo* nucleation activity of cardiac leiomodin2, which can be explained by different structural compatibilities [72, 74]. There is no evidence concerning how leiomodin decorates the whole thin filament or how it changes the ATPase activity of myosin.

I.2. Gelsolin is a reorganizer of filamentous actin

Gelsolin plays an important role in the dynamics of the actin cytoskeleton, reorganization of filamentous actin and regulation of filament lengths [56, 70]. Calcium ions activate gelsolin to sever filaments leaving the gelsolin cap at their barbed ends.

I.2.1. The conserved gelsolin domain

Gelsolin contains six copies of homologous domain usually called as the gelsolin domain (Fig 4.). This domain is built up by 97 – 118 residues folded into a 5- or 6-stranded β sheet sandwiched between a long helix that is almost parallel, and a short helix which is nearly perpendicular, to the strands in the sheet (Fig 5.) [83, 84]. Different proteins from gelsolin superfamily contain multiple copies of this domain by this way earn novel functions of protein [85].

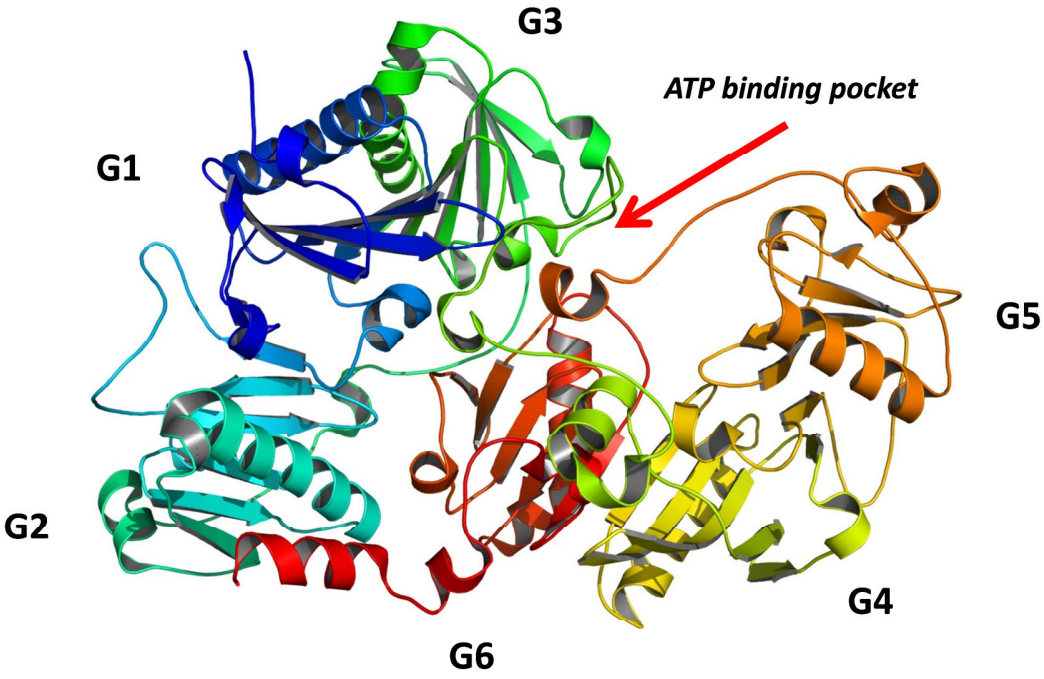

Figure 4. *Structure of inactive gelsolin.* The gelsolin contains six homologous domains, all of them can bind a calcium ion thereby through a step-by-step processes effectuate its activation. An ATP-binding site is localized on the linker between G5 and G6 and forms a deep binding pocket (PDB ID: 3FFN).

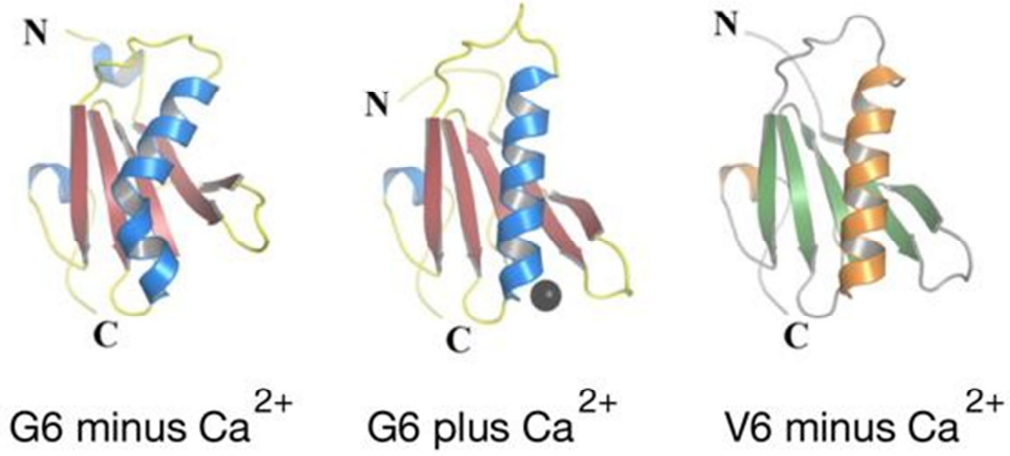

Figure 5. *X-ray crystallography, coupled with computer-generated simulations, to model activation of gelsolin and villin in the context of calcium and actin.* Hui, together with supervisor Les Burtnick of the CBR and collaborators in the Bob Robinson and Ivana Mihalek laboratories in Singapore, discovered that the long helix that forms the backbone of the calcium-free structure of the isolated V6 domain of villin is

elongated, and closely matches that in the activated calcium-bound G6 domain of gelsolin. This conformation is in striking contrast to the kinked conformation of the long helix in intact inactive G6 found under calcium-free conditions.

Eight mammalian proteins of the gelsolin superfamily contain at least one of this type of domain: CapG, adseverin, gelsolin, flightless I, advillin, villin, villin-like protein and supervillin. CapG has three, supervillin has five, and others have six gelsolin domains. Severin, fragmin and fragmin60 [86, 87] have three gelsolin domains are known from lower eukaryotes. The three- or six-domain contained proteins, probably developed by a similar process from a single domain prototype protein, which was first triplicated then duplicated [88, 89]. In addition to CapG, gelsolin, and villin type proteins [90], other proteins from gelsolin superfamily are also found in invertebrates and adopt structures that have two, four or five gelsolin-type domains, which indicates a complex evolutionary development which is still unresolved [91-94]. We should interpret the evolution of the gelsolin superfamily as a whole in order to understand their functional and regulatory diversity, which leads to their roles in the background of disorders. Single domain proteins of gelsolin superfamily have not been found yet, but the gelsolin domain partially resembles the ADF/cofilin family members [95] , which have been investigated. The gelsolin domain is different from the cofilin domain since it has a calcium ion-binding site (termed type-2), which comprises a glutamic acid at the beginning of the long helix and an aspartic acid on the β-sheet. An unrelated calcium ion-binding site (type-1) exists at each of the actin interfaces with G1 and G4. The type-2 site is found in many proteins of the gelsolin family, and in the case of gelsolin there is one on each domains [96]. Sequence analysis shows that CapG, adseverin, advillin and villin have the type-2 sites, however adseverin has a homologous site in domain 3 (Asp281Glu). By contrast, flightless I contains only two of the six type-2 sites (domain 1 - Glu557Lys, domain 2 - Asp646Phe, Glu668Ser, domain 3 - Asp774Cys, Glu796Val, domain 4 - Glu996Gly). Domains 5 and 6 have complete type-2 sites and probably they can bind calcium although one residue of domain 5 (Asp1083Glu) has a substitution to adseverin domain 3. Villin-like protein is missing the domain 1 type-2 site (Asp39His, Glu72Ala) while those in domains 4 (Asp418Asn) and 5 (Glu559Gln) may be compromised. Supervillin lacks the type-2 sites in domain 5 (Asp1484Thr, Glu1508Thr) and domain 6

(Asp1616Pro, Glu1641Lys), while the site in domain 3 (Asp1167Glu, Glu1189Gln) may be compromised. These calcium-binding signatures suggest that flightless I, villin-like protein and supervillin will be sensitive to calcium in a different manner and perhaps in a different range than has been determined for the case of gelsolin. Asp to Asn and Glu to Gln mutations made in gelsolin partially compromises the calcium-binding sites [97]. These mutations destabilize both the inactive and activate conformations of gelsolin and the mutants are likely to lose some affinity for calcium. The structure in the type-2 sites can be changed by calcium binding, changing the precise positioning of the long helix relative to the β-sheet, and straightening of the long helices of domains 3 and 6 [98]. The long helix can be generalized in function as a calcium sensor that links the calcium binding sites and other areas to transmit structural changes between domains and initialize large-scale rearrangements of domain positions, while keeping the structural integrity of the individual domains [96, 99, 100]. Previously published calcium dissociation constants for gelsolin type-2 sites are between 0.2 μM to 600 μM, *e.g.*, 600 μM [101], 0.7 μM [102], 1.8 μM [103], 100 μM [104], and 0.2 μM [103] for G1, G2, G4, G5, G6, respectively. The *Kd* of G3 is unknown yet. It is possible that the domains bind calcium sequentially on increasing calcium concentrations, thus defining a range of calcium concentrations that can potentially regulate protein activity. Calcium affinities of isolated domains can be modified in the context of other domains, or by activator molecules, or in the presence of actin as the target protein [101-103, 105, 106].

I.2.2. The role of calcium in activation

Calcium is a well-known intracellular signaling molecule and an important regulator of gelsolin activity. It can cause large conformational change in gelsolin leading to its activation. Calcium binding dislodges the tail region that clamps G6 to G2 and straightens the kink in the G4 long helix to induces steric clashes that assist in separating the G4-G6 half of gelsolin [98]. Additional calcium is necessary for adopting the active conformation that required for actin binding [103, 104]. Changes in interactions between the two halves of gelsolin may encourage straightening of the G3 long helix, and separating G1 from G3, resulting in its activation without addition of more calcium ions. The N-terminal half of gelsolin alone can sever actin filaments in the absence of calcium ions,

but addition of calcium improves severing efficiency. Accordingly, during the calcium-initialized conformational changes in the structure of gelsolin the actin-binding sites are uncovered [107-111]. The comparison of active and inactive gelsolin structures refers to the beginning and the end of the activation, though its mechanism of interchange is mainly unknown. Our understanding of the intermediate stages during the activation is based on contradictory data of variable assays of calcium dependent conformational changes. The multidomain nature of gelsolin provides challenges to describe the specific conformational changes of gelsolin by each calcium-binding event. Calcium affects the affinity [112, 113] and the binding rate [111, 114] of gelsolin actin complex [115]. Previous publications did not resolve the number of calcium-binding events occurring during gelsolin activation, avoided the interpretation of which calcium levels can cause structural transitions, and the function of calcium-binding sites in the activation process. Two or three conformational changes happen in gelsolin activation when the calcium concentration rises from 10 nM to ~5 μM, through the binding of two or three calcium ions with dissociation constants estimated to be 0.1 μM and 0.3 μM and 6.4 μM [116, 117]. These events may refer to the release of the tail latch [96, 116-123], which implicates a cooperative event at the type-2 sites on G2 and G6 [97]. Sequence analysis shows that members of human gelsolin superfamily which lack a full set of the six type-2 sites still retain one site in domain 2 (supervillin) or domain 6 (flightless I), which points to the importance of the interaction between domain 2 and domain 6 during activation. Additional calcium ions in the concentration range between 0.2 mM complete the activation process [116, 117, 124-127] but the intracellular concentrations cannot reach this level of calcium ions, despite that such levels exist in the extracellular space. To resolve this contradiction, we must assume that actin is able to modify the affinity of gelsolin for calcium, and can reduce the levels of calcium needed for conformational changes leading to active gelsolin [119, 128]. Therefore, actin can stabilize the active conformation of gelsolin thus facilitates the sequestration of calcium by gelsolin [100, 110, 116, 128]. Low pH also can reduce the calcium levels which are required for full gelsolin activation, e.g. the severing activity at pH 5.0 and 40 nM Ca^{2+} is similar to that observed at pH 8.0 and 1 mM Ca^{2+}. Lower pH partially activates gelsolin even in the absence of Ca^{2+} [120, 129, 130]. Thus their co-dependence, activation by pH and Ca^{2+}

occurs through different conformational states, and these mechanisms are less studied [123, 130]. Therefore, calcium binding destabilizes interactions between domains of inactive gelsolin and stabilizes the active state in a specific cooperative manner and it also depends on the H^+ and actin concentrations, both of which are able to destabilize the inactive and stabilize the active conformation of gelsolin. In case of a genetic disease, familial amyloidosis (FAF) the effect of calcium on the structure gelsolin is significant [131]. A point mutation in the type-2 calcium-binding site of domain G2 (D187N or D187Y) causes the calcium bound active gelsolin to be suitable for cleavage by furin protease during the transport through the Golgi apparatus [102](Fig 6.). The cleaved product undergoes further proteolysis in the extracellular space to produce 5 and 8 kDa peptides. They are able to stack into, amyloid fibrils, causing proteotoxicity and cytotoxicity to cells. Amyloid fibril production results dysfunctional tissues and organs, with the most severe cases associated with eyes, nerves, skin and kidneys. The partial calcium binding of G2 slightly destabilizes the domain structure during activation of gelsolin, contributing to the disease [99, 132, 133]. Thus, the loss of calcium binding by mutant G2 most likely causes aberration in the activation process, holding it in an intermediate state in which the furin cleavage site is accessible and primed to initiate the first step in the amyloidogenic pathway [97, 100].

I.2.3. Actin binding

The net result of conformational changes is to open up the actin-binding sites of gelsolin. The regulatory functions of gelsolin are localized in several regions in its structure. These are three major actin-binding sites of G1, G2 and G4, respectively. They are able to bind to actin through residues on their conserved long helices [83, 96, 100, 103, 134-136]. The actin-binding sites on G1, on G2 and on G4 are well conserved in all human gelsolin superfamily proteins, excluding supervillin, which looks different by having incompatible residues on domain 2. Other actin-binding sites have been identified on G3 [100] and G6 [136], in the G1-G2 linker [137], and on a second patch of G2 [100]. The G3 actin-binding site appears to be conserved in all human proteins of the gelsolin superfamily, while that on the WH2-like G1-G2 linker is present in all proteins except supervillin. It is also interesting that the G3-G4 linker can bind to actin. This region dis-

plays conservation between gelsolin, adseverin, advillin, villin and villin-like protein, and rather weaker similarity in supervillin and flightless I. The actin-bound structure of G1-G3 is similar to G4-G6 reveals that G4 binds to actin analogously as G1, in the gap between actin subdomain 1 and 3. G5 acts as a bridge to allow G6 to bind to subdomain 3 on an actin monomer, by contrast the G1-G2 linker is extended on the surface of actin to allow G2 to bind to subdomain 2. The role of G3 in this activated complex is to connect G2 to actin, at the junction between actin subdomains 1 and 2. In the actin-gelsolin complex the domains of G1 and G4 each bind an additional calcium ion. These conserved type-1 calcium-binding sites are necessary for the interaction with actin on residue Glu167 and complete the coordination sphere of the bound calcium ion [83, 96, 136]. Thus, calcium forms bridges between actin and gelsolin, stabilizing interactions and regulating the affinity between the two proteins. The type-1 site in domain 4 is maintained in all members of human gelsolin superfamily, excluding flightless I (Asp to Phe). In domain 1 this site is conserved in gelsolin, adseverin, advillin and villin, and modified in CapG (Asp to Asn) and villin-like protein (Asp to Gln), and changed to arginine in flightless I, where the arginine may mimic a calcium-bound aspartic acid. Maximal activation of gelsolin results by eight calcium ions saturating all type-1 and type-2 sites on gelsolin. However, lower levels of calcium produce lower activity in severing [96, 97]. In summary, calcium-activated gelsolin presents actin-binding sites on the extended interdomain linkers and on each domain, excluding G5.

I.2.4. Actin severing by gelsolin

To understand how gelsolin interacts with actin, in the first instance, we should focus on the mechanism of filamentous actin severing. Basically, the severing activity of gelsolin refers to the braking of the polymers and capping their barbed ends, which results in modified filamentous actin dynamics and a pool of short, capped oligomers. Domain G1 and G4-G6 terminal fragment are effective capping proteins, which are each able to bind to one actin monomer. They compete for the same site on actin [134], that is located in the gap between actin subdomain 1 and 3 [83, 136]. The minimum required set of domains for severing activity is G1 plus the G1-G2 linker [112, 118], in intact gelsolin the interaction between G2 and F-actin is most likely the first step of severing. The G1-G2

linker binds to the filament and localizes the position of G1 near its binding site on actin [100, 137]. The first step is that gelsolin initially binds to the side of the filament, where the G2G3 unit is targeted to subdomain 2 of actin, as observed in the structure of G1-G3 complex with actin [100, 138], and to subdomain 1 on the next axial actin monomer (protomer 5). G3 fixed upon against G2 and aids it in anchoring gelsolin to the filament at protomer 7. The extended G1-G2 linker interacts with the surface of actin protomer 7, positioning G1 to bind between subdomains 1 and 3, connected to protomer 9 (Fig 6.). Similarly, the G3-G4 linker extended between the two sides of the filament to fix the activated C-terminal half of gelsolin near the gap between subdomains 1 and 3 of protomer 4, which forms contacts with protomer 6. As shown (Fig 6.), this model predicts that the gelsolin domains bind actin cooperatively, and severing is the consequence of clamping movement sourced from simultaneous parallel steps when G1 and protomer 9 compete for binding to protomer 7, while G4 and protomer 6 compete for binding to protomer 4. We anticipate that this mechanism will apply to all human gelsolin superfamily members, excluding CapG and supervillin. Three-domain CapG caps but does not sever actin filaments [139], and supervillin lacks many of the actin-binding sites needed for severing.

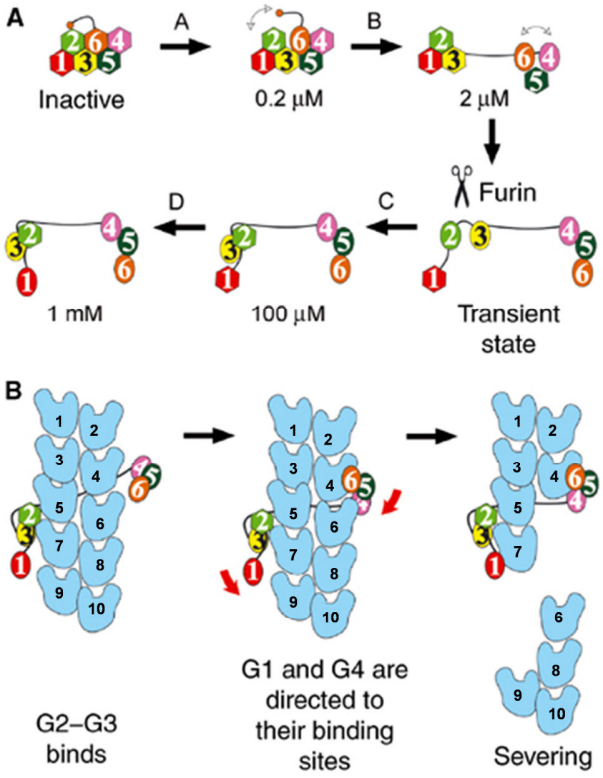

Figure 6. [100] *Calcium-induced activation of gelsolin and the severing of F-actin.* (**A**) Levels of calcium activation. Ca^{2+}-free gelsolin domains are shown as hexagons and calcium-bound domains are depicted as ovals. Calcium ion concentrations are indicated for each step. The scissors represent the stage at which FAF gelsolin is cleaved. (**B**) The sequence of events during severing of actin by fully activated gelsolin. Actin protomers are shown in blue.

Actin severing by gelsolin is an event that relies on fluctuations in the structure of the actin filament in order to access the G1 and G4 binding sites. However, binding of the G2G3 fragment to actin may facilitate changes in the twist of the filament that could weaken longitudinal interactions between neighbouring protomers and tip the scales in favor of severing [140-142] [143]. Furthermore, previous reports have suggested that the actin filament behaves as a mechanosensor of environmental changes, reacts with changes in its twist, curvature and flexibility [144, 145]. These introduce protein-specific activities, as cofilin binding is inhibited by increased tension on a filament, while gelsolin severs more rapidly when a filament is under tension [144]. A possible

mechanism for G2 induced actin filament changes belongs to the predicted interaction of Arg221 from G2 with Glu167 from actin [100]. Actin residue Glu167 forms part of a cation-binding site (K^+ or Mg^{2+}) that provides stiffness to the actin filament [146]. Thus, binding of G2 may reorder this cation-binding site and alter the flexibility and twist of the filament. Arg221 is conserved in all human gelsolin superfamily members, excluding flightless I (Asn) and supervillin (Gln), where the substitution for polar residues may stabilize cation binding. However, actin residue Glu167 completes the coordination sphere of the type-1 calcium-binding sites that are sandwiched between gelsolin domains G1 and G4 with actin subunits 3 and 4. Thus, exchange the K^+ or Mg^{2+} bound to Glu167 in the stiffness of actin-actin cation-binding site with Ca^{2+} bound to Glu167 at the G1-actin and G4-actin type-1 sites will enhance the severing process. CapG and villin-like protein are similar in their domain 1 type-1 sites, containing Asn and Gln, respectively, which caused loss of severing in case of CapG. Flightless I lacks both type-1 sites, containing Arg and Phe in domains 1 and 4. The role of the potential flightless I actin-binding sites on domains 1 and 4 is not clear as to whether they provide an interface for capping instead of severing. Gelsolin is partially activated at cytoplasmic calcium concentrations so that the actin binding or capping sites are only partially revealed, and filament driven conformational changes and filament associations are thought to compensate each other. Furthermore, cellular actin monomers are sequestered by monomer binding proteins, such as profilin and thymosin-β4, which reduce the free G-actin concentration. Nucleation of actin filaments by gelsolin is likely to be prevented *in vivo* by competition from G-actin complexes with profilin or with thymosin-β4 and being sterically inhibited by partial activation. Furthermore, profilin or with thymosin-β4 are prevented from joining to the free pointed ends of gelsolin-capped actin oligomers due to steric reasons. Thus, gelsolin is able to bind on both sides of an actin filament and order its capping domains to directly compete with actin:actin interactions in order to disrupt the filament.

I.2.5. The gelsolin in vivo

Gelsolin plays roles in the dynamics and regulation of actin filament lengths [147]. Calcium ions activate gelsolin to sever actin filaments, leading to one of the two resulting

filaments being capped at its barbed end. F-actin severing, capping and uncapping by gelsolin, close to the cell membrane, are thought to contribute to cell movement and shape [148, 149]. Gelsolin can dissociate from the barbed end of capped filaments to provide a free interface for a directed polymerization near to the cell membrane. Phosphatidylinositides are involved in signaling to the actin cytoskeleton by modifying the activity of various actin-binding proteins, including the gelsolin superfamily proteins [150]. In particular, phosphatidylinositol 4,5-bisphosphate (PIP_2) is a major regulator of actin cytoskeletal organization [151, 152] that modulates many actin regulating proteins [153], including: gelsolin [154]; capping proteins, CapG [155] and CapZ [156]; actin monomer-binding proteins, profilin [157], cofilin [158] and twinfilin [159]; actin filament nucleation effectors, WASP [160], N-WASP [161] and dynamin2/cortactin [162]; actin filament crosslinking proteins, α-actinin [163], filamin [164] and cortexillin [165]; and actin filament membrane tethering proteins, vinculin [166], talin [166] and ERM proteins [167]. Gelsolin localizes to PIP_2-rich areas of a membrane [168], thus PIP_2 inhibits interactions between free gelsolin and actin [154, 169-172] and removes gelsolin caps from actin filaments [154]. There is a strong evidence to suggest that PIP_2 islands in the membrane lead to the uncapping of filaments, resulting a rapid, directed filament elongation pushing the membrane [154, 173].

Three PIP_2-binding sites have been identified on gelsolin, between residues 135-142; 161-169, which overlaps with F-actin binding site; and between residues 621-634, which overlaps with the ATP binding site [172, 174-177]. The second site is well conserved within the gelsolin superfamily. The mechanism of uncapping is not fully understood, however PIP_2 may either directly compete with actin for binding to gelsolin, and/or it may change the conformation of the actin-binding sites to become incompatible with binding to actin [84, 171, 176, 177]. There are several reports of a correlation between PIP_2 and calcium binding to gelsolin, however it is controversial whether this correlation is positive or negative [172, 174, 178].

Gelsolin can bind to the ATP-mimetic resin Cibracon-Blue and can be liberated from the resin by a range of nucleotides including ATP, ADP, GTP and GDP [179, 180]. Equilibrium dialysis experiments were used to determine dissociation constants of 0.28 μM and 1.8 μM of gelsolin for ATP and GTP, respectively, at high NaCl concentrations,

while ADP and GDP showed no significant association under these conditions [181]. The affinity of ATP for gelsolin decreases to 2.4 μM in the presence of 0.2-2.0 mM Mg^{2+}. No ATP binding to gelsolin was detectable in solutions that contain more than 10 μM Ca^{2+}, and conversely, the presence of ATP reduces the affinity of gelsolin for Ca^{2+} [182]. Gremm and Wegner reported a lower affinity of calcium-free gelsolin for ATP (*Kd* = 32 μM) than discussed above [182]. This may reflect differences in analytical techniques, fluorescence analysis versus equilibrium dialysis, or differences in experimental buffer conditions, including pH, $MgCl_2$ and $CaCl_2$. Gelsolin does not show any detectable ATPase activity [181, 183]. The discovery of the ATP: gelsolin interaction led to the suggestion that ATP maybe important in some of the multiple functions of gelsolin. At high calcium concentrations, gelsolin is almost fully activated, implying that the loss of its ATP-binding ability is due to disruption of the interaction site within gelsolin due to a conformational change [181]. The structure of the gelsolin: ATP complex revealed the basis for its sensitivity to calcium ion concentration. ATP interacts with the two halves of calcium-free gelsolin, which change conformation on binding to calcium [136, 176, 184-188]. The phosphate groups of ATP interact with basic residues of gelsolin domain 5 (G5). These residues also comprise part of a region that previously had been determined as bind to PIP_2 [172]. Gelsolin is also sensitive to the type of nucleotide, which bound by actin, severing ADP-actin but cannot ADP-Pi-actin filaments [189]. Accordingly, G4-G6 shows a preference for ADP containing actin monomers while G1-G3 binds to ATP- and ADP-actin with comparable affinities [190]. In contrast, ATP (but not ADP) concentrations in the 0.5 mM range inhibit the binding of G1-G3 to actin monomers [190].

Generally, the free calcium concentration in cells oscillates on the nanomolar scale [191, 192], while in stimulated cells these concentrations can increase to micromolar levels [193, 194], In some species the calcium level can reach ten micromolar [195]. Local calcium concentrations near a cell membrane may increase up to one hundred micromolar during the influx of millimolar calcium ion from the extracellular field [196]. Cytoplasmic free magnesium levels are regulated in the 0.5-1.0 mM range [197, 198]. Intracellular ATP concentrations vary on a wide range depending on the type, stage and state of the cell, and these levels play a regulatory role in membrane channel function [199-

206]. Stimulated cells can display complex calcium oscillations and have high ATP consumption [207].

I.3. Leiomodin is a thin filament length optimizer

I.3.1. Leiomodins

Leiomodins (Lmods) are vertebrate members of the tropomodulin (Tmod) gene family, which were recently recognised as regulators of muscle function. Lmods are expressed in different muscle tissues [208]. Lmod1 can be found in smooth muscle [209, 210] and was recently reported as a megacyst microcolon intestinal hypoperistaltic syndrome (MMIHS) disease gene in humans and mice [211]. Transcripts encoding the *LMOD2* gene are present in fetal and adult heart and also in adult skeletal muscle [72, 79, 212]. The human *LMOD2* gene is located near the hypertrophic cardiomyopathy locus *CMH6* on human chromosome 7q3, potentially implicating this protein in the disease [208]. The third form, the fetal Lmod3 is required for embryonic myofibrillogenesis and implicated in nemaline myopathy in both humans and mice [213-215].

Tropomodulins and leiomodins are built from homologous domain structures (Fig 7.). Both proteins contain two tropomyosin-binding domains (TMBS1/2), an actin-binding domain (ABS1) and a leucine-rich repeat (ABS2/LRR) that also binds to monomeric actin [74, 77, 79]. In addition to these homologous domains, the structure of Lmods diverge from Tmods by possessing a C-terminal extension (Cterm), which contains a proline-rich region (PR, a potential recognition site of intracellular signalling), helical domains and a Wiskott–Aldrich syndrome protein (WASP)–homology 2 (WH2) domain [74, 79, 216]. In cardiac sarcomeres the expression of Lmod2 and Tmod1 depends on the maturation stage of myofibrils. Tmod1 is associated to actin filaments at the early stages of myofibril assembly, before the striated pattern is established [217]. Lmod2 appears later and its expression correlates with the development of myofibrils *in situ* and in some cases it associates with sarcomeres in matured cardiac muscle [72]. Depletion or overexpression of either of these proteins compromises sarcomeric thin filament length and organisation. Overexpression of Tmod1 or deletion of Lmod2 both caused the early lethality of embryos by dilated cardiomyopathy [72, 218], suggesting that they regulate

sarcomeric actin dynamics through different mechanisms. Both proteins localize to the pointed end of actin filaments [72, 219, 220]. However it was proposed that their localisation is manifested through fundamentally different mechanisms to the pointed ends of two distinct subsets of actin filaments in cardiac myofibrils [77]. While Tmods inhibit sarcomeric actin filament lengthening by capping pointed ends [219, 221, 222], Lmod2 maintains pointed end dynamics and antagonises the capping effect of Tmod [72, 77]. Based on their effects on thin filament length *in vivo*, Lmods were proposed to act as actin filament nucleators in muscle cells [77, 79]. Indeed, they accelerate actin assembly *in vitro* [77, 79, 214]. However, the nucleating ability of Lmods has not been demonstrated *in vivo*. Chicken Lmod2 expression is first detected in the heart after it has started to beat [72], indicating that this protein plays a role in the regulation of thin filament lengthening during the maturation of the heart tissues, rather than in initial filament nucleation. According to the recently proposed model of human cardiac Lmod2-actin interaction [74], Lmod2 can bind three actin monomers simultaneously through its ABS1/2 and WH2 motifs (Fig 7). Efficient enhancement of actin polymerisation requires both the N-terminal ABS1 and the C-terminal WH2 domains [77, 79]. The WH2 domain alone is not sufficient for actin nucleation, in agreement with recent views [223, 224]. The WH2 domain of Lmod2 seems to be required for filament elongation because its removal results in shorter actin filaments in rat cardiomyocytes, suggesting pointed end capping by isolated N-terminal of Lmod2, similarly to Tmod1 [72]. Lmods interact with tropomyosin (Tpm) in an isoform specific manner and this interaction affects the actin polymerization promoting effect of Lmods [79-82]. It was suggested that tropomyosin modifies the pointed-end interaction but not the *de novo* nucleation activity of cardiac Lmod2, which can be explained by different structural compatibilities [72, 74]. Considering the functional and structural differences between Tmod1 and Lmod2, one can hypothesise that the members of tropomodulin gene family were possibly developing through exon duplications and deletions, thus their evolution shows similarities with fuzzy proteins [225]. Both *in vitro* and *in vivo* observations support that one of the main functions of Lmod and Tmod proteins is related to pointed end-binding. Through this interaction they tune the length of the thin filaments in a competitive fashion to maintain the final organisation and sarcomere architecture.

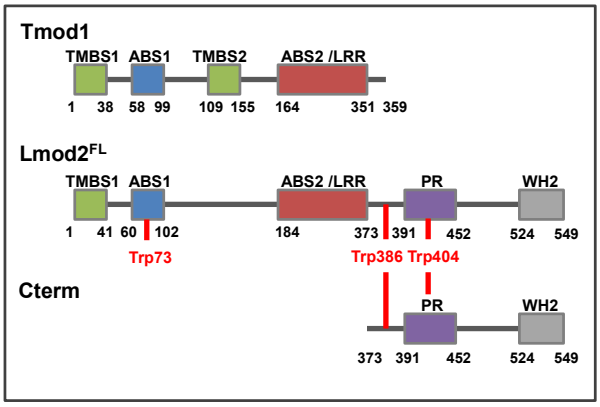

Figure 7. *Domain structure of human tropomodulin1 and Rattus norvegicus cardiac leiomodin2.* The scheme compares the domain organisation of Tmod1 to the full length (Lmod2^{FL}) and the C-terminal region (Cterm) of cardiac leiomodin2. Tmod1 and Lmod2^{FL} contain different tropomyosin binding domains (TMBS1/2), homolog actin binding domains (ABS1) and leucine-rich repeats (ABS2/LRR). Lmod2 contains an additional C-terminal extension (Cterm) comprising a proline-rich (PR) and a Wiskott–Aldrich syndrome protein (WASP)–homology 2 (WH2) domain. Tryptophans used in our spectroscopy experiments are marked with red.

I.3.2. Leiomodin binds to the sides and the pointed end of actin filament

Interestingly, while Tmod1 localises only to pointed ends towards the M-lines, Lmod2 can be found near the M-lines and also shows diffuse distribution along the entire length of the thin filaments in rat cardiomyocytes, which belongs to its ABS2/LRR domain [72, 77]. A previous study reported that the expression and sarcomeric localisation of Lmod are enhanced during myofibril maturation [78]. Immunofluorescent images of three days old rat cardiac cells show comparable fluorescent emission intensities of actin as leiomodin. Lmod-GFP localises along the thin filaments, and more importantly anti-Lmod antibodies reveal an elevated physiological expression level of leiomodin along the thin filaments distinct from M-lines in matured chicken cardiac cells and zebrafish skeletal muscle cells. Cellular localization of Lmod can be labelled at both sides from myomesin in M-lines, and it is well separated from α-actinin in Z-discs, frequently flanks single or

double bands of Tmod, and partially overlaps with the myosin thick filaments in matured cardiac sarcomeres. Probably, indirect effect of growth factors can enhance the expression of leiomodin and by the absence of tropomyosin or by the low number of acto-myosin complexes of unmatured thin filaments leiomodin can find several binding sites therefore the localization and expression of leiomodin can be changed during the maturation and by the actual state of muscle cells. This suggests that leiomodins bind directly to the sides of thin filaments and besides the pointed end-binding related functions leiomodins may regulate other aspects of sarcomeric thin filament function/organization through their side-binding ability.

I.3.3. Lmod2 regulates thin filament lengths

Lmods and Tmods have different biochemical activities, domain organizations and sarcomeric localizations. Functional studies have led to the idea that the two subfamilies compete with each other for pointed end capping, and that Lmods might additionally promote pointed-end elongation [72, 212, 213] a function proposed earlier for SALS, an unrelated protein from Drosophila [226]. Thus, overexpression of Lmod2 in cardiac myocytes reduces Tmod1 localization at pointed ends, resulting in slightly longer (by ~ 6 – 8 %) thin filaments. The overexpression of a Lmod2 construct lacking the WH2 domain (residues 1–514) did not lead to longer thin filaments, nor did overexpression of Lmod2 with a mutation in TMBS1 reduces TM binding [72, 82]. Interestingly, deletion of LMOD2 in the developing mouse heart results in ~15% shorter thin filaments, without affecting sarcomere organization, Tmod1 levels or localization in cardiac myocytes Lmod3 levels are unaffected by Lmod2 deletion in cardiac myocytes [212]. Lmod2 appears to regulate thin filament lengths by enhancing actin assembly at pointed ends, examined on adenovirus-mediated expression of GFP-Lmod2 in cultured Lmod2 -/- neonatal cardiomyocytes, which increases the incorporation of rhodamine-actin at pointed ends and rescues normal thin filament length [212]. Moreover, FRAP experiments also show that GFP-Lmod2 increases mCherry-actin turnover near pointed ends but not close to the barbed ends, again suggesting that Lmod2 promotes actin monomer incorporation in the vicinity of pointed ends. Lmod2 -/- mouse hearts with shorter thin filaments show reduced systolic performance after birth, progressing to dilated

cardiomyopathy and juvenile lethality [212, 218]. Lmod2 -/- cultured neonatal cardiac myocytes also display reduced contractile force, suggesting that abnormal thin filament length regulation and force generation are the primary causes of cardiomyopathy. Longer thin filaments may be required to sustain cardiac force generation at longer sarcomere lengths during systolic function [212]. The cardiac Lmod2 deletion phenotype is strikingly similar to a transgenic Tmod1 overexpression phenotype, characterized by shorter thin filaments, sarcomere disarray, and heart degeneration that progresses to dilated cardiomyopathy and results in death a few weeks after birth [227, 228]. In other words, loss of Lmod2 appears to functionally phenocopy overexpression of Tmod1 in the mouse heart. Unlike the loss of Tmod1, the loss of Lmod2 does not interfere with myofibril assembly during heart development, indicating that Lmod2 regulates thin filament lengths subsequent to sarcomere assembly. Furthermore, while shorter thin filaments are detected as early as E12.5 phase of cell cycle, sarcomere organization remains relatively normal until the development of cardiomyopathy symptoms at phase of P15, indicating that sarcomere disarray is likely a degenerative phenotype, possibly due to increased mechanical load on the heart after birth [212]. Possibly, sarcomeric formins could work synergistically with Lmods, whereby Lmods nucleate new filaments whose barbed ends are then elongated by formins and mediate thin filament organization in sarcomeres but not polymerization [229, 230] (Fig 8.). In addition to sarcomere disarray, another study also observed abnormal intercalated disc morphology and reduced expression of some intercalated disc genes at P25, which may reflect degenerative processes in the absence of Lmod2 [218]. However, an additional role for Lmod in myofibril assembly in the developing heart cannot be excluded, because Lmod1 expression from E9.5– E12.5 may compensate for loss of Lmod2 during this stage of development [210]. Possible effect of Lmod2 on myosin activity is unknown yet.

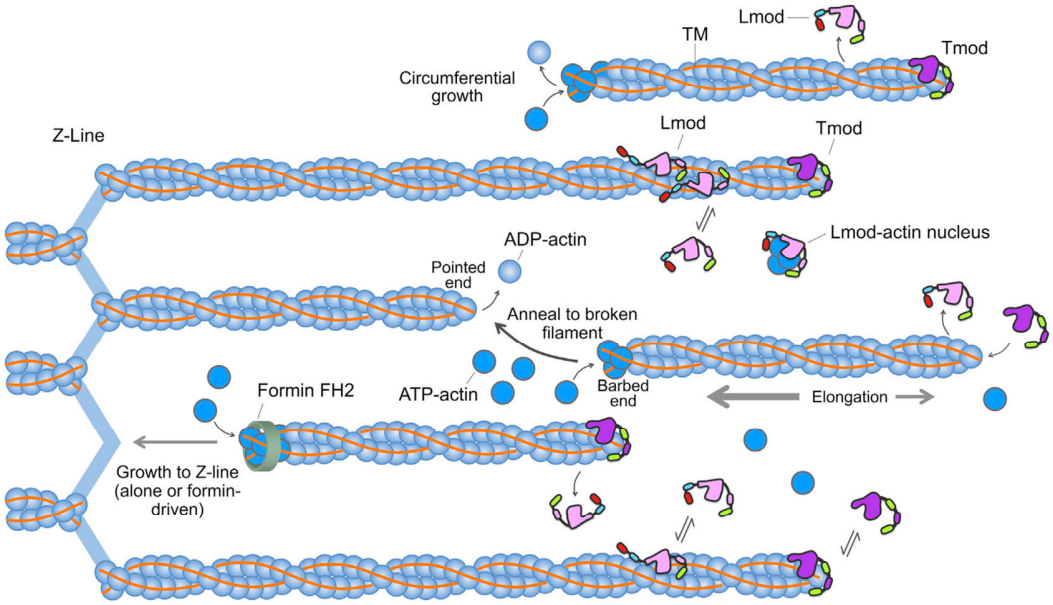

Figure 8. [71] *A model for Lmod nucleation of new filaments that are integrated into sarcomeres during normal filament turnover and repair in mature muscle, or during myofibrillogenesis in development.* Lmod catalyzes the formation of an actin nucleus (dark blue, ATP-bound actin subunits). After Lmod dissociates from the actin nucleus, actin subunits add rapidly to free barbed ends, either spontaneously or catalyzed by formins (green ring), leading to filament growth towards the Z-line. Actin hydrolyses ATP in the filament, and older filament consist mainly of ADP-bound actin subunits (light blue). During sarcomere turnover and repair, the barbed ends could either anneal to the pointed ends of preexisting filaments damaged during contraction, or elongate to the Z line where they are capped by CapZ and captured by α-actinin. Actin subunits also add slowly to the pointed ends of newly formed filaments, resulting in elongation toward the M-line, where the pointed end can be dynamically capped by Tmod. Cycles of Lmod nucleation, dissociation, and pause (possibly characterized by attachment of Lmod to thin filament sides) could permit a single Lmod molecule to assemble many new thin filaments. During myofibrillogenesis, new Lmod-nucleated filaments may also add to the periphery of sarcomeres, contributing to circumferential growth. In the case of Lmod overexpression, abundant nucleation generates an excess of free pointed ends, which are less frequently capped by Tmods. This can result in increased actin subunit addition at pointed ends and longer thin filaments [71].

II. Issues addressed in the thesis

The aim of this work was to obtain more information about actin filament length regulator proteins by two important proteins that bind to its ends, the barbed end binding cytoplasmic gelsolin or pointed end binding cardiac leiomodin2. The description of missing steps in recycling of gelsolin in its severing cycle are needed for a better understand of cytoskeletal system remodeling nearby of the cell membrane. A deeper understanding of the function of cardiac leiomodin2 in enhancing the length of actin filaments and modifying the actin-tropomyosin-myosin complex will lead to insights to the maintenance of cardiac muscle cell contractility. The major goals were:

1. Describe the interplay between ATP and calcium, which may modify PIP_2 binding of gelsolin.

2. Identify the missing steps in the recycling gelsolin from the membrane to the cytoplasm.

3. Characterize the intrinsic structural features of cardiac leiomodin2 and the differences between leiomodin and tropomodulin.

4. Investigate the actin assembly efficiencies of leiomodin2.

5. Explore the thin filament side binding activity of leiomodin2 and its potential functional consequences.

III. Materials and Methods

III.1. Protein preparation

III.1.1. Preparation of rabbit skeletal muscle α-actin

Calcium bound G-actin was prepared from rabbit muscle acetone powder (Pel Freez, Biologicals) according to the method of Spudich and Watt with a slight modification introduced by Mossakowska and co-workers. [231, 232]. For each gram of acetone-dried muscle powder was extracted by stirring in 20 ml of buffer A containing (4 mM Tris-HCl, pH 8.0, 0.2 mM ATP, 0.1 mM $CaCl_2$, 0.5 mM DTT and 0.005 % NaN_3) at 4 °C. After 30 minutes of gentle stirring the liquor was filtered through 4 layers of gauze and then the extraction step was repeated with the same volume of fresh buffer A. After the second filtration the filtered liquid was collected in a cylinder and was polymerized at room temperature by the addition of 100 mM KCl and 2 mM $MgCl_2$. 2 hours later after the initiation of polymerization, 0.6 M solid KCl was added to the liquor which was gently stirred and kept at 4 °C for 30 minutes. After which, the KCl had completely dissolved, the liquid was centrifuged at 100,000 x *g* for 30 minutes. The pellets were swollen on ice for at least 2 hours by the addition of given amount of storage buffer (4 mM Tris-HCl, 0.2 mM ATP, 0.1 mM $CaCl_2$, 0.5 mM MEA, and 0.005% NaN_3) needed for further procedures. The swollen pellets were gently homogenized and then were dialysed against the same storage buffer at pH 8.0. The absorption of G-actin was measured by a spectrophotometer and the concentration of G-actin was calculated by using an absorption coefficient of 1.11 mg ml^{-1} cm^{-1} and 0.63 mg ml^{-1} cm^{-1} at 280 nm and 290 nm, respectively [233]. The relative molecular mass of 42,300 Da was used for G-actin [234].

III.1.2. Preparation of rabbit skeletal muscle tropomyosin

Skeletal muscle tropomyosin (Tpm1.1/2.2) [235] was purified as described earlier [236, 237] then applied to hydroxyapatite chromatography and stored frozen in 5 mM Tris-HCl, pH 7.8, 1 mM DTT.

III.1.3. Expression and purification of human cytoplasmic gelsolin

To label selected domains of gelsolin with maleimide-conjugated fluorophores we needed to make constructs that lacked native cysteine residues. It was required to replace the cysteines with other amino acids by mutation of DNA constructs to keep on structurally intact gelsolin. First we mutated out the native cysteines (Cys93Thr, Cys304Val, Cys645Val), which are not the members of the disulfide-bridge in G2 (Cys188, Cys201) made by QuikChange Lightning Site-Directed Mutagenesis Kit (Agilent Technologies) the construct is referred to as gelsolin M3. M3 mutant was used as a tool to show if any structural or functional change could happen if we mutate out cysteines compared to wild-type gelsolin. If we retain any native cysteine we can have constructs for selective labeling of G1, G3 or G6. The mutant gelsolin M2 contains only the mutations of Cys93Thr and Cys304Val. Thus M2 retains Cys645 in G6 to provide a suitable construct for selective labeling of G2, Cys645 under oxidative than Cys188 and/or Cys201 under reductive conditions.

The plasmid constructs of wild type gelsolin, M3 and M2 mutant gelsolins containing the nucleotide sequence of His-tagged human wild type gelsolin in a pSY5 plasmid (Invitrogen), were transformed into *E. coli* Rosetta2 (DE3) pLyS cells. The cells were grown on 37 ^{o}C in Luria Broth media until the optical density reached 0.6. Then the expression was induced by 1 mM isopropyl-β-D-1-thiogalactosidase (IPTG). After an overnight induction at 20 ^{o}C, cells were harvested by centrifugation (90 mins, 4,000 rcf at 4 ^{o}C) then dissolved in lysis buffer (4 mM imidazole, 10 mM Tris.HCl, 150 mM NaCl, 1 mg/ml lysozyme, pH 8) and subjected to sonication. The slurry was ultracentrifuged (2 hours, 150,000 rcf, at 4 ^{o}C) then the supernatant was loaded onto a Ni-NTA affinity column, followed by overnight on-column cleavage step by PreScission protease. The protein was eluted by elution buffer (20 mM Tris-HCl, 300 mM imidazole, 150 mM NaCl, pH 7.5) then loaded on a Superdex75 column in a gel filtration buffer (2 mM Tris-HCl, 150 mM NaCl, pH 7.5). Chromatographies were carried out with ÄKTA purifier system (Amersham Biosciences, Piscataway, NJ, USA). The peak fractions were collected and concentrated 5 times by Vivaspin 30 kDa mwco tube (4,000 rcf at 4 ^{o}C) then dialysed against storage buffer (2 mM-Tris HCl, 1 mM EGTA, pH 7.5). The dia-

lysed sample was concentrated again. The absorption of gelsolin was measured by a Nanodrop spectrophotometer and the concentration was calculated at 280 nm by using an absorption coefficient of 115,530 M^{-1} cm^{-1}. Purified human gelsolin sample was divided into small aliquots, frozen in liquid nitrogen, and kept at -80 °C. The frozen protein was used within few months and centrifuged prior to the measurements. Expression and purification of mutant gelsolins M2 and M3 proceeded by same protocol for wild type protein.

III.1.4. Expression and purification of cardiac leiomodin2 from *Rattus norvegicus*

Rattus norvegicus full length cardiac Lmod2 (NP_001094434.1; $Lmod2^{FL}$) and the C-terminal fragment (373-549 aa; Cterm) were expressed and purified using the Twin-CN (NE BioLabs) chitin-intein self-cleavage and purification system. DNA constructs were obtained from Roberto Dominguez's lab and cloned into pTyB1 vectors. Fusion proteins containing chitin-binding and intein tags were expressed for 20 hours at 20 ^{o}C in ER2566 *E.coli* cells. Cells were harvested by centrifugation (6000 x *g*, 10 min, 4 ^{o}C) then lysed with sonication in Column Buffer (20 mM Tris-HCl, 500 mM NaCl, pH 8.5). The supernatant of the ultracentrifuged (100.000 x *g*, 1 h, 4 ^{o}C) sample was loaded onto a chitin column, where intein self-cleavage was induced by a thiol reaction using 50 mM DTT, followed by the elution of the target protein from the column. $Lmod2^{FL}$ and Cterm concentrations were determined by either measuring the absorption spectra (Jasco V-550 spectrophotometer) and using the extinction coefficients of 23950 $M^{-1}cm^{-1}$ and 12490 $M^{-1}cm^{-1}$, respectively, or with the Bradford Protein assay (Bio-Rad). The two methods gave comparable results.

III.2. Fluorescent labeling of proteins

III.2.1. Labeling of actin

The labeling of the Cys-374 residue of actin with Alexa488-maleimide or Alexa532-maleimide (Life Technologies) was performed in the form of F-actin (2 mg/ml) which was incubated with 10-fold molar excess of Alexa for 16 hours at 4 °C. After the incu-

bation 1 mM DTT was added to the solution to terminate the labeling process. The sample was centrifuged at 100.000 rcf for 1 hour at 4 °C. The pellet was dissolved in buffer A, homogenized and dialyzed overnight. On the following day the labeled actin was centrifuged and the concentration of the supernatant was determined with a Nanodrop spectrophotometer. The Alexa488 label has significant absorption at 495 nm, similarly Alexa532 has at 532 nm, and the concentration of Alexa was calculated by using their extinction coefficient of 71,000 M^{-1} cm^{-1} for Alexa488 and 81,000 M^{-1} cm^{-1} for Alexa532. The measured absorbance of Alexa labeled G-actin was measured at 280 nm and 290 nm, where the extinction coefficient is 1.11 mg ml^{-1} cm^{-1} and 0.63 mg ml^{-1} cm^{-1} respectively, were used for calculating the concentration of actin [233]. The labeling ratio of five independent preparations was between 0.7 and 0.82. Cys374 of actin was labelled with either IAEDANS (5-((((2-iodoacetyl) amino) ethyl) amino) naphthalene-1-sulfonic acid) as a FRET donor or IAF (5-iodoacetoamidofluorescein) as FRET acceptor as described earlier [238-240]. Pyrene (N-1-pyrene-iodoacetamide) labelling was carried out by a standard protocol as described earlier [241]. Actin concentration and labelling ratios were determined from the absorption spectra (Jasco V-550 spectrophotometer). The labelling ratios were 0.8-0.9 for IAEDANS, 0.7–0.8 for IAF and 0.6-0.8 for pyrene.

III.2.2. Labeling of gelsolin

Alexa488-maleimide and Alexa532-maleimide (Life Technologies) were used to modify the cysteine residues of gelsolin (Cys93, Cys188, Cys201, Cys304 and Cys645). Before the labeling, gelsolin was dialyzed against in a calcium free buffer (2 mM Tris-HCl, 1 mM EGTA, pH 8); Alexa was dissolved in a same buffer and added to the gelsolin solution in 10-fold molar excess. The reaction mixture was incubated on ice overnight then dialyzed overnight to eliminate the unbound fluorophores. The sample was centrifuged at 100,000 rcf for 30 minutes on 4 °C. The measured absorbance of Alexa labeled gelsolin was measured at 280 nm where the extinction coefficient is 115,530 M^{-1} cm^{-1} were used for calculating the concentration of actin. The absorption of Alexa488 was measured by a Nanodrop spectrophotometer at 495 nm, Alexa532 at 532 nm; the concentration of Alexa was calculated by using their extinction coefficient of 71,000 M^{-1} cm^{-1} and

81,000 M^{-1} cm^{-1}, respectively. The labeling efficiencies of five independent preparations were between 60 and 68 %.

In case of M2 mutant gelsolin it was possible to label selectively G2 and G6, where Cys645 was exposed under oxidative conditions. Therefore M2 was incubated overnight in the presence of 2 µM $CuSO_4$ and 10-fold molar excess of Alexa532. The next day 1 mM DTT was added to the solution to reduce the disulfide-bridge and dialyzed overnight before adding 10-fold molar excess of Alexa 488. Free fluorophores were removed by an additional dialysis.

III.3. Preparation of membrane vesicles

III.3.1. Preparation of Rhodamine590 filled phospholipid vesicles

Phospholipid vesicles were prepared by a modified protocol from James H. Morrissey (Protocol from James H. Morrissey , Dept. of Biochemistry, University of Illinois at Urbana-Champaign, Urbana, IL 61801, USA). A mixture of 1% PIP_2 (PtdIns-(4,5)-P_2(1,2-dipalmitoyl)) (Cayman Chemicals), 79% PC (L-α-phosphatydilcholine) (Sigma-Aldrich) and 20% PS (3-sn-phosphatidyl-L-serine) (Sigma-Aldrich) was dissolved in 20 µM rhodamine 590 N-succinimidyl ester (Sigma-Aldrich) in chloroform. The dried lipid mixture was suspended in 2 mM Tris-HCl, 200 mM NaCl, pH 7.4, and sonicated until the solution became visually homogeneous. Vesicles were collected by centrifugation at 22 °C for 10 min at 5,000 x g, and stored at 4 °C.

III.4. Fluorescence spectroscopy methods

III.4.1. Characterization of intrinsic tryptophans fluorescence

$Lmod2^{FL}$ contains 3 tryptophans; one is in the N-terminal ABS1 (W73) and two are in the C-terminal extension (W386, W404). These tryptophans were used as intrinsic probes for the fluorescence emission coupled structural dynamics measurements in Lmod2. Structural changes of amino acids neighbouring the tryptophans can affect the

excitation and emission spectra. Fluorescence spectra were measured with Perkin Elmer LS 50B spectrofluorimeter (λ_{ex} = 282 nm, λ_{em} = 354 nm).

The intrinsic fluorescence emission assays from the tryptophans of gelsolin (residue numbers: W67, W111, W203, W223, W341, W392, W446, W489, W601, W637, W699, W706, W755, W759, W764) were carried out with a Perkin Elmer LS-50 spectrofluorimeter. The excitation and emission monochromators were set to 288 nm and 332 nm, respectively, and the excitation and emission slits to 5 nm. 5 µM gelsolin was incubated under physiological salt conditions (100 µM $CaCl_2$, 100 mM KCl, 1 mM $MgCl_2$, 0.2 mM ATP, 2 mM Tris-HCl, pH 7.4) supplemented with EGTA or $CaCl_2$ to vary the free calcium levels (calculated with Maxchelator Stanford http://maxchelator.stanford.edu): pCa 9: 6 mM EGTA; pCa 6: 100 µM EGTA; pCa 3: 1 mM $CaCl_2$. Steady-state fluorescence intensities were measured after sequential addition of appropriate stock solutions to attain: **1)** 2 µM PIP_2, **2)** 0.5 mM ATP, and **3)** pCa 6.

III.4.2. Steady-state fluorescence quenching

Steady-state fluorescence quenching measurements were carried out on a Perkin-Elmer LS55B spectrofluorometer equipped with a thermostable cuvette holder. Cys645 in the M2 mutant gelsolin (M2 GSN) was labeled by Alexa488-maleimide the protein concentration was set to 5 µM in all measurements. The fluorescence signal of Alexa was quenched by adding acrylamide in a final concentration of 2 mM in 10 steps. The excitation wavelength was set at 488 nm and the emission spectra were recorded between 505 nm and 600 nm at 22 °C. The ratio of the fluorescence intensity of Alexa488-M2 GSN in the absence and presence of the quencher was plotted against the quencher concentration (so called Stern-Volmer plot). The Stern-Volmer constant (K_{SV}) characterizing the accessibility of the fluorophore was derived from the slope of the straight line fitted on the experimental data according to the classical Stern-Volmer equation (Equation 1)

$$\frac{F_o}{F} = 1 + K_{SV}[Q] \qquad \text{(Eq. 1.)}$$

where F_0 is the fluorescence intensity of the fluorophore in the absence of the quencher, and F is in the presence of different quencher concentration [Q].

III.4.3. Steady-state and time dependent fluorescence anisotropy measurement

Steady-state anisotropy of gelsolin binding fluorescent derivatives of ATP and PIP_2 were measured on a Safire^2 monochromator microplate reader (TECAN). The steady-state anisotropy resulting from intrinsic fluorescence of the tryptophans in leiomodin2 was measured with Horiba Jobin Yvon spectrofluorimeter. Fluorescence lifetime and anisotropy decay resulting from intrinsic fluorescence of the tryptophan of leiomodin2 were measured using the cross-correlation phase-modulation method (ISS K2 multi-frequency phase fluorimeter) [239]. The emission polarizer was set to 0° and 90° as compared to the excitation polarizer to measure I_{VV} (t) and I_{VH} (t), where V and H sub-scripts refer to vertical and horizontal setting of excitation and emission polarizers, re-spectively. The instrument response function (IRF) was determined by measuring light scattering of a glycogen solution. The G value was determined by measuring the ratio of I_{HV} (t) / I_{HH} (t). The intensity decay data were analysed assuming the following multi-exponential decay law:

$$I_{total}(t) = I_{VV}(t) + 2I_{VH}(t) = \sum_i a_i \exp(-t/\tau_i) \qquad \text{(Eq. 2.)}$$

where a_i and τ_i are the normalised pre-exponential factors and decay times, respectively. Anisotropy values were calculated using Equation 3.[242]:

$$r(t) = \frac{I_{VV}(t) - I_{VH}(t)}{I_{VV}(t) + 2I_{VH}(t)} \qquad \text{(Eq. 3.)}$$

We used a fluorescent derivative of PIP_2 **(**PtdIns-(4,5)-P_2-fluorescein**,** Cayman Chemicals, NU-10010388, λ_{ex}= 493 nm, λ_{em}= 520 nm, abbreviated as PIP_2-F) and a fluorescent derivative of ATP (N^6-(6-amino)hexyl-ATP-ATTO-532, Jena Bioscience, NU-805-532, λ_{ex}= 532 nm, λ_{em}= 553 nm, abbreviated as ATP-N) as probes for the binding of PIP_2 and ATP to gelsolin.

The dissociation constants of gelsolin for ATP and PIP_2 were calculated using a hyperbolic model [243] from anisotropy data that had reached saturation during the gelsolin titrations:

$$r = r_f + (r_b - r_f)\left(\frac{K_d+[G]+[L]-\sqrt{(K_d+[G]+[L])^2-4[G][L]}}{2[L]}\right) \quad \text{(Eq. 4.)}$$

where r_f is the anisotropy of free ligand, r_b is the anisotropy of gelsolin-bound ligand, *[L]* is the total concentration of ligand, *Kd* is the dissociation constant and *[G]* is the total concentration of gelsolin. The anisotropy of 0.5 µM ATP-N was measured in the presence of gelsolin concentrations: 0, 0.2, 1.5, 2, 3, 5 and 8 µM. Saturation was evident at 5 µM characterized by an anisotropy value of 0.15 ± 0.006. The calcium and magnesium sensitivities of ATP binding to gelsolin were characterized by the change in anisotropy of solutions containing 0.5 µM ATP-N in the presence of 5 µM of gelsolin over a range of divalent cation concentrations of pCa 2-12 or pMg 1-12, where pCa and pMg refer to -log[Ca^{2+}] and -log[Mg^{2+}], respectively. The affinity of the PIP_2-gelsolin interaction was measured by the anisotropy change of 0.5 µM or 0.25 µM PIP_2-F in the presence of 0, 0.2, 2, 1.5, 3, 5 and 8 µM gelsolin, which showed saturation at 4 µM. Anisotropy of 0.5 µM or 0.25 µM solutions of PIP_2-F in the presence of 5 µM gelsolin was used to probe the changes in binding of the complexes under different calcium, magnesium, salt and ATP conditions.

Anisotropy decay data of leiomodin were analysed using Equation 5.:

$$r(t) = \sum_i r_{0i}\exp(-t/\theta_i) \quad \text{(Eq. 5.)}$$

where r_{oi} are fractional anisotropies, which decay with rotational correlation time of θ_i. Steady-state anisotropy values correspond to the rotational diffusion of the protein/protein complexes containing fluorophores, which reflect the rotational movement of the whole protein and the flexibility of protein chains containing the fluorophore. Rotational correlation times derived from anisotropy decay measurements depend on the mobility of fluorophores, as well as on the protein chains.

The steady-state anisotropy of intrinsic tryptophans in Lmod2^{FL} (9 µM) and Cterm (4.8 µM) fragments was measured with λ_{ex} = 282 nm, λ_{em} = 354 nm. Fluorescence lifetime and anisotropy decay of the intrinsic tryptophan of Lmod2^{FL} and Cterm were measured using the excitation and emission wavelengths at 280 nm and 350 nm, respectively. The average fluorescence lifetimes were found to be $\tau_{Lmod2FL} = 2.92 \pm 0.24$ ns and $\tau_{Cterm} = 3.26 \pm 1.41$ ns for Lmod2^{FL} and Cterm, respectively.

III.4.4. FRET measurements

For interdomain FRET we used 0.2 µM of an engineered mutant (M2) of gelsolin, which contains only the disulfide-bridge and one more residual cysteine for labelling with donor or acceptor in 1:1 ratio. Under oxidative conditions, provided by 1 µM $CuCl_2$ in a buffer of 2 mM Tris-HCl and pH7.4, Cys645 in G6 was amenable to be labelled with acceptor. This was followed by dialysis and 1 mM DTT treatment. Thus, the disulphide-bridge in G2 was reduced and Cys201 became exposed for labelling with the donor. From the two cysteines of disulphide-bridge only the Cys201 turned to be exposed, a situation we determined by solving the X-ray structure of Alexa488-maleimide labelled M3-gelsolin (data not shown). The gelsolin M2 mutant was labeled with Alexa488-maleimide as donor and with Alexa532-maleimide as acceptor to measure FRET transfer in the presence of 100 µM PIP_2 or 1 mM ATP or pCa6 or pCa3. The energy transfer between the two fluorophores was determined in a temperature dependent manner between 5 °C to 35 °C in 5 °C steps. The excitation wavelength was set to 488 nm and the emission spectra were monitored between 505 nm and 600 nm, and was corrected for the emission of acceptor. Both side slits were set to 5 nm.

For inter-monomer FRET measurements actin monomers were labelled separately with donor or with acceptor then mixed in a donor/acceptor ratio of 1: 10 [238, 244] then polymerized under medium salt conditions (1 mM $MgCl_2$, 50 mM KCl). To investigate the Lmod induced structural changes in F-actin, IAEDENS was used as the donor and IAF as the acceptor. The temperature-dependent inter-monomer FRET efficiency of IAEDENS-IAF F-actin (4 µM) was measured in the presence or absence of Lmod2^{FL} (5 µM) (Horiba Jobin Yvon spectrofluorimeter, λ_{ex} = 350 nm, λ_{em} = 380 – 600 nm). The temperature was set between 5-35 ^{o}C.

The obtained intensities of the donor were corrected for the inner filter effect by applying the Equation 6.

$$F_{corr} = F_{obs} antilog[(OD_{EX} + OD_{EM})/2] \quad \text{(Eq. 6.)}$$

where F_{corr} is the corrected fluorescence intensity, F_{obs} is the measured fluorescence intensity, and OD_{EX} and OD_{EM} are the optical densities of the sample at the excitation and emission wavelengths, respectively. In order to calculate the fluorescence resonance energy transfer efficiency (E), the intensity of the donor was measured in the presence (F_{DA}) and absence (F_D) of the acceptor. The energy transfer efficiency was calculated from the Equation 7.

$$E = \{1 - (F_{DA}/c_{DA}/F_D/c_D)\}/\beta \quad \text{(Eq. 7.)}$$

where β is the labeling ratio of the acceptor, c_{DA} and c_D are the concentrations of the donor molecule in the presence and absence of the acceptor, respectively.

It was shown previously that the energy transfer efficiency (E) normalized by the intensity (F_{DA}) of the donor in the presence of the acceptor could provide information about the flexibility of the protein matrix between the FRET fluorophore pair. This normalized energy transfer efficiency is called as relative transfer (f') that was introduced in 1984 by Somogyi et al [245]. The relative transfer can be calculated by using the Equation 8.

$$f' = E/F_{DA} \quad \text{(Eq. 8.)}$$

The flexibility of the proteins is related to the thermal fluctuations of protein segments relative to each other. It is expected that the increase in temperature generates higher amplitude of relative motion between donor-acceptor fluorophores. Fluctuations with a higher amplitude refers to a more flexible protein structure and results a higher value of relative transfer [246]. In our experiments each relative transfer value was normalized by the flexibility parameter obtained at the lowest temperature level (5 $^{\circ}$C) and this relative flexibility parameter was plotted against the temperature. The slope of the curve

corresponds to the flexibility of the protein structure between the donor and acceptor fluorophores.

III.4.5. Actin polymerization assay

To study actin polymerization the time dependent intensity of pyrene-labelled actin was measured. The actin concentration was 4 µM containing 5 % pyrene actin. The effects of the Lmod2 constructs were investigated at different salt conditions: low salt (0.5 mM $MgCl_2$, 10 mM KCl); medium salt (1 mM $MgCl_2$, 50 mM KCl); and high salt (2 mM $MgCl_2$, 100 mM KCl). The final ionic strength (IS) at each condition was derived using the following equation:

$$[IS] = \frac{1}{2}\sum_{i=1}^{n} c_i z_i \qquad \text{(Eq. 9.)}$$

where c_i and z_i are the molar concentrations and charge of the ions, respectively. The polymerization rates were determined in the absence or presence of $Lmod2^{FL}$ and Cterm from the slope of the pyrene curves at 50 % of maximal change. The normalized polymerization rate was calculated as the ratio of the slope obtained in the presence of Lmod2 constructs to the slope determined for spontaneous actin assembly.

III.4.6. Critical concentration measurements

To determine the critical concentration of actin assembly, we measured the fluorescence emission of 0.03; 0.05; 0.1; 0.3; 0.5; 0.7; 1; 3; and 5 µM actin (5 % pyrene labelled) in the absence or presence of $Lmod2^{FL}$ (100 nM) or Cterm (4 µM) under high salt conditions. The critical concentration, corresponding to the free G-actin concentration at steady-state was determined from the actin concentration ([a]) dependence of the pyrene fluorescence emission (F) using Equation 10:

$$F = F_c + \left[(L_s + R_s)\frac{[a]-cc}{2}\right] - \left[(L_s - R_s)\frac{[a]-cc}{2}\right] \qquad \text{(Eq. 10.)}$$

where F_c is the fluorescence emission corresponding to the critical concentration, L_s and R_s are the slopes of the function below and over the critical concentration, respectively, and *cc* is the critical concentration.

III.4.7. Fast kinetic measurements of the interaction of Lmod2 with actin filaments

To measure the binding kinetics of leiomodin to F-actin, the real time change of pyrene F-actin fluorescence (5 % pyrene labelled) mixed with leiomodin2 under medium salt conditions was measured by a stopped-flow fast kinetic system (Applied Photophysics Ltd.). The change in pyrene fluorescence as a function of time ($y(t)$) was fitted using the following function:

$$y(t) = A_1\left(1 - exp\left(-\frac{t}{t_1}\right)\right) + A_2\left(1 - exp\left(-\frac{t}{t_2}\right)\right) \qquad \text{(Eq.11.)}$$

where A_1 and A_2 are the amplitude of the first and second exponential, respectively, t_1 and t_2 are the corresponding times.

III.5. Crystallization

III.5.1. Crystallization and data collection of gelsolin mutants

Crystals of calcium-free, human gelsolin mutant M3 and Alexa488-maleimide labeled gelsolin M3 were obtained after added 5 µl of a 10 mg/mL solution of protein to 5 µl precipitating solution (24% glycerol, 1.7 M ammonium sulfate, and 100 mM Bis-Tris-HCl, pH 8.5) at 22 °C by using the sitting-drop vapor diffusion method. The crystals were frozen in liquid nitrogen after soaking in 20 % glycerol. X-ray diffraction data were collected on beamline BL13B1 by an Area Detection Systems Corporation Quantum-315 CCD detector at the National Synchrotron Research Center (Hsinchu, Taiwan). The wavelength was set to 1 Å and the data collected at 105 K. Data were indexed, scaled, and merged in HKL2000. Molecular replacement and refinement were carried out using the native gelsolin structure (3FFN PDB ID), in PHENIX 1.9 (NIH General

Medical Sciences). The final statistics were: space group $P42_12$, resolution: 3.04 Å, R free: 0.2751, R work: 0.2155.

III.6. Critical micelle concentration

III.6.1. Determination of lipid critical micelle concentration

The critical micelle concentrations of PIP_2 and 1-(1-octadecanoyl-fluorescein-2R-octadecanoylphosphatidyl)inositol-4,5-bisphosphate (Cayman Chemical, abbreviated as PIP_2-F) were determined by dynamic light scattering [247]. Fifty microliter samples were prepared by serial dilution of PIP_2 or PIP_2-F into a low salt buffer (2 mM Tris-HCl, pH 7.4), or the same buffer supplemented with 100 mM KCl, 1 mM $MgCl_2$, and/or 1 mM $CaCl_2$. After incubation for 30 min, the samples were centrifuged at 15,000 x g for 10 min, transferred into a 384-well clear bottom plate, and light scattering was measured using a Wyatt Dynapro plate reader at room temperature. The concentrations of PIP_2-F were subsequently determined by light absorbance at 494 nm with a Nanodrop spectrophotometer.

III.7. Microscopy imaging

III.7.1. Confocal microscopy imaging of vesicles

10% (v/v) rhodamine590-filled vesicles and 5 µM Alexa488-labeled gelsolin were incubated together and a drop of the mixture was placed on a clean glass slide, which was then covered by, and separated from, a second slide by a parafilm gasket. In this setup, buffer conditions surrounding the vesicles can be changed by laminar flow between the two slides. A 2 mm x 2 mm piece of tissue (KimWipes) was used to secure the vesicles. The sample was washed (2 mM Tris-HCl, pH 7.4) for 1 min and then placed on the glass slide before being covered. In the flow cell, vesicles were kept in the field of view by the tissue fibres. Fluorescence emission-based imaging was carried out using a Zeiss LSM 510 META Confocal Microscope. The two different fluorophores were detected in two separate channels; Alexa488 (gelsolin) was excited by 477 nm laser light and emis-

sion was detected in the 505-530 nm channel, while rhodamine590 (vesicles) was excited by 545 nm laser light and emission was detected in the 585-630 nm channel.

III.8. Cosedimentation

III.8.1. High-speed cosedimentation assays

F-actin (4 µM) was incubated with Lmod2^{FL} under medium and high salt conditions. Samples were centrifuged at 258,000 x *g* for 30 min at room temperature. The pellets were resuspended and analysed by SDS-PAGE. The band intensities were derived by GeneTools software (Synaptics Ltd.) and corrected for the molecular weight of the proteins and for the staining efficiency of Coomassie blue. The ratio of the MW corrected band intensities of pelleted Lmod2^{FL} to pelleted actin was derived (protein ratio, *y*) and plotted as a function of total Lmod2^{FL} concentration. Data was fitted with sigmoidal function (Eq.12.).

$$y = \frac{y_{min} - y_{max}}{1+\exp(x-x_0)/dx} + y_{max} \qquad \text{(Eq. 12.)}$$

where y_{min} and y_{max} are the protein ratios in the absence and presence of saturating amount of Lmod2, respectively, x is the total Lmod2 concentration, x_0 is the Lmod2 concentration corresponding to the inflection point and dx is the slope of the linear segment of the sigmoidal.

III.9. Coupled assay

III.9.1. Mg^{2+}-ATPase activity of HMM in the presence of leiomodin2

The Mg^{2+}-ATPase activity of HMM was measured with a Jasco V-550 spectrophotometer. The assay is based on a reaction in which the regeneration of hydrolysed ATP is coupled to the oxidation of NADH. The reaction buffer contains 100 mM KCl, 20 mM

MOPS, 0.5 mM $MgCl_2$, 0.5 mM ATP, 1 mM PEP, 0.5 mM EGTA, 5-10 µl PK (2 U/µl), 10 µl LDH (4 U / µl) in 60 % glycerol, 0.15 mM NADH, pH 7.0. Following each cycle of ATP hydrolysis of 0.5 µM HMM (heavy-meromyosin) with or without 1 µM F-actin in the presence or absence of 1 µM $Lmod2^{FL}$, the regeneration system consisting of phosphoenol-pyruvate (PEP) and pyruvate kinase (PK) converts one molecule of PEP to pyruvate when the ADP is converted back to the ATP. The pyruvate is subsequently converted to lactate by L-lactate dehydrogenase (LDH) resulting in the oxidation of one NADH molecule. The assay measures the rate of NADH absorbance decrease at 340 nm, which is proportional to the rate of steady-state ATP hydrolysis. The constant regeneration of ATP allows monitoring the ATP hydrolysis rate over the entire course of the assay. The rate of ATP hydrolysis is calculated from the following equation:

$$k = -\frac{dA_{340}}{dt} x\, E_{path}^{-1} x\, M_{ATP}^{-1} \qquad \text{(Eq. 13.)}$$

where k is the ATPase activity, A_{340} is the measured absorbance at 340 nm, t is the elapsed time, E_{path} is the molar absorption coefficient of NADH, M_{ATP} is the molarity of ATP. k values were corrected for the HMM concentrations.

IV. Results and Discussion

IV.1. Results

IV.1.1. ATP and PIP_2 binding to gelsolin

IV.1.1.1. Structural dynamics of ATP or PIP_2 bound gelsolin under different salt conditions

In order to probe the interplay between PIP_2, ATP and Ca^{2+} in binding to gelsolin, we first characterized the binding of fluorescent derivatives of PIP_2 and ATP to gelsolin using steady-state anisotropy measurements. The fluorescent derivative of ATP (0.5 μM), N^6-(6-amino)hexyl-ATP-ATTO-532 named ATP-N hereafter, binds to gelsolin with a *Kd* of 0.71 ± 0.52 μM in the absence of divalent cations determined by analysis of steady-state anisotropy measurements (Fig 10*A*). This value is within experimental error of that previously reported for the gelsolin: ATP interaction (0.28 μM), as measured by equilibrium dialysis [183]. In case of M3 mutant of gelsolin, the affinity (*Kd*) was changed to 1.55 ± 0.74 μM (Fig 10*A*). Interestingly, we found that the crystal structures of wild type and M3 mutant gelsolin were identical, only the Cys645 residue may be implicated in ATP binding because it is directly linked to the ATP-binding pocket thus the mutation of Cys645Val possibly modified the dynamics of ATP binding (Fig 9*A*, *B*). Micromolar levels of calcium ions or millimolar levels of magnesium ions were able to effectively dissociate ATP-N from gelsolin (5 μM), characterized by 50% of the ATP-N remaining bound at 6.3 ± 0.2 μM calcium or 5.0 ± 1.1 mM magnesium (Fig 10*B*). Furthermore, the first evidence of the competition between ATP and PIP_2 in binding to gelsolin was observed from the elevated anisotropy (0.12, Fig 10*C*) of PIP_2-F (0.5 μM), characteristic of its association with gelsolin (5 μM), being lost on the addition of 0.2 or 0.5 mM ATP, or 1 mM Ca^{2+} (Fig 10*D*).

The calcium range that induces ATP dissociation is in line with physiological calcium signaling levels and with calcium concentrations that are able to initiate conformational changes in gelsolin, which disrupt the ATP-binding site leading to ATP release [186]. However, the effective concentration of magnesium is higher than the normal free physiological levels (0.5 - 1.0 mM) [197]. The presence of potassium ions weakens the gel-

solin: ATP-N interaction (Fig 11*A-B*). Under physiological potassium ion concentrations, the ATP-N interaction with gelsolin was characterized by *Kd*s of 1.27 ± 0.60 µM and 1.42 ± 0.27 µM at 100 mM and 120 mM KCl, respectively, values which were reduced slightly by the addition of 1 mM $MgCl_2$ (*Kd*s of 1.58 ± 0.85 µM and 2.34 ± 0.73 µM, respectively) (Fig 11*C,D*). Similarly, in 50 mM KCl and 1 mM $MgCl_2$, a condition commonly used for *in vitro* actin polymerization experiments [248], gelsolin binding of ATP-N and unlabeled ATP was determined by titration with gelsolin and via competition with ATP-N, and the *Kd* values were 1.8 µM and 2.2 µM respectively (Fig 12*A*,*B*). The effect of calcium under the actin polymerization conditions recapitulated the observation made under the low salt conditions, with micromolar and higher concentrations of calcium negatively impacting the gelsolin: ATP-N interaction (Fig 12*A* vs Fig 10*B*). Collectively, these data indicate that under buffer conditions modelling the physiological state gelsolin binds to both ATP-N and unlabeled ATP in similar fashion, and that calcium acts as a regulator for the binding.

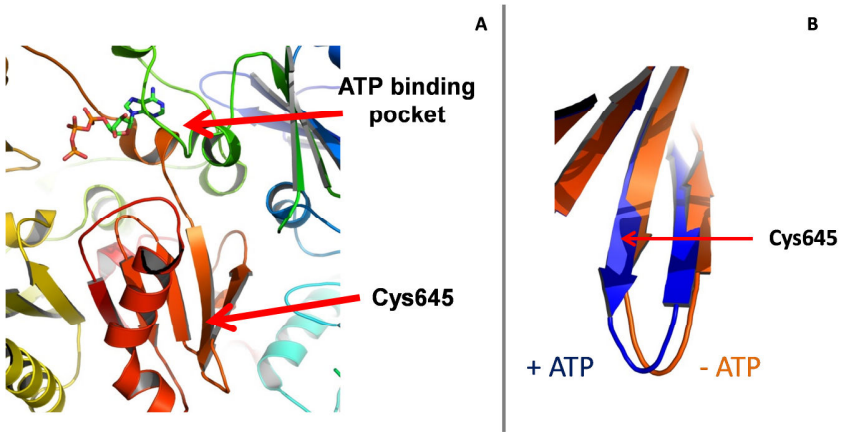

Figure 9. *Structural importance in ATP binding of gelsolin.* (**A**) From the three mutations of native cysteines Cys93Thr, Cys304Val and Cys645Val in M3 gelsolin only the Cys645Val can be expected to influence ATP binding. (**B**) The structure of ATP-bound and ATP-free gelsolin around the Cys645 are almost identical. Possibly, Cys645 is involved in structural dynamics of the binding pocket, therefore its mutation to valine decreased the affinity for ATP.

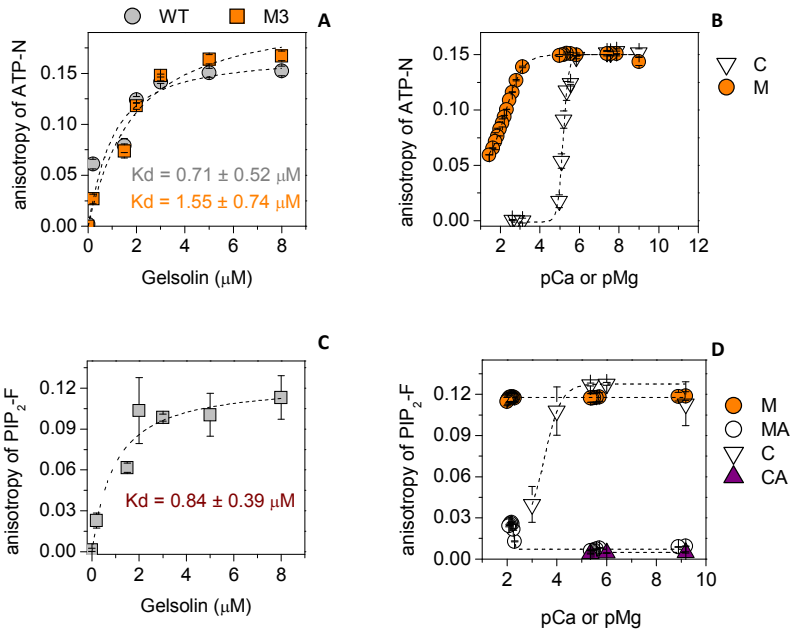

Figure 10. *The interplay between calcium, magnesium, ATP and PIP_2 for binding to gelsolin.* (**A**) In the absence of divalent cations, the anisotropy of ATP-N (0.5 μM) increased with increasing gelsolin concentration and reached steady-state at ~ 5 μM wild type gelsolin (grey circles) and M3 mutant gelsolin (orange squares), indicating saturation of binding. Dashed line shows the fit to the data (Eq. 4). (**B**) Micromolar calcium levels (C, open triangles, inflection point at pCa 5.2) or millimolar magnesium levels (M, orange circles, inflection point at pMg 2.3) were able to reduce the anisotropy of ATP-N (0.5 μM) in the presence of gelsolin (5 μM), indicating the dissociation of ATP-N from gelsolin. Dashed line means simple sigmoidal fitting. (**C**) In the absence of divalent cations, the anisotropy of PIP_2-F (0.5 μM) increased with increasing gelsolin concentration and reached steady-state at ~ 5 μM gelsolin, indicating saturation of binding. Dashed line shows the fit to the data (Eq. 4). (**D**) The anisotropy of PIP_2-F (0.5 μM) in the presence of gelsolin (5 μM) was not changed on titration with magnesium (M, orange circles), but inclusion of 0.5 mM ATP (MA, white circles) lowered the anisotropy to the value characteristic to free PIP_2-F, indicating complete dissociation of the gelsolin/PIP_2-F complex by ATP. This effect was diminished by magnesium concentrations above 7 mM. In the absence of ATP, PIP_2-F (0.5 μM) binds to gelsolin (5 μM), as revealed by the increase in anisotropy across a wide range of calcium concentrations (C, white triangles). Inclusion of ATP (0.2 mM, CA, purple triangles) lowered the anisotropy to the value characteristic to free PIP_2-F, indicating complete dissociation of the gelsolin/PIP_2-F complex by ATP.

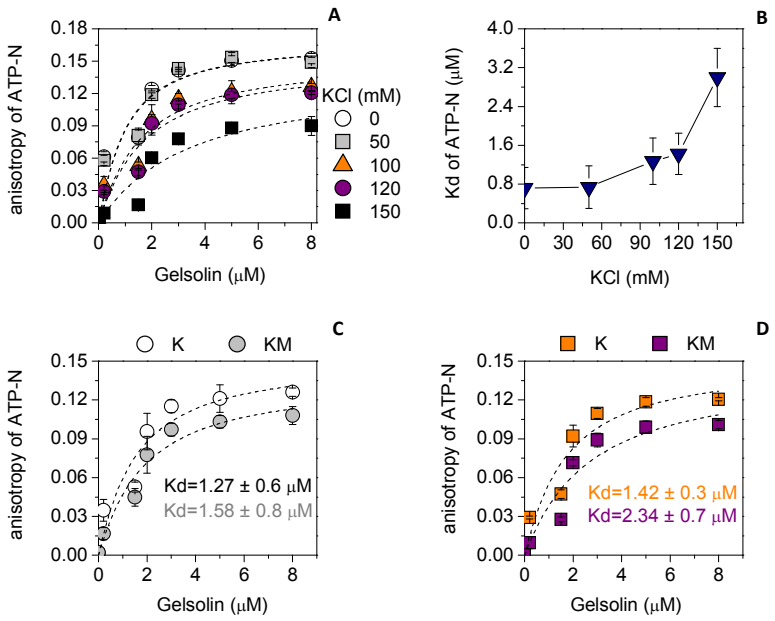

Figure 11. *The interplay among calcium, magnesium and potassium ions on ATP-N binding to gelsolin.* (**A**) In the absence of divalent cations, the anisotropy of ATP-N (0.5 μM) increased with increasing gelsolin concentration and this interaction was potassium ion dependent. Dashed lines show the fit to the data (Eq. 4). (**B**) The *Kd*s calculated from the binding curves in Fig 11*A* showed diminishing affinities with increasing potassium ion concentrations. (**C,D**) Inclusion of 1 mM $MgCl_2$ slightly weakened the affinity of ATP-N for gelsolin at (**C**) 100 mM and (**D**) 120 mM KCl (K, potassium ions, KM, potassium and magnesium ions). Dashed lines show the fit to the data (Eq. 4).

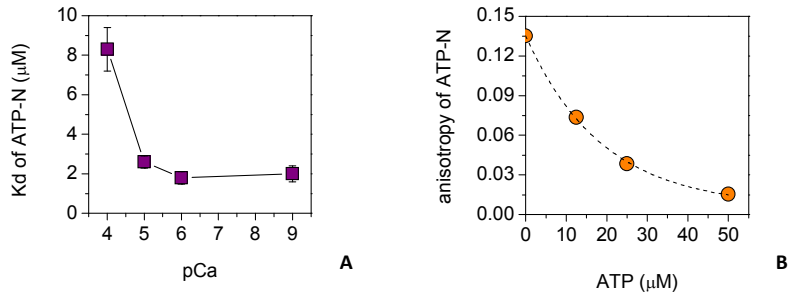

Figure 12. *ATP binding to gelsolin under actin polymerization conditions.* (**A**) The calcium-dependent gelsolin binding affinity for ATP under actin polymerization conditions was determined by the change in ATP-N anisotropy. *Kd*s were calculated to be between 1.51 μM and 2.35 μM in the 1 nM to 10 μM calcium concentration range, and the value increased to 8.05 ± 1.32 μM above 100 μM calcium. (**B**) The anisotropy of ATP-N (0.5 μM) bound to gelsolin (5 μM) was measured upon titrating with unlabeled ATP in the absence of calcium. 50 μM ATP was sufficient to remove the gelsolin bound ATP-N. The affinity of unlabeled ATP for gelsolin, under actin polymerizing salt conditions, was calculated to be *Kd* = 2.2 ± 0.17 μM measured by labeled/unlabeled ATP competition on gelsolin, which is similar to the affinity of ATP-N derived from Fig 11*C* (*Kd* = 1.58 ± 0.8 μM). Data were analyzed by the method of Kubala [249] with the modification that the change in anisotropy of ATP-N was substituted for the change in fluorescence emission as the indication of ATP competition.

Gelsolin has been shown to have three PIP_2-binding sites, which have previously been characterized to display *Kd* values for gelsolin binding in the 1-20 μM range [172, 174, 177]. In a similar strategy to that adopted for characterizing the ATP-gelsolin interaction, a soluble fluorescent derivative of PIP_2, PtdIns-(4,5)-P_2-fluorescein named PIP_2-F hereafter, was used to probe the gelsolin-PIP_2 interaction using steady-state anisotropy measurements. In this assay the binding of PIP_2-F (0.5 μM) to gelsolin in the absence of divalent cations was characterized by a *Kd* of 0.84 ± 0.39 μM (Fig 10*C*). This value increased to 1.35 ± 0.7 μM and 3.12 ± 1.7 μM in the presence of 100 mM and 120 mM KCl, respectively, and these values remained constant within the experimental error on the further addition of 1 mM $MgCl_2$ (Fig 13*A-D*). Under high concentration of salt 400

mM KCl or NaCl both removed PIP_2, refers to ionic strength dependent interaction between PIP_2 and gelsolin (Fig 13*E*). Briefly, the interactions of PIP_2-F and ATP-N with gelsolin lie in the same range under physiological salt conditions.

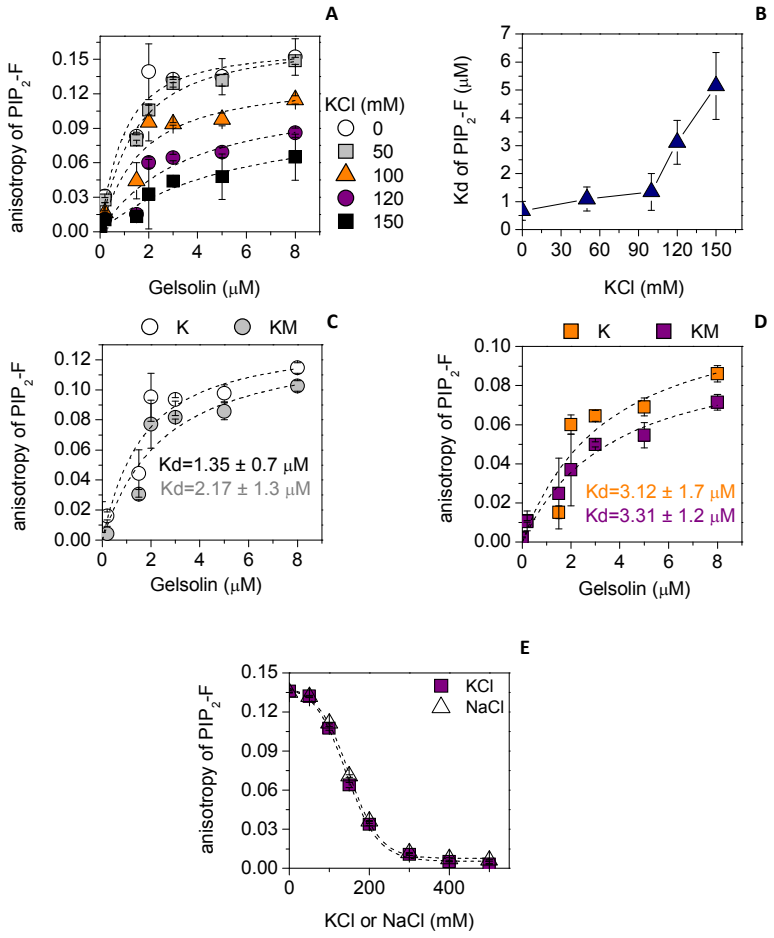

Figure 13. *The interplay between calcium, magnesium and potassium ions on PIP_2-F binding to gelsolin.* (**A**) In the absence of divalent cations, the anisotropy of PIP_2-F (0.5 μM) increased with increasing gelsolin concentration and this interaction was potassium ion dependent. Dashed lines show the fit to the data (Eq. 4). (**B**) The *Kd*s calculated from the binding curves in Fig 13A showed diminishing affinities with increasing potassium ion concentrations. (**C,D**) Inclusion of 1 mM $MgCl_2$ had relatively little effect on the affinity of PIP_2-F for gelsolin at (**C**) 100 mM and (**D**) 120 mM KCl (K, potassium ions, KM, potassium and magnesium ions). Dashed lines show the fit to the data (Eq. 4). (**E**) Anisotropy of PIP_2-F (0.5 μM) in

the presence of gelsolin (5 μM) as a function of KCl or NaCl concentration. Fitted with simple sigmoidal. The decrease in anisotropy indicates that PIP_2-F is dissociated from gelsolin by increasing potassium or sodium ion concentrations, with the half-effective concentrations of 141.2 ± 3.0 mM and 143.3 ± 1.6 mM, respectively. This indicates the effect of KCl on gelsolin: PIP_2-F binding is largely ionic and nonspecific.

In the absence of salts the ATP, PIP_2 and calcium binding based structural dynamics of gelsolin was investigated by using FRET measurements. PIP_2 and ATP increased the FRET transfer efficiency between the Alexa488 (donor) labeled G6 and Alexa532 (acceptor) labeled G2 (Fig 14*A*) and the relative transfer shows lower values in the presence than in the absence of ATP or PIP_2 and increased in a temperature dependent manner (Fig 14*B*). Interestingly, gelsolin had less flexible dynamics by ATP binding but PIP_2 binding resulted the lowest flexibilty of the gelsolin. The FRET transfer efficiency between the donor and the acceptor was decreased by the binding of calcium and caused a more flexible structure of gelsolin in a concentration dependent manner (Fig 14*C*). The relative transfer generated by the ratios of transfer efficiencies and donor emissions increases by the temperature relates to an increased thermal motion of protein matrixbetween Alexa labeled G2 and G6 (Fig 14*D*). Alexa488-Cys645 fluorescence emission was less sensitive to acrylamide quenching in the presence of PIP_2 suggesting that Cys645 was buried in the gelsolin structure but in the presence of millimolar calcium the Alexa probe turned to become more exposed.

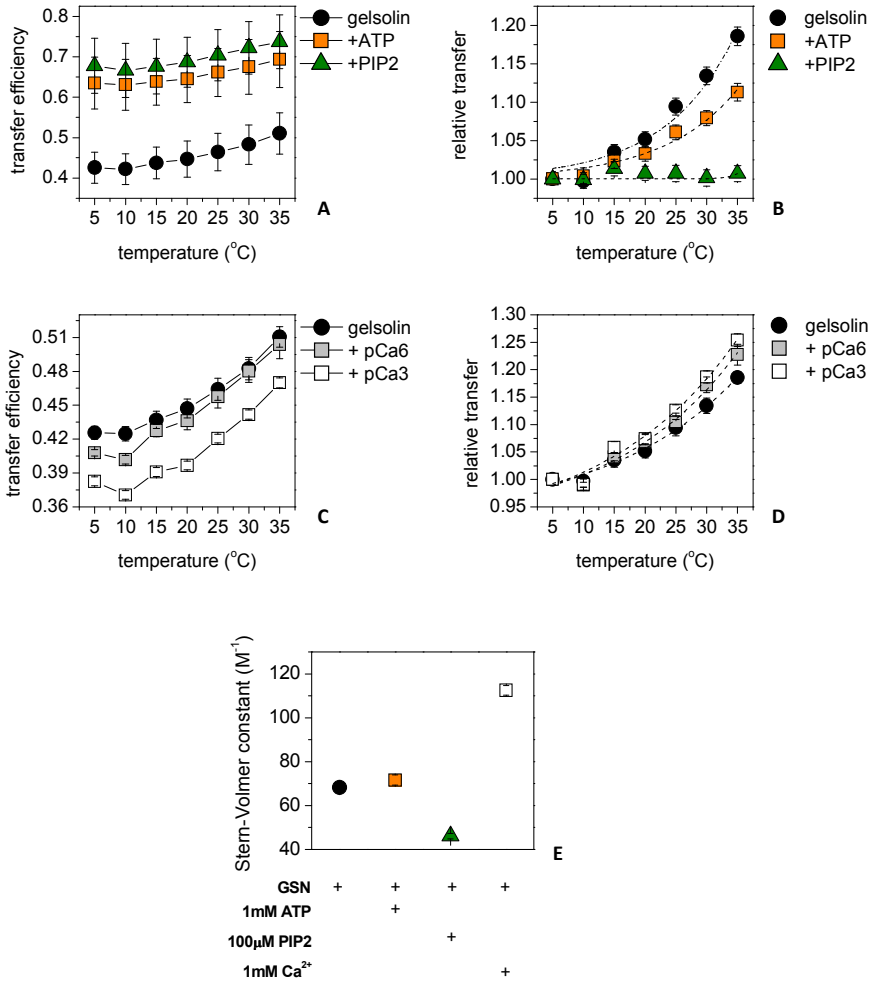

Figure 14. *ATP, PIP_2 and calcium binding based structural dynamics of gelsolin.* (**A**) PIP_2 and ATP binding increased the FRET transfer between Alexa488 (donor) labeled G6 and Alexa532 (acceptor) labeled G2 while the (**B**) relative transfer decreased by the temperature which indicates a less flexible structure of gelsolin. In case of PIP_2 binding gelsolin shows a stiff, well packed structure. (**C**) The FRET transfer between donor and acceptor was decreased slightly by micromolar and intensively by millimolar calcium. (**D**) Calcium ions caused a change in the gelsolin structure in becoming more flexible, which fits with the higher relative transfer between Alexa labeled G2 and G6. (**E**) Alexa488-Cys645 fluorescence emission was less sensitive to acryl-amide quenching in the presence of PIP_2 suggesting that it was buried in the gelsolin structure, but in the presence of millimolar calcium Alexa became more exposed.

IV.1.1.2. ATP and PIP_2 binding to gelsolin under physiological salt conditions

The ability of ATP to dissociate PIP_2-F remained constant over a wide range of Mg^{2+} concentrations, from picomolar to the physiologically relevant millimolar range, becoming less effective above 7 mM magnesium. Hence, ATP can effectively compete with PIP_2 for binding to gelsolin under physiological Mg^{2+} conditions. In the absence of ATP, PIP_2-F was able to bind gelsolin, characterized by a steady-state anisotropy value increment from approximately 0.002 to 0.12, over the 0-10 µM range of Ca^{2+} (Fig 10*D*). At higher calcium levels the anisotropy decreased, reaching 0.04 at 1 mM Ca^{2+} (Fig 10*D*). The PIP_2-F/gelsolin interaction was characterized by *Kd* values less than 20 µM across the entire calcium range in line with previously reported PIP_2/gelsolin affinities [172, 174, 177], and below 1 µM in the 1-10 µM range (Fig 15*A,B*), in the absence of KCl and magnesium. In the presence of 0.2 mM ATP in the 0-10 µM calcium range, the anisotropy was close to the baseline characteristic of free PIP_2-F, indicating the effective dissociation of the PIP_2-F from gelsolin (Figs 10*D* and 15*C*) with estimated *Kd*s in excess of 300 µM (Fig 15*B*). Higher calcium levels were not obtainable in the presence of ATP due to precipitation of these reagents in the absence of salt (Fig. 15*D*). In a control experiment, PIP_2 had no observable effect on the binding of calcium to FURA-2FF, implying that any calcium binding by PIP_2 is substantially weaker than that of FURA-2FF (*Kd* = 25 µM of calcium to FURA-2FF, Fig 15*E*), and it is unlikely to have had a significant effect in these experiments. Thus, these data suggest that ATP can release PIP_2-F from gelsolin effectively in the 0-10 µM calcium concentration range. With this results we confirmed that the PIP_2-F-gelsolin complex remained intact under actin polymerization conditions, and that PIP_2-F was released from gelsolin when these conditions were supplemented with 0.5 mM ATP (Fig 16*A*).

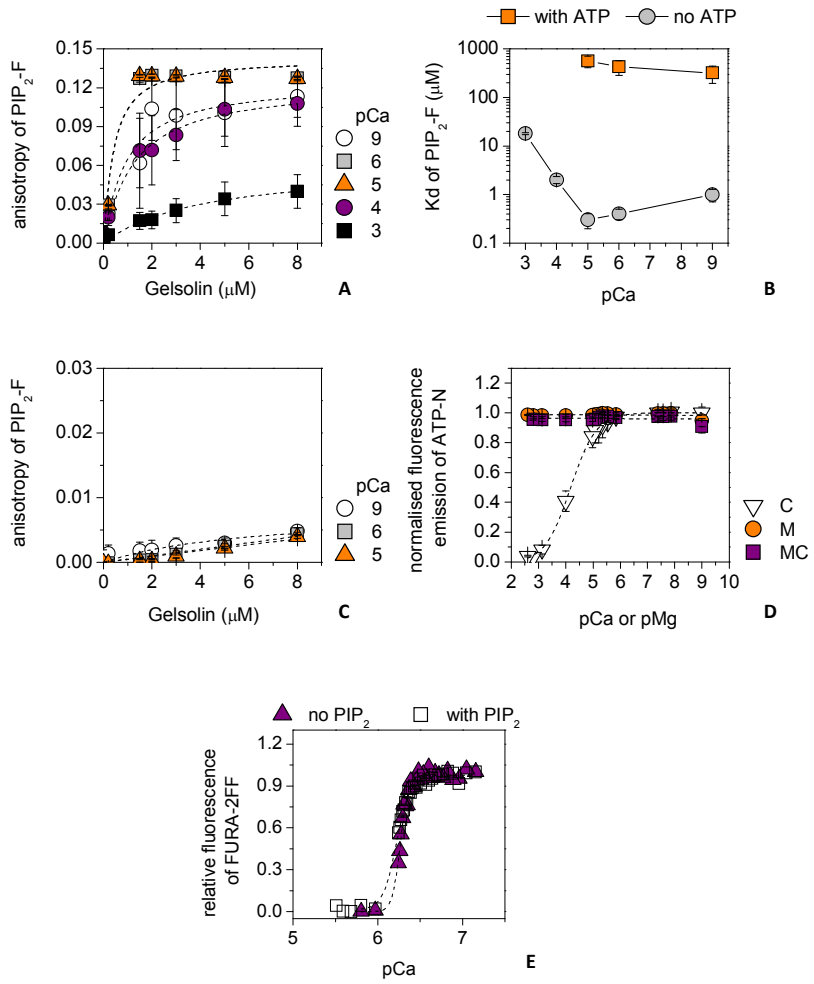

Figure 15. *Assessment of the effects of calcium and ATP on the binding of ATP-N and PIP_2-F to gelsolin.* (**A**) Gelsolin:PIP_2-F binding under different calcium concentrations in the absence of ATP. Part of the data have been shown in Fig 10*D* (white triangles). In the absence of ATP, PIP_2-F (0.5 μM) binds to gelsolin, as reflected by the increase in anisotropy, across a wide range of calcium concentrations. Dashed lines show the fit to the data (Eq. 4). (**B**) *Kd*s were calculated from the data shown in Fig 15*A*. In the absence of ATP, the affinity of gelsolin for PIP_2-F varied in the 0.5-20 μM range with calcium concentration. In the presence of ATP, the interaction of PIP_2-F with gelsolin was very weak below 10 μM calcium (*Kd* = 563.0 ± 3.6 μM at 10 μM calcium). (**C**) Gelsolin:PIP_2-F binding under different calcium concentrations in the presence of ATP. Part of the data have been shown in Fig 10*D* (purple triangles). In the presence of 0.2 mM ATP, PIP_2-F (0.5 μM) showed no binding to gelsolin, as measured by anisotropy, across a wide range of calcium concentrations. Dashed lines show the fit to the data (Eq. 4). (**D**) In the absence of

gelsolin, calcium directly precipitates ATP-N (C, open triangles) with a half-maximum value of 70.4 ± 0.7 μM. Magnesium has no effect on the fluorescence emission of ATP-N either in the absence (M, orange circles) or presence of calcium (MC, purple squares). Fitted with simple sigmoidal curve. (**E**) The reported FURA-2FF dissociation constant for calcium ions is 25 μM (A.G. Scientific Inc.). The calcium-dependent fluorescence emission profile of FURA-2FF (2 μM) over pCa range of 5-7 was similar in the presence and absence of 20 μM PIP_2. Fitted with simple sigmoidal. The half-saturation pCa values were = 6.265 ± 0.004 and 6.217 ± 0.011 in the absence and presence of PIP_2, respectively, suggesting that PIP_2 does not interact with calcium with a *Kd* less than 25 μM. The measurement was carried out by Perkin Elmer LS-55 spectrofluorimeter (λ_{ex} = 340 nm, λ_{em} = 505 nm).

Subsequently, we used the intrinsic tryptophan fluorescence emission at 332 nm, emitted by the 15 tryptophan residues that are evenly distributed across the 6 domains of gelsolin, to probe the effects of PIP_2 and ATP on gelsolin at concentration higher than could be probed by the PIP_2-F and ATP-N anisotropy assays. Since gelsolin contains 6 calcium-binding sites, some of which have *Kd* values below the protein concentration used in the experiment, we turned to an EGTA-buffered calcium system to control the free calcium levels. Gelsolin was incubated under physiological salt conditions (100 μM $CaCl_2$, 100 mM KCl, 1 mM $MgCl_2$, 0.2 mM ATP, 2 mM Tris-HCl, pH 7.4) and was supplemented with various concentration of EGTA or $CaCl_2$ to establish the free calcium levels. Gelsolin (5 μM) showed lower tryptophan emission levels when bound to ATP (0.5 mM) relative to PIP_2 (2 μM) at 1 μM and 1 nM $CaCl_2$ (Fig 16*B*). This difference was used to demonstrate the cycling between gelsolin binding to PIP_2 and ATP. Gelsolin showed a decrease in tryptophan fluorescence in moving from 1 nM free calcium to activating levels of calcium (1 μM and 1 mM, Fig 16*C*). Subsequent addition of PIP_2 (2 μM) to these samples raised the intrinsic tryptophan fluorescence at 1 nM and 1 μM, but not at 1 mM free calcium, indicating that tryptophan fluorescence is a sensitive signal to the gelsolin : PIP_2 interactions in the 1 nM to 1 μM range. Subsequent addition of ATP (0.5 mM) led to a reduction in the intrinsic fluorescence at both 1 nM and 1 μM free calcium. Finally, the tryptophan fluorescence converged on adjusting each condition to 1 μM free calcium, indicating that the interplay between calcium with gelsolin in PIP_2/ATP was in equilibrium and reversible. Thus, the tryptophan assay showed that ATP could exert competitive effects against PIP_2 in the 1 nM and 1 μM calcium range.

Next we probed the effect of actin on the competition between ATP and PIP_2 in binding to gelsolin. The association of PIP_2-F (0.25 μM) with gelsolin (5 μM) was investigated as a function of free Ca^{2+} concentration under physiological model conditions (100 mM K^+, 1 mM Mg^{2+}). Addition of 0.5 mM ATP caused an almost complete loss of PIP_2-F anisotropy across the entire calcium range both in the absence and presence of 50 μM actin (Fig 16*D*). Together these data indicated that ATP could release PIP_2 from gelsolin in the presence of salt, calcium ions and actin.

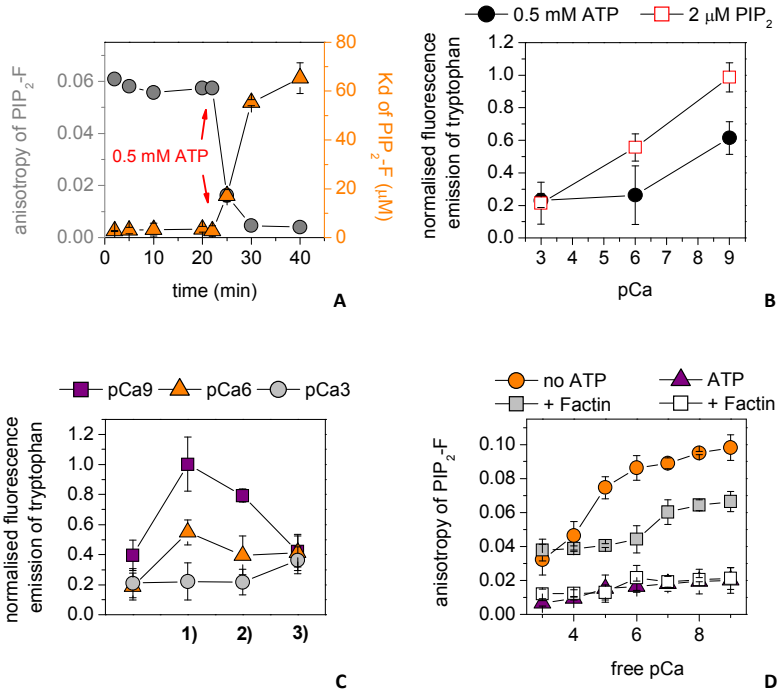

Figure 16. *PIP_2 binding to gelsolin under actin polymerizing conditions.* (**A**) The anisotropy of PIP_2-F (0.25 μM) was measured as a function of time in the presence of 5 μM gelsolin, 10 μM Ca^{2+}, 1 mM Mg^{2+} and 50 mM K^+ (gray circles). After 20 min, ATP (0.5 mM) was added. The resulting decrease in anisotropy indicates the release of PIP_2-F from gelsolin. The calculated *Kd*s (orange triangles) ranged from 2.7 ± 0.2 μM in absence of ATP followed by a substantial rise to 65.4 ± 6.2 μM after the addition of ATP. (**B**) Tryptophan fluorescence emission of gelsolin (5 μM) was measured at steady-state at three free-calcium concentrations: 1 nM (pCa 9), 1 μM (pCa 6) and 1 mM (pCa 3) in the presence of 2 μM PIP_2 (red open squares) or 0.5 mM ATP (filled black circles). (**C**) Tryptophan fluorescence emission of gelsolin (5 μM) was measured at steady-state at three free-calcium concentrations: 1 nM (pCa 9, purple squares), 1 μM

(pCa 6, orange triangles) and 1 mM (pCa 3, gray circles) through a cycle of **1)** 2 μM PIP_2 addition, **2)** 0.5 mM ATP addition and **3)** calcium levels set to 1 μM. (**D**) The steady-state anisotropy of PIP_2-F (0.25 μM) in the presence of gelsolin (5 μM) under physiological salt conditions (1 mM Mg^{2+}, 100 mM K^{+}, orange circles) followed a similar profile to that without salt across a wide range of calcium ion concentrations (see data presented on Fig 10*D*). Addition of F-actin (50 μM, gray squares) reduced the anisotropy, but still indicated significant binding. Inclusion of ATP (0.5 mM) reduced the anisotropy to close to background levels, to the value characteristic to free PIP_2-F both in the presence (white squares) and absence (purple triangles) of F-actin (50 μM) indicating the dissociation of the gelsolin/PIP_2-F complex across the entire calcium concentration range.

IV.1.2. Membrane binding of gelsolin

IV.1.2.1. Micelle formation of PIP_2 under different salt conditions

Subsequently, we studied the sensitivity of PIP_2-F (0.5 μM) binding to gelsolin (5 μM) in the absence/presence of ATP and divalent cations (magnesium and calcium). It is known that divalent cations, calcium in particular, cause PIP_2 to aggregate [250, 251]. Therefore, we evaluated the effects of cations on the critical micelle concentrations (CMCs) of PIP_2 and PIP_2-F by dynamic light scattering [247]. Under the buffer conditions tested, PIP_2-F was free from micelle formation at concentrations of 0.5 μM or below, whereas PIP_2 was more sensitive to cations and had a greater tendency to form micelles (Fig 17). Thus, we used 0.5 μM PIP_2-F to probe these interactions.

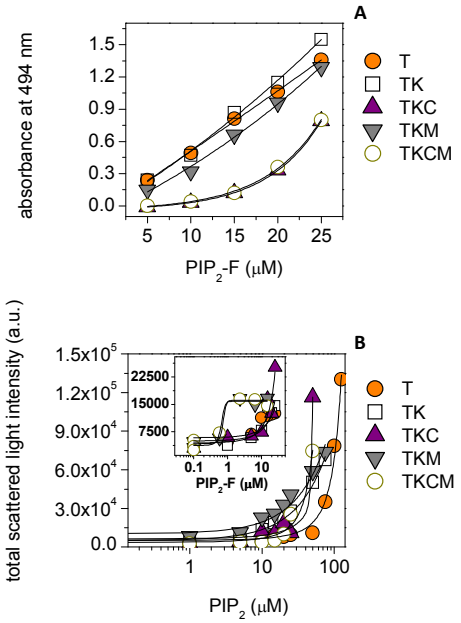

Figure 17. *Assessment of the solubility of PIP_2 and PIP_2-F in the experimental buffers.* (**A**) Determination of the actual concentrations of PIP_2-F after incubation with different cations by light absorbance at 494 nm. T, 2 mM Tris-HCl, pH 7.4; K, 100 mM KCl; C, 1 mM $CaCl_2$; M, 1 mM $MgCl_2$. (**B**) Determination of critical micelle concentrations of PIP_2 and PIP_2-F by dynamic light scattering.

The results clearly indicate that the CMCs are affected by the cations. Calcium, but not magnesium or potassium ions, precipitated PIP_2-F, causing a substantial amount of PIP_2-F being removed from solution by centrifugation (Fig 17A). After taking the concentration changes into account, the CMC of PIP_2-F was estimated to be ~10 µM in the absence of calcium, and this value was lowered to ~ 0.5 µM in the presence of 1 mM $CaCl_2$, either in the presence of 100 mM KCl or 100 mM KCl and 1 mM $MgCl_2$ (Fig 17B). These values are in agreement with those reported in the literature [247]. Unlike PIP_2-F, the actual concentrations of PIP_2 could not be determined photometrically. Therefore, the CMC of PIP_2 reported here were estimated based on the nominal rather than the actual PIP_2 concentrations. The obtained values were 20 µM in the absence of cations, 2 µM and < 1 µM in the presence of 100 mM KCl or 100 mM KCl and 1 mM

$MgCl_2$, respectively, which again are in concordance with the literature data [250]. Introduction of calcium into the buffer raised the CMC of PIP_2 to ~ 10 µM, which is considered as an overestimation due to likely precipitation of PIP_2 by calcium in a similar way to that observed for PIP_2-F (Fig 17A). Taken together we concluded that under the buffer conditions tested PIP_2-F was free from micelle formation at concentrations of 0.5 µM or below, whereas PIP_2 was more sensitive to cations and had a greater tendency to form micelles than PIP_2-F.

IV.1.2.2. Gelsolin can bind to the membrane within PIP_2 and can be released by ATP

We used the technique of confocal microscopy to determine whether ATP can be observed to release gelsolin from phospholipid vesicles. PIP_2-containing rhodamine590-filled phospholipid vesicles were observed to bind to Alexa488-labelled gelsolin in the absence of ATP, calcium and magnesium (Fig 18, upper panel). This gelsolin was subsequently released by the addition of 0.5 mM ATP (Fig 18, middle panel). A second round of labeled gelsolin could be bound to the vesicles after the solution had been exchanged to remove the ATP (Fig 18, lower panel). During the release of gelsolin by ATP, some vesicles were observed to display shape changes (Fig 19, Fig 20). This suggests that gelsolin binds to PIP_2 in the vesicles and may induce deformation or local structural changes in the vesicles, and that ATP can effectively dissociate gelsolin from the vesicles.

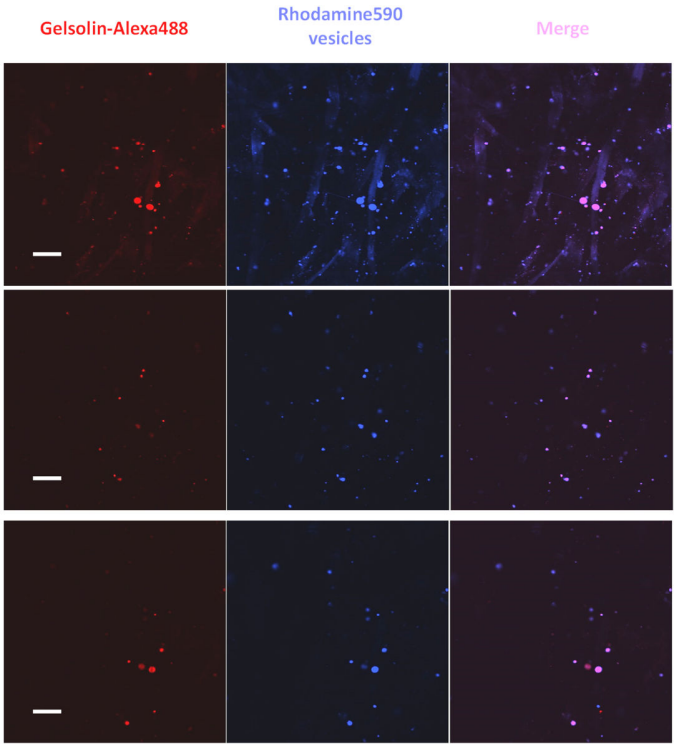

Figure 18. *Cycle of gelsolin binding to the surface of PIP_2-containing membrane vesicles.* Gelsolin-Alexa488 (GSN, 5 µM, red) was incubated with rhodamine590-filled, PIP_2-containing membrane vesicles (blue) and visualized by confocal microscopy. The merged image indicates that gelsolin and vesicles colocalized (top panel). After ATP (0.5 mM) was added, the majority of gelsolin-Alexa488 was released from the vesicles (middle panel). Following removal of ATP via buffer exchange and addition of fresh gelsolin-Alexa488 (15 µM), gelsolin re-associated with the vesicles (bottom panel). Scale bar = 10 µm.

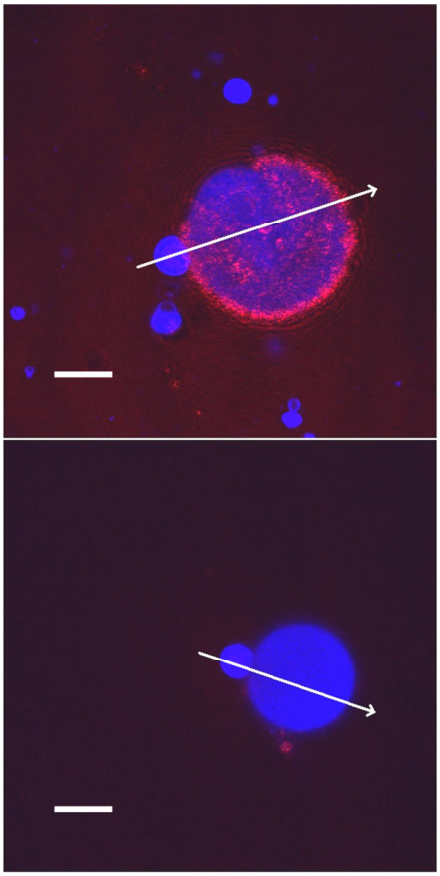

Figure 19. *ATP dependence of gelsolin binding to the surface of PIP_2-containing membrane vesicles.* Representative image of gelsolin-Alexa488 (15 µM, red) localized to the surface of a large rhodamine590-filled PIP_2-containing vesicle (blue) (top panel). After the addition of ATP (0.5 mM) the vesicle changed morphology concurrently with the release of gelsolin (red) from the vesicle surface (blue) (bottom panel). Scale bar = 10 µm. Fig 20*A* and 20*B* show line scans across the images as indicated by the arrows. The confocal slice thickness was ~ 3 µm. There are two vesicles in focus, a small (d = 7 µm) and a large (d = 22.5 µm) one, the outer layer of the bigger vesicle is attached to the coverslip.

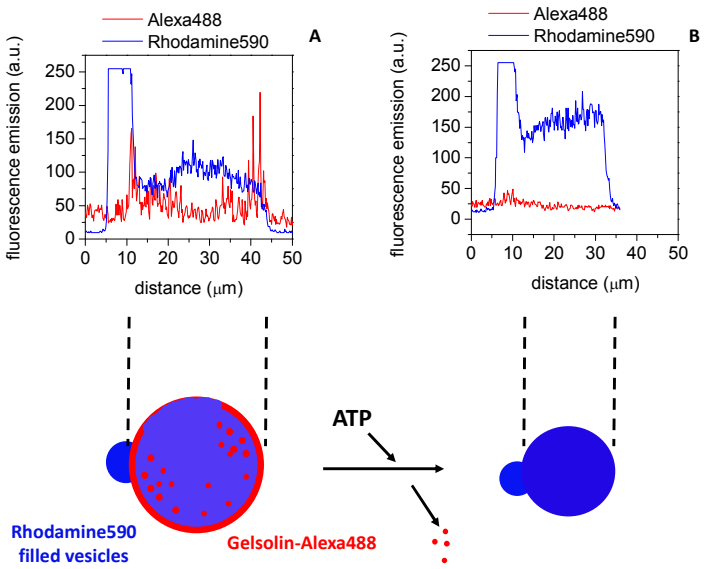

Figure 20. *Line scans of fluorescence intensity versus distance along the arrows shown in Fig. 19.* (**A**) Profiles of gelsolin-Alexa488 (red) and PIP_2-containing membrane vesicles filled with rhodamine590 (blue) in the absence of ATP. (**B**) Gelsolin-Alexa488 (red) was released and the size of vesicle (filled by rhodamine590, blue) was changed by 0.5 mM ATP treatment in Fig 19.

IV.1.3. Intrinsic structural dynamics of leiomodin2

The crystal structure of the C-terminal regions of human Lmod2 in complex with actin was recently reported [74], which shows that Lmod2 possesses well-structured regions, as well as probably highly flexible elements, which are missing from the structure. In agreement with this, our bioinformatics analysis predicts structural elements in Lmod2, which are characterised by relatively large disorder probabilities, characteristic for intrinsically disordered protein regions (IDRs) (disorder probability > 0.5, Fig 21*A*) [252-254]. *Rattus norvegicus* leiomodin2 contains three tryptophans (W73, W386 and W404), which are located in segments with high predicted disorder (Fig 21*A*). Multiple sequence alignment predicts that the W73 of cardiac Lmod2 is located at same position as L71 in human tropomodulin1. W386 and W404 are conserved between *Rattus norvegicus* Lmod2 and human Lmod1 (corresponding residues are W347 and W365 in the human protein, respectively). L71 resides on a flexible chain of actin binding site ABS1 in Tmod1 (PDB ID: 4PKG [222]). The structural similarities implicate that the

W73 residue in Lmod2 would be localised on a flexible chain of the actin binding domain ABS1 (Fig 21*B*) [82]. The C-terminal tryptophan of human Lmod1 is found in a highly flexible region (residues 339-388) that is missing from the crystal structure (PDB ID: 4RWT [74], Fig 21*C*), suggesting similar structural environments for W386 and W404 in Lmod2.

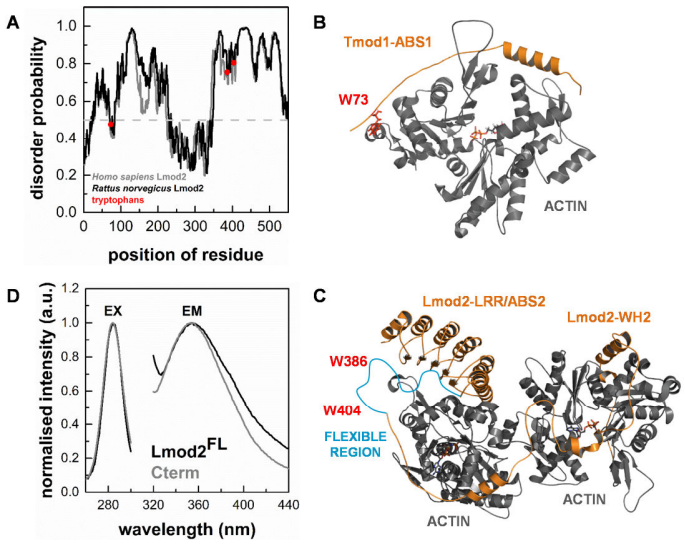

Figure 21. *Intrinsic structural properties of Lmod2.* **(A)** Bioinformatics analysis of Lmod protein sequences predicts intrinsically unstructured protein regions. The disorder probability in *Homo sapiens* Lmod2 and *Rattus norvegicus* Lmod2 (Uniprot accession numbers are Q6P5Q4 and A1A5Q0, respectively). The analysis was performed by IUPred [255, 256]. The tryptophan residues of *Rattus norvegicus* Lmod2 are highlighted by red. (**B**) Structural features of the interactions of Tmod1 with actin. The complex between Tmod1 ABS1 and actin is shown (PDB ID: 4PKG). The position of W73 of *Rattus norvegicus* cardiac leiomodin2 is predicted by multiple sequence alignment and highlighted by red. (**C**) Structural features of the interactions of Lmod2 with actin. The complexes between Lmod2 ABS2/LRR or WH2 actin-binding sites and actin monomers are shown (PDB ID: 4PKG). The position of W386 and W347 (red) of *Rattus norvegicus* cardiac leiomodin2 are predicted to localize in a flexible protein region (blue) by multiple sequence alignment (PDB ID: 4RWT). This flexible region between residues 339-388 is missing from the structure of 4RWT. (**D**) Tryptophan fluorescence spectra of Lmod2. Excitation (EX) and emission (EM) spectra of the intrinsic tryptophans of $Lmod2^{FL}$ (1 µM, black line) and Cterm (4 µM, grey line) were obtained at emission wavelength of 354 nm and excitation wavelength of 282 nm.

We used these intrinsic fluorophores to characterise the structural dynamics of full length cardiac leiomodin2 ($Lmod2^{FL}$) and its truncated C-terminal segment (Cterm) in

fluorescence spectroscopic experiments. First, to describe the spectral properties of tryptophan residues we recorded their emission and excitation spectra (Fig 21*D*). The spectra obtained for Lmod2^{FL} and Cterm showed identical excitation maxima at ~ 282 nm, and the wavelength corresponding to the emission maxima were also close for the two proteins (~ 354 nm). This indicates that the microenvironments of the tryptophan residues were similar in the full length leiomodin2 and its C-terminal fragment. We carried out the subsequent spectroscopic measurements using the above identified maximum excitation and emission wavelengths.

To describe the flexibility of the protein matrix we also measured the steady-state anisotropy (r) of the fluorescence emission. The values were 0.083 ± 0.015 and 0.038 ± 0.005 for Lmod2^{FL} and Cterm, respectively. Taking into account the size of the proteins (Lmod2^{FL}: 62 kDa and Cterm: 19.5 kDa) and the theoretical maximum of the steady-state anisotropy for a perfectly immobilised system (0.4), these are relatively low anisotropy values, indicating that the tryptophans are located in unstructured and flexible protein regions in both Lmod2^{FL} and Cterm. To further explore the structural properties of leiomodin we also carried out time-dependent anisotropy decay experiments. The anisotropy decay was fitted with double exponential functions and the fits provided two rotational correlation times for each protein (data not shown). The shorter correlation times were sub-nanosecond values. Although, due to the resolution limits of the experiments the proper interpretation of the actual values is difficult, we attributed these short correlation times to the wobbling motion of the tryptophan in their flexible protein environment [239, 257-259]. The longer rotational correlation time was 35.9 ± 6.5 ns and 6.9 ± 1.6 ns for Lmod2^{FL} and Cterm, respectively. These values characterise the rotational diffusion of the entire protein in both cases. Lmod2 (62 kDa) is a larger protein than Cterm (19.5 kDa), which explains the longer correlation times obtained for Lmod2^{FL}. In these experiments we observed that the probes located in a flexible protein regions, where little limitation was posed on their wobbling rotational motion.

In conclusion, our experimental data suggests that the tryptophan residues of Lmod2 are located in disordered and flexible regions, consistently with the structural and bioinformatics prediction (Fig 21*A*).

IV.1.4. The effects of cardiac leiomodin2 on thin filaments

IV.1.4.1. The effects of purified cardiac leiomodin2 on actin assembly dynamics

To test whether our proteins are functional, pyrene actin polymerisation assays were carried out in the absence or presence of Lmod2^{FL} or Cterm (25-1500 nM) (Fig 22*A*). In these experiments the increase of the pyrene fluorescence reported on the increase of the actin filament concentration. The rate of actin polymerisation increased in the presence of Lmod2^{FL} (Fig 22*A, B*), in agreement with previous reports [72, 74, 79]. This increase was Lmod2^{FL} concentration dependent and followed a saturation curve, its maximal value being ~ 12 times larger in the presence than in the absence of Lmod2^{FL}. This substantial increase of the polymerisation rate indicated that Lmod2^{FL} can effectively accelerate actin assembly. Cterm did not influence significantly actin polymerisation in the concentration range tested (Fig 22*A, B*).

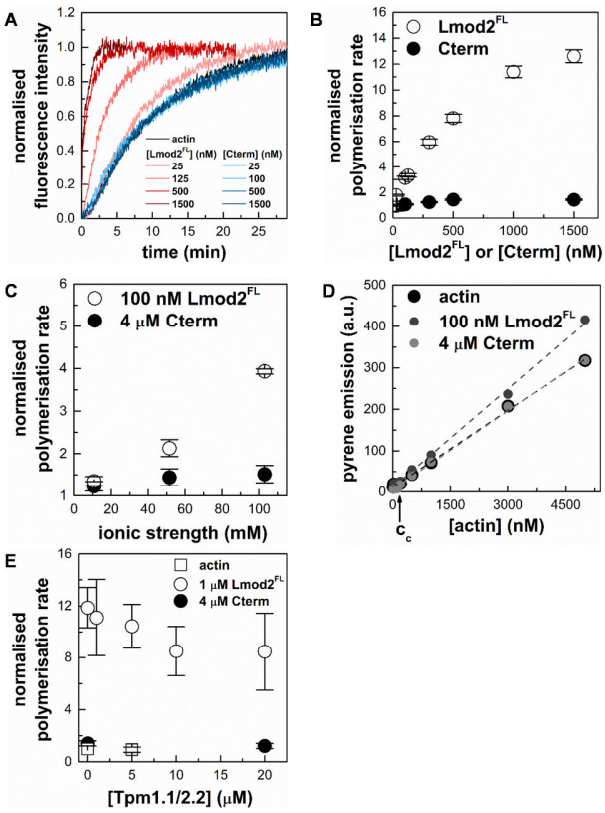

Figure 22. *The effects of purified cardiac leiomodin2 on actin assembly dynamics.* (**A**) Effects of cardiac Lmod2 and Cterm on the polymerisation kinetics of actin. The kinetics of actin assembly (4 μM, containing 5 % pyrene labelled actin) in the absence and presence of different concentrations of $Lmod2^{FL}$ or Cterm. Pyrene fluorescence was measured at excitation and emission wavelengths of 350 nm and 404 nm, respectively. Salt conditions: 100 mM KCl, 2 mM $MgCl_2$. (**B**) Cardiac Lmod2 influences actin polymerisation in a concentration dependent manner. Polymerisation rates were determined from the slope of the pyrene curves (shown on panel (A)) at 50 % polymerisation and normalised by the rate measured for spontaneous actin assembly. The actin polymerisation rates are plotted as a function of $Lmod2^{FL}$ (empty circles) and Cterm (filled circles) concentrations. (**C**) Ionic strength dependence of the effects of cardiac Lmod2 and Cterm on actin polymerisation. Pyrene-actin (4 μM, 5 % labelled) was polymerised in the absence or presence of 100 nM $Lmod2^{FL}$ (empty circles) or 4 μM Cterm (filled circles) under low (10 mM KCl, 0.5 mM $MgCl_2$), medium (50 mM KCl, 1 mM $MgCl_2$) and high (100 mM KCl, 2 mM $MgCl_2$) salt conditions. Normalised polymerisation rates were derived as described above and plotted as a function of ionic strength (Eq. 9.). (**D**) The effect of cardiac Lmod2 on the critical concentration of actin assembly. Pyrene intensities as a function of actin concentration were measured in the absence (black circles) or presence of 100 nM $Lmod2^{FL}$ (grey circles) or 4 μM Cterm (light grey circles) under high salt conditions (100 mM KCl, 2 mM $MgCl_2$). Actin (5 % pyrene labelled) concentrations were 30; 50; 100; 300; 500; 700 nM and 1; 3; 5 μM. The critical concentrations were determined by using Eq. 10. and were found to be 120 ± 83 nM in the absence of $Lmod2^{FL}$ and 117 ± 68 nM and 132 ± 58 nM in the presence of $Lmod2^{FL}$ and Cterm, respectively. Dashed lines in the corresponding colour show the fit to the data. (**E**) Skeletal tropomyosin (Tpm1.1/2.2) reduces the polymerisation activity of Lmod2. Pyrene-actin (4 μM, 5 % labelled) was polymerised in the absence (empty squares) or presence (empty circles) of 1 μM $Lmod2^{FL}$ or 4 μM Cterm (filled circles) under high salt conditions (100 mM KCl, 2 mM $MgCl_2$) in the presence of different concentrations of skeletal muscle tropomyosin. Data are presented as mean ± SD (n = 3).

Protein-protein interactions often depend on the ionic strength. To describe whether the effect of leiomodin on actin polymerisation is salt dependent we measured the rates of actin polymerisation under low salt (0.5 mM $MgCl_2$, 10 mM KCl), medium salt (1 mM $MgCl_2$, 50 mM KCl) or high salt (2 mM $MgCl_2$, 100 mM KCl) conditions in the absence and presence of $Lmod2^{FL}$ (100 nM) or Cterm (4 μM). We found ionic strength dependence in all cases (Fig 22*C*), although the salt dependence was much more pronounced for $Lmod2^{FL}$ than for Cterm. In the presence of $Lmod2^{FL}$ the increase in the rate of actin polymerisation was 1.2 fold at low salt and 4 fold at high salt conditions.

To further investigate the effects of Lmod2 on actin dynamics, we measured the critical concentration of actin in the absence and presence of $Lmod2^{FL}$ and Cterm (Fig 22*D*).

Pyrene labelled actin was incubated under polymerising conditions at various concentrations and then the pyrene fluorescence intensity was measured. The plot of these intensities as the function of the actin concentration showed a breaking point, corresponding to the critical concentration (Fig 22*D*). In the absence of Lmod2^{FL} the critical concentration was 120 ± 83 nM at high salt conditions, in good agreement with the well-established value [238, 260]. In the presence of 100 nM Lmod2^{FL} or 4 μM Cterm the critical concentration was not significantly affected (117 ± 68 nM and 132 ± 58 nM, respectively). The close agreement between these critical concentration values indicated that the amount of actin that was polymerised in the absence and presence of Lmod2 proteins was similar. The lack of the shift in the breaking point is in agreement with the observations that Lmod2 does not affect barbed end dynamics, consistently with its pointed end localisation [72, 74, 79].

The above observations indicate that the Cterm, possessing a single actin-binding WH2 domain is not sufficient for enhancing actin polymerisation. The efficient actin assembly promoting activity of Lmod2 requires the N-terminal actin-binding domains. Our data are in agreement with previous reports and show that *Rattus norvegicus* cardiac Lmod2 behaves similarly to the human protein in terms of actin dynamics regulation [77, 79].

IV.1.4.2. Tropomyosin influences the leiomodin2-mediated actin polymerization

In muscle cells actin dynamics is regulated by a large repertoire of ABPs [261, 262]. An essential member of this family in muscle cells is tropomyosin that decorates the side of actin filaments [263, 264]. To extend our investigations, we tested whether the presence of skeletal muscle tropomyosin (Tpm1.1/2.2) can change the effect of leiomodin on actin polymerisation. The polymerisation kinetics of pyrene labelled actin was monitored in the presence of Lmod2^{FL} (1 μM) or Cterm (4 μM) and in the presence of various concentrations (0-20 μM) of tropomyosin (Fig 22*E*). Tropomyosin did not affect actin polymerisation in the absence of Lmod2^{FL}. In the presence of Lmod2^{FL} tropomyosin induced a concentration dependent decrease in the rate of actin assembly. At the highest concentration of tropomyosin (20 μM) the rate of Lmod2^{FL} mediated actin polymerisation was decreased to ~ 70 % of its value measured in the absence of tropomyosin. Statistical analysis revealed that this change was not significant ($p = 0.2017$). We found

that tropomyosin did not influence significantly actin assembly in the presence of Cterm (Fig 22*E*).

In conclusion, skeletal muscle tropomyosin influences Lmod2 mediated actin polymerisation. Our observations suggest, that the inhibitory effect of tropomyosin on leiomodin mediated actin polymerisation could appear due to enhanced capping activity of the N-terminal of Lmod2, consistently with recent findings [72].

IV.1.4.3. Lmod2 affects the structure of filamentous actin

In the above experiments the pyrene intensity after saturation was increased in a Lmod2^{FL} concentration dependent manner, addition of 5 µM Lmod2^{FL} resulted in a ~ 4 fold increase (Fig 23*A*). The PDB structures of 4PKG and 4RWT clearly show that ABS1 and helical domains from Cterm both bind nearby of Cys374 on actin, which can affect the freedom and fluorescence emission of fluorophores on cysteine. Considering that the actin polymerisation assays were carried out with 4 µM actin and assuming that the value of the critical concentration is 100 - 150 nM, (Fig 22*D* and [224, 238, 260]), we estimate that approximately 95 % of actin polymerises in the absence of leiomodin. Therefore, the large (~ 4 fold) increase in the maximum fluorescence intensity observed with Lmod2^{FL} cannot be explained by assuming that more actin was in polymer form in the presence of Lmod2^{FL} than in its absence. Considering the above observations, we interpret our data by proposing that Lmod2^{FL} interacts with actin filaments and its binding substantially increases the fluorescence quantum yield and thus the intensity of pyrene.

To further confirm the fluorescence increase of leiomodin binding we carried out rapid kinetic stopped-flow experiments using prepolymerised actin filaments. The adventage of these experiment is that the optical properties of the solution are the same during the recording of signals before and after the binding of leiomodin, therefore eliminating the possible artefacts arising from the mixing of buffers. We wanted to characterise a second order binding process therefore the leiomodin concentration was designed to cover a broad concentration range, where the faster binding rates could also be determined. These rapid kinetic assays showed that Lmod2^{FL} increased the fluorescence emission of 1 µM pyrene labelled actin filaments in a concentration dependent manner (Fig 23*C*). In

subsequent experiments we found that Lmod2^{FL} could also amplify the emission of IAEDANS labelled actin filaments as well (data are not shown). These observations suggest that Lmod2 affects the structure of actin filaments, and could serve as a basis for further spectroscopic and kinetic experiments.

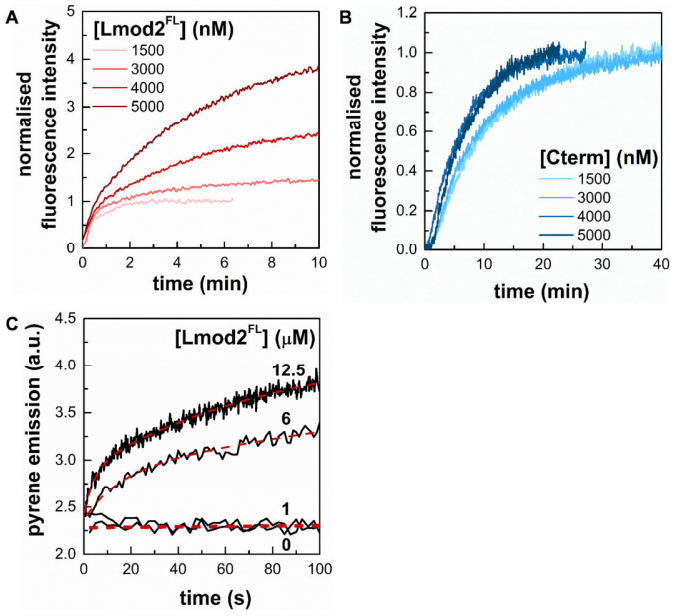

Figure 23. *Lmod2 influences pyrene emission in actin filaments.* (**A**) Polymerisation kinetics of actin assembly (4 µM; 5 % labelled) in the presence of Lmod2^{FL} show increased saturation of pyrene fluorescence emission in a concentration dependent manner. (**B**) Cterm does not affect the steady-state value of pyrene actin fluorescence. The actin concentration was 4 µM, containing 5 % labelled actin. (**C**) Rapid kinetics measurements of the time dependent change in pyrene F-actin fluorescence. Stopped-flow measurements of the kinetics of pyrene fluorescence emission of prepolymerised F-actin (1 µM, 5 % pyrene labelled) in the absence or presence of different concentrations of Lmod2^{FL} (1 µM, 6 µM and 12.5 µM, as indicated). Salt conditions: 100 mM KCl, 2 mM $MgCl_2$. Dashed lines show the fit using Eq. 11.

IV.1.4.4. Lmod2 binds to the side of actin filaments

The fluorescence quantum yield of actin bound probes increased in the presence of leiomodin. One explanation for this observation is to consider that leiomodin2 through its pointed-end binding ability [72, 77, 79] induces structural changes in F-actin, which affects the fluorescence emission of actin-bound probes. Similar long range effects were

reported for other ABPs; e.g. for gelsolin and formins [141, 238, 239, 265]. As an alternative explanation one can consider that Lmod2, besides end binding, can bind to the sides of actin filaments, i.e. it can decorate the filaments along their length [78]. This way Lmod2 could directly alter the quenching processes that determine the fluorescence intensity of the probes.

To test how Lmod2^{FL} binds to the sides of actin filaments we carried out high-speed co-sedimentation experiments (Fig 24). We tested only Lmod2^{FL} for this ability, since Cterm failed to increase the pyrene signal in spectroscopic experiments (Fig 23). In these experiments actin (4 μM) and Lmod2^{FL} (0-5 μM) were co-incubated and centrifuged. The pellets and supernatants were analysed by SDS-PAGE. We observed that increasing the total concentration of leiomodin resulted in increased leiomodin concentration in the pellets (Fig 24*A*). In control experiments, Lmod2^{FL} did not appear in the pellet in the absence of actin (Fig 24*B*). Since the concentration of pointed ends of micromolar actin filaments is a few nanomolar, the amount of leiomodin detected in the pellets was much greater than that expected from only filament end binding. Therefore, our observation can only be explained by assuming that Lmod2^{FL} bound to the side of actin filaments and pelleted with them as a complex. The binding of Lmod2 to F-actin was salt sensitive, its binding affinity was decreased by increasing ionic strength (from medium salt to high salt conditions) (Fig 24*C*). In conclusion, in addition to its pointed end binding ability, leiomodin binds to the sides of actin filaments *in vitro*.

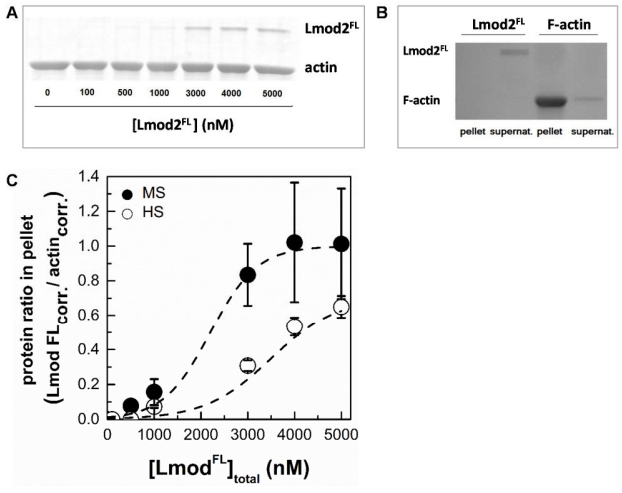

Figure 24. *Cardiac leiomodin2 binds to the sides of actin filaments.* (**A**) In high-speed cosedimentation assays F-actin (4 µM) and Lmod2^{FL} (0-5 µM) was incubated under high salt conditions (100 mM KCl, 2 mM $MgCl_2$) and centrifuged at 258,000 x g for 30 min at room temperature. The pellets were analysed by SDS-PAGE. Representative Coomassie stained SDS-PAGE gel of the pellets is shown. (**B**) Lmod2^{FL} (5 µM) does not sediment in the absence of actin. Leiomodin was centrifuged in the absence of F-actin (left two columns) or F-actin (5 µM) was pelleted in the presence of Lmod2^{FL} (right two columns). Pellets and supernatants are indicated on the figure. (**C**) Actin-Lmod2^{FL} ratios in pellet were calculated from SDS-PAGE analysis of under high salt (HS, 100 mM KCl, 2 mM $MgCl_2$) and medium salt (MS, 50 mM KCl, 1 mM $MgCl_2$) conditions, and plotted as the function of Lmod2^{FL} concentration. Dashed lines show the fit using Eq. 12. Data are presented as mean ± SD (n = 3).

IV.1.4.5. Structural consequences of F-actin binding by Lmod2

The above observations suggest that by binding to actin filaments Lmod2 can affect the structural properties of F-actin. To address this issue, inter-monomer FRET measurements were carried out with double labelled actin filaments [238]. Actin monomers were labelled separately with IAEDANS as a donor or with IAF as an acceptor. The two pools of labelled actin monomers were mixed and then co-polymerised. Using this strategy, the energy transfer between neighbouring actin protomers in the filament, i.e. the inter-monomer FRET can be investigated. As expected, we observed a decrease in the donor emission in the presence of the acceptor (Fig 25*A*). The inter-monomer FRET efficiency within filaments (4 µM) in the absence of Lmod2 was found to be 26 %. Addition of Lmod2^{FL} (5 µM) resulted in an increase of the inter-monomer FRET efficiency to 32 %. We interpret this increase as a consequence of binding of leiomodin to the filaments. The first possible explanation is that Lmod2^{FL} binding changes the radial coordinate of the fluorescently labelled residue, whereas the second interpretation is that it changes the flexibility of actin filaments [238, 244, 245]. In the first explanation would assume that the fluorophores moved closer to the longitudinal axis of the filament, leading to a more compact and probably stiffer structure and thus to an increase in the FRET efficiency. In the second case, the binding of leiomodin would make the structure of the filament more dynamic, thereby increasing the frequency and/or the amplitude of the relative oscillations of the fluorophores, resulting in larger FRET efficiencies [238, 245,

259]. To test which of the two explanations are valid we carried out temperature-dependent FRET experiments, where the determined FRET efficiencies are normalized by the fluorescence intensity of the donor measured in the presence of acceptor. The resulted temperature dependence of the normalized energy transfer provides information on the flexibility of the protein matrix between the donor and the acceptor [245]. The theory has been shown to be valid even if multiple fluorophore systems are applied, e.g. when one donor is in FRET interaction with more than one acceptor [266], as it is the case here. Our normalized FRET data showed steeper temperature dependence in the presence than in the absence of leiomodin (Fig 25*B*), indicating that the structure of the filaments become more flexible upon the binding of Lmod2^{FL}. Considering that the Lmod2^{FL} induced effects on the fluorescence emission of the probes, as well as on the inter-monomer FRET efficiency were observed at relatively large protein concentrations (~ 5 μM), we propose that these effects originate mainly from side-binding and that the binding of Lmod2^{FL} affects the structural dynamics of actin filaments.

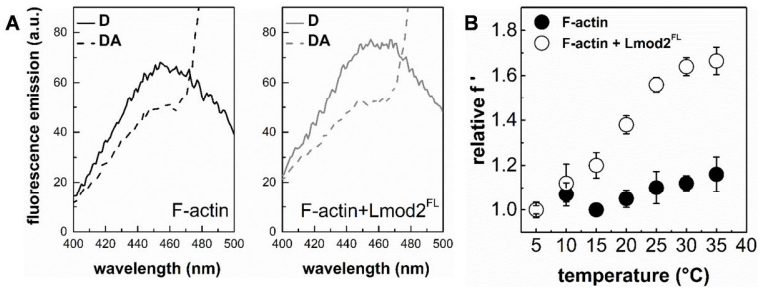

Figure 25. *The effect of leiomodin2 on the flexibility of actin filaments.* (**A**) Emission spectra of IAEDANS (D, donor) in the absence and presence of IAF (A, acceptor), and in the absence and presence of Lmod2^{FL}. The actin filament concentration was 4 μM. Note the acceptor induced decrease in the donor emission due to FRET. (**B**) Temperature-dependent FRET measurements were performed on IAEDENS-IAF actin filaments (4 μM) in the absence and presence of different concentrations of Lmod2^{FL}. FRET efficiencies calculated from the emission spectra (representative spectra are shown on panel (A) with Eq. 7.) were normalised by FRET efficiency measured at the lowest temperature (relative f ', Eq. 8.) and plotted as a function of temperature. Data obtained in the absence (filled circles) or presence (empty circles) of Lmod2^{FL} (5 μM) are shown. Data are presented as mean ± SD (n = 3).

IV.1.4.6. Functional consequences of F-actin binding by Lmod2

Myosin is a prominent actin-binding protein playing central role in muscle function. To further elaborate on the functional consequences of the side-binding ability of Lmod2, we investigated whether the ATPase activity of skeletal muscle myosin II is altered by leiomodin. A truncated form of skeletal muscle myosin, the double-headed heavy meromyosin (HMM) was used in these studies. The Mg^{2+}-ATPase activity of HMM was measured by using a coupled assay in the absence or presence of actin filaments (1 μM) and / or leiomodin (1 μM). In control experiments, in the absence of HMM, ATPase activity was not detected for either F-actin or $Lmod2^{FL}$ (Fig 26*A*). The basal and the F-actin (1 μM) activated Mg^{2+}-ATPase activities of HMM (0.5 μM) were 0.04 $\mu M_{ATP}\ s^{-1}\ \mu M_{protein}^{-1}$ and 0.164 $\mu M_{ATP}\ s^{-1}\ \mu M_{protein}^{-1}$, respectively, consistent with previous data [267]. We observed that the actin-activated Mg^{2+}-ATPase activity of HMM decreased in the presence of $Lmod2^{FL}$ in a concentration-depended manner (Fig 26) reaching ~ 40 % of its original value at 3 μM $Lmod2^{FL}$ concentration (Fig 26*B*).

The above observations show that by binding to actin filaments $Lmod2^{FL}$ can regulate the ATPase activity of myosin. This can be explained either by direct or indirect structural effects. Lmod2 may directly block the ATP binding cleft on HMM or the Lmod2 binding site may overlap with that of myosin II. Alternatively, a mechanism based on allosteric structural changes in actin filaments can be considered; the binding of Lmod2 to filaments may induce long-range structural changes, which may affect myosin II and F-actin interaction. Several ABPs, including formins, gelsolins and ADF-cofilins and myosin were reported to impose allosteric effects to actin filaments upon binding [141, 238, 239, 265, 268-270]. Allosteric regulation upon cooperative structural changes in actin filaments were shown to contribute to the mutually exclusive binding of myosin and ADF/cofilin proteins [271].

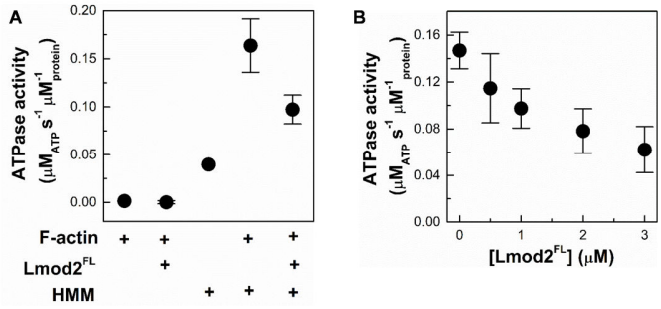

Figure 26. *Functional consequences of F-actin binding by Lmod2.* (**A**) The effect of Lmod2^{FL} on the Mg^{2+}-ATPase activity of HMM measured with coupled assay. The Mg^{2+}-ATPase activity of HMM (0.5 μM) in the absence and presence of actin and/or Lmod2^{FL} was measured under low salt conditions (10 mM KCl, 0.5 mM $MgCl_2$). (**B**) The Mg^{2+}-ATPase activity of HMM (0.5 μM) in the presence of F-actin (1 μM) as the function of Lmod2^{FL} concentration. Data are presented as mean ± SD (n = 3).

IV.2. Discussion

IV.2.1. Activation cycle of gelsolin

ATP and PIP_2 have been shown to compete in binding to K_{ATP} channels [207]. Here, we have demonstrated that ATP can displace PIP_2 from gelsolin in solution under physiological buffer conditions *in vitro*. Furthermore, ATP is able to release PIP_2-bound gelsolin from the surface of phospholipid vesicles. These observations suggest that ATP is likely to dissociate gelsolin from PIP_2 at plasma membranes, and this ATP-driven dissociation is the missing step in recycling of gelsolin during its actin filament remodeling cycle. In a background of high cellular ATP, PIP_2 will not generally bind to gelsolin. However, in the situation where gelsolin-capped filaments point at the plasma membrane, the filament barbed-end bound gelsolin becomes greatly reduced in its mobility, and it is in close proximity to membrane-bound PIP_2 that can move within the membrane and increase its local concentration by forming clusters [272]. All these factors favor the binding between gelsolin and PIP_2, and hence filament uncapping. We propose that effective competition by ATP will dominate following filament uncapping and the dissociation of PIP_2-bound gelsolin is increased.

The cartoon presented in Figure 26 details the postulated stages of this remodeling cycle under standard cellular conditions. Activation: elevation of calcium levels above 10 nM leads to a conformational change in gelsolin that releases ATP and allows gelsolin to recognize an actin filament. Severing: competition for actin-actin interactions by gelsolin-actin interactions leads to the severing of the filament. Capping: gelsolin remains bound to the barbed-end of the severed filament, preventing its elongation. Uncapping: when a gelsolin-capped filament encounters PIP_2 in the plasma membrane, the cap is removed through an unknown mechanism [190]. The uncapped filament is then free to elongate and exert force on the plasma membrane. Release: gelsolin is released from PIP_2 at the plasma membrane through ATP competition, leading to diffusion of the gelsolin: ATP complex away from the plasma membrane. Gelsolin will return to its inactive state in low calcium environments. Thus, gelsolin is likely removed from PIP_2 at the plasma membrane in an ATP-dependent manner that distinguishes it from other PIP_2-

sensing actin-regulating proteins, allowing gelsolin to cycle in a background of elevated PIP_2.

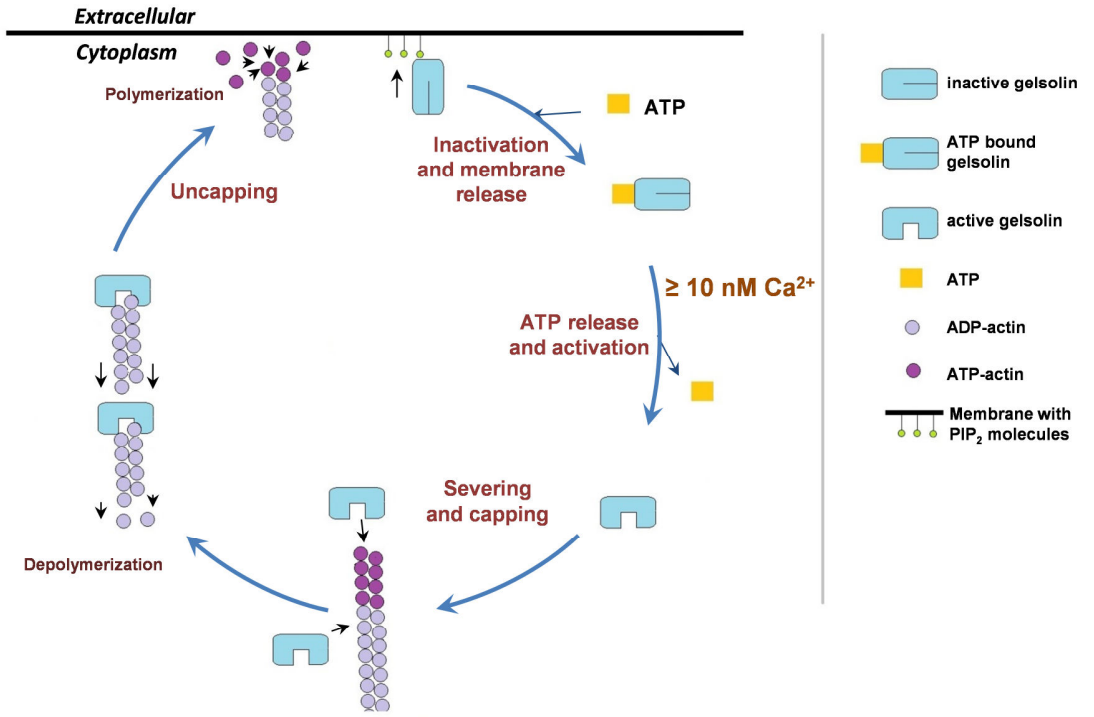

Figure 27. *Model of the severing, capping, uncapping and inactivation/release cycle of gelsolin.* The cartoon presents a model for the cycle of activation and function of gelsolin. Severing and capping: Free calcium levels above 10 nM Ca^{2+} activate gelsolin, releasing ATP, leading to severing and capping of actin filaments. Depolymerization: Gelsolin-capped filaments will depolymerize from their pointed ends. Uncapping and polymerization: Gelsolin-capped actin filaments will be uncapped on encountering PIP_2 in the membrane, resulting in force being exerted on the membrane from the polymerization of the uncapped filaments. Inactivation and membrane release: Gelsolin will be released from PIP_2 and the membrane by competition with ATP. Following its release gelsolin is able to undergo subsequent cycles of severing, capping, uncapping and inactivation/release.

IV.2.2. Structural dynamics and function of cardiac leiomodin2

We have shown that *Rattus norvegicus* cardiac leiomodin2 possesses similar structural and functional features as human leiomodin2. *Rattus norvegicus* Lmod2 contains highly flexible, intrinsically disordered regions, similar to its Tmod homologues and other Lmods [74, 222]. In terms of actin dynamics, we demonstrated that *Rattus norvegicus*

Lmod2 influences the rate of actin polymerization in an ionic strength dependent manner (Fig 22). This indicates that leiomodin2 may play a role in the regulation of actin filament generation in locations where tropomyosin and matured actin filaments are present, and new actin filaments are not needed.

Apart from its already known colocalization with filament ends, Lmod2 was detected along the length of thin filaments in rat cardiomyocytes, as well as in M-lines [77, 78]. Consistently with these observations, we demonstrated that $Lmod2^{FL}$ can bind to the sides of actin filaments *in vitro* (Fig 24). The binding of leiomodin to actin filaments made the structure of the filaments more flexible (Fig 25). As a functional consequence, $Lmod2^{FL}$ decreased the actin enhanced Mg^{2+}-ATPase activity of myosin upon F-actin binding (Fig 26). These novel interactions of leiomodin have functional implications. The localization of leiomodin in living muscle cells is not limited to the ends of the thin filaments, the presence of Lmod along the actin filaments, as well as in regions where myosin II is localized indicates that Lmod may influence acto-myosin activity in the cellular context. Leiomodin by reducing the activity of myosin, as we detect in our experiments even in the presence of lower amount ($\leq$ 1 μM) of Lmod2, may decrease the generated force during the interaction of thin and thick filaments. Interestingly, the inhibition of myosin II activity with blebbistatin resulted in the delocalization of leiomodin in cultured cardiomyocytes, which was interpreted as a lack of need for *de novo* actin polymerization considering the *in vitro* nucleation activity of Lmod2 [78]. Blebbistatin preferentially binds to the weak-binding ADP.P_i intermediate of myosin II and slows down phosphate release, thereby it blocks myosin heads in their low-affinity complexes [273]. This way blebbistatin alters the equilibrium between the actin bound and unbound myosin populations. Considering this, we propose an alternative explanation for the blebbistatin-induced Lmod2 dissociation from actin filaments. Active and contractile sarcomeres require the actin filament localization of Lmod2 to properly tune the force-generation by the acto-myosin system. The inactivity of myosin II upon blebbistatin treatment results in uncontractile machinery, which does not require the optimization of acto-myosin interaction. This may result in the dissociation of Lmod2 from actin filaments. Our findings on the Lmod2 dependent activity of myosin II can supplement the

recently published new model of cyclic activities of Lmod in sarcomeric functions and provides an *in vivo* support for the interpretation of our results [71].

Considering that previous data indicated important roles of leiomodin in the developing heart [212], the regulation of the acto-myosin cross-bridge activity by leiomodin maybe essential in developing heart muscle cells, where larger than optimal forces may perturb the proper formation of the sarcomeric structure.

IV.2.3. Plasticity of actin filaments provided by different length regulator proteins

The functions of actin polymers varies within a wide range of activities, and this variation is based on the plastic dynamics of filaments controlled by the effects of ABP proteins. Capping the barbed-end or pointed-end of a filament modifies the kinetics and dynamics of filamental turnover, allowing actin oligomers to be mobilized to remodel the whole cytoskeleton by gelsolin or for long polymers to be built in the stiff structural system of sarcomeres by leiomodin. Gelsolin and leiomodin are both recycling and implicated in crucial steps of cell migration or maturation of embryonic muscle. They bind the opposite ends of filament and show opposite effects on filament length, but both bind to the sides of filaments for two different purposes. Their physiological functions are composed by several different types of complexes for a well-tuned process of actin filament length regulation.

V. References

1. Doherty, G.J. and H.T. McMahon, *Mediation, modulation, and consequences of membrane-cytoskeleton interactions.* Annu Rev Biophys, 2008. **37**: p. 65-95.
2. Baum, D.A. and B. Baum, *An inside-out origin for the eukaryotic cell.* BMC Biol, 2014. **12**: p. 76.
3. Lestourgeon, W.M., et al., *Contractile proteins. Major components of nuclear and chromosome non-histone proteins.* Biochim Biophys Acta, 1975. **379**(2): p. 529-52.
4. Clark, T.G. and R.W. Merriam, *Diffusible and bound actin nuclei of Xenopus laevis oocytes.* Cell, 1977. **12**(4): p. 883-91.
5. Clark, T.G. and J.L. Rosenbaum, *An actin filament matrix in hand-isolated nuclei of X. laevis oocytes.* Cell, 1979. **18**(4): p. 1101-8.
6. Pederson, T. and U. Aebi, *Actin in the nucleus: what form and what for?* J Struct Biol, 2002. **140**(1-3): p. 3-9.
7. Visa, N. and P. Percipalle, *Nuclear functions of actin.* Cold Spring Harb Perspect Biol, 2010. **2**(4): p. a000620.
8. Zhao, K., et al., *Rapid and phosphoinositol-dependent binding of the SWI/SNF-like BAF complex to chromatin after T lymphocyte receptor signaling.* Cell, 1998. **95**(5): p. 625-36.
9. Kapoor, P. and X. Shen, *Mechanisms of nuclear actin in chromatin-remodeling complexes.* Trends Cell Biol, 2014. **24**(4): p. 238-46.
10. Grosse, R. and M.K. Vartiainen, *To be or not to be assembled: progressing into nuclear actin filaments.* Nat Rev Mol Cell Biol, 2013. **14**(11): p. 693-7.
11. Gieni, R.S. and M.J. Hendzel, *Actin dynamics and functions in the interphase nucleus: moving toward an understanding of nuclear polymeric actin.* Biochem Cell Biol, 2009. **87**(1): p. 283-306.
12. Castano, E., et al., *Actin complexes in the cell nucleus: new stones in an old field.* Histochem Cell Biol, 2010. **133**(6): p. 607-26.
13. Kristo, I., et al., *Actin, actin-binding proteins, and actin-related proteins in the nucleus.* Histochem Cell Biol, 2016. **145**(4): p. 373-88.
14. Stuven, T., E. Hartmann, and D. Gorlich, *Exportin 6: a novel nuclear export receptor that is specific for profilin.actin complexes.* EMBO J, 2003. **22**(21): p. 5928-40.
15. Dopie, J., et al., *Active maintenance of nuclear actin by importin 9 supports transcription.* Proc Natl Acad Sci U S A, 2012. **109**(9): p. E544-52.
16. Revenu, C., et al., *The co-workers of actin filaments: from cell structures to signals.* Nat Rev Mol Cell Biol, 2004. **5**(8): p. 635-46.
17. Salbreux, G., G. Charras, and E. Paluch, *Actin cortex mechanics and cellular morphogenesis.* Trends Cell Biol, 2012. **22**(10): p. 536-45.
18. Lanzetti, L., *Actin in membrane trafficking.* Curr Opin Cell Biol, 2007. **19**(4): p. 453-8.
19. Thery, M., et al., *The extracellular matrix guides the orientation of the cell division axis.* Nat Cell Biol, 2005. **7**(10): p. 947-53.
20. Parsons, J.T., A.R. Horwitz, and M.A. Schwartz, *Cell adhesion: integrating cytoskeletal dynamics and cellular tension.* Nat Rev Mol Cell Biol, 2010. **11**(9): p. 633-43.

21. Le Clainche, C. and M.F. Carlier, *Regulation of actin assembly associated with protrusion and adhesion in cell migration.* Physiol Rev, 2008. **88**(2): p. 489-513.
22. Zhao, H., A. Pykalainen, and P. Lappalainen, *I-BAR domain proteins: linking actin and plasma membrane dynamics.* Curr Opin Cell Biol, 2011. **23**(1): p. 14-21.
23. Mogilner, A. and G. Oster, *Force generation by actin polymerization II: the elastic ratchet and tethered filaments.* Biophys J, 2003. **84**(3): p. 1591-605.
24. Carlsson, A.E. and P.V. Bayly, *Force generation by endocytic actin patches in budding yeast.* Biophys J, 2014. **106**(8): p. 1596-606.
25. Footer, M.J., et al., *Direct measurement of force generation by actin filament polymerization using an optical trap.* Proc Natl Acad Sci U S A, 2007. **104**(7): p. 2181-6.
26. Hartman, M.A. and J.A. Spudich, *The myosin superfamily at a glance.* J Cell Sci, 2012. **125**(Pt 7): p. 1627-32.
27. Kull, F.J. and S.A. Endow, *Force generation by kinesin and myosin cytoskeletal motor proteins.* J Cell Sci, 2013. **126**(Pt 1): p. 9-19.
28. Winder, S.J. and K.R. Ayscough, *Actin-binding proteins.* J Cell Sci, 2005. **118**(Pt 4): p. 651-4.
29. Kawska, A., et al., *How actin network dynamics control the onset of actin-based motility.* Proc Natl Acad Sci U S A, 2012. **109**(36): p. 14440-5.
30. Ireton, K., *Molecular mechanisms of cell-cell spread of intracellular bacterial pathogens.* Open Biol, 2013. **3**(7): p. 130079.
31. Costa, C.F., et al., *Myopathy mutations in alpha-skeletal-muscle actin cause a range of molecular defects.* J Cell Sci, 2004. **117**(Pt 15): p. 3367-77.
32. Sequeira, V., et al., *The physiological role of cardiac cytoskeleton and its alterations in heart failure.* Biochim Biophys Acta, 2014. **1838**(2): p. 700-22.
33. Alberts B, J.A., Lewis J, et al., *Chapter 16 The Cytoskeleton*. 4 ed, ed. G. Science. Vol. pp. 907–982. 2002, Molecular biology of the cell: Garland Science. 75.
34. Korn, E.D., M.F. Carlier, and D. Pantaloni, *Actin polymerization and ATP hydrolysis.* Science, 1987. **238**(4827): p. 638-44.
35. Sept, D. and J.A. McCammon, *Thermodynamics and kinetics of actin filament nucleation.* Biophys J, 2001. **81**(2): p. 667-74.
36. Pollard, T.D. and M.S. Mooseker, *Direct measurement of actin polymerization rate constants by electron microscopy of actin filaments nucleated by isolated microvillus cores.* J Cell Biol, 1981. **88**(3): p. 654-9.
37. Vavylonis, D., Q. Yang, and B. O'Shaughnessy, *Actin polymerization kinetics, cap structure, and fluctuations.* Proc Natl Acad Sci U S A, 2005. **102**(24): p. 8543-8.
38. Tobacman, L.S. and E.D. Korn, *The regulation of actin polymerization and the inhibition of monomeric actin ATPase activity by Acanthamoeba profilin.* J Biol Chem, 1982. **257**(8): p. 4166-70.
39. Fujiwara, I., D. Vavylonis, and T.D. Pollard, *Polymerization kinetics of ADP- and ADP-Pi-actin determined by fluorescence microscopy.* Proc Natl Acad Sci U S A, 2007. **104**(21): p. 8827-32.
40. Pollard, T.D. and G.G. Borisy, *Cellular motility driven by assembly and disassembly of actin filaments.* Cell, 2003. **112**(4): p. 453-65.
41. Zheng, X., K. Diraviyam, and D. Sept, *Nucleotide effects on the structure and dynamics of actin.* Biophys J, 2007. **93**(4): p. 1277-83.
42. Wegner, A. and J. Engel, *Kinetics of the cooperative association of actin to actin filaments.* Biophys Chem, 1975. **3**(3): p. 215-25.

43. Gutsche-Perelroizen, I., et al., *Filament assembly from profilin-actin.* J Biol Chem, 1999. **274**(10): p. 6234-43.
44. Wanger, M. and A. Wegner, *Binding of phosphate ions to actin.* Biochim Biophys Acta, 1987. **914**(2): p. 105-13.
45. Rickard, J.E. and P. Sheterline, *Cytoplasmic concentrations of inorganic phosphate affect the critical concentration for assembly of actin in the presence of cytochalasin D or ADP.* J Mol Biol, 1986. **191**(2): p. 273-80.
46. Kuhn, J.R. and T.D. Pollard, *Real-time measurements of actin filament polymerization by total internal reflection fluorescence microscopy.* Biophys J, 2005. **88**(2): p. 1387-402.
47. Bindschadler, M., et al., *A mechanistic model of the actin cycle.* Biophys J, 2004. **86**(5): p. 2720-39.
48. Watanabe, N. and T.J. Mitchison, *Single-molecule speckle analysis of actin filament turnover in lamellipodia.* Science, 2002. **295**(5557): p. 1083-6.
49. Pollard, T.D., *Rate constants for the reactions of ATP- and ADP-actin with the ends of actin filaments.* J Cell Biol, 1986. **103**(6 Pt 2): p. 2747-54.
50. Pollard, T.D., L. Blanchoin, and R.D. Mullins, *Molecular mechanisms controlling actin filament dynamics in nonmuscle cells.* Annu Rev Biophys Biomol Struct, 2000. **29**: p. 545-76.
51. Waterman-Storer, C., et al., *Microtubules remodel actomyosin networks in Xenopus egg extracts via two mechanisms of F-actin transport.* J Cell Biol, 2000. **150**(2): p. 361-76.
52. dos Remedios, C.G., et al., *Actin binding proteins: regulation of cytoskeletal microfilaments.* Physiol Rev, 2003. **83**(2): p. 433-73.
53. Ono, S., *Mechanism of depolymerization and severing of actin filaments and its significance in cytoskeletal dynamics.* Int Rev Cytol, 2007. **258**: p. 1-82.
54. Oh, M.A., et al., *PKCdelta and cofilin activation affects peripheral actin reorganization and cell-cell contact in cells expressing integrin alpha5 but not its tailless mutant.* J Cell Sci, 2007. **120**(Pt 15): p. 2717-30.
55. Bearer, E.L., et al., *VASP protects actin filaments from gelsolin: an in vitro study with implications for platelet actin reorganizations.* Cell Motil Cytoskeleton, 2000. **47**(4): p. 351-64.
56. Nag, S., et al., *Gelsolin: the tail of a molecular gymnast.* Cytoskeleton (Hoboken), 2013. **70**(7): p. 360-84.
57. Dominguez, R., *Actin filament nucleation and elongation factors--structure-function relationships.* Crit Rev Biochem Mol Biol, 2009. **44**(6): p. 351-66.
58. Kostyukova, A.S., E.I. Tiktopulo, and Y. Maeda, *Folding properties of functional domains of tropomodulin.* Biophys J, 2001. **81**(1): p. 345-51.
59. Helft, L., et al., *LRR conservation mapping to predict functional sites within protein leucine-rich repeat domains.* PLoS One, 2011. **6**(7): p. e21614.
60. Korenbaum, E. and F. Rivero, *Calponin homology domains at a glance.* J Cell Sci, 2002. **115**(Pt 18): p. 3543-5.
61. Xu, Y., et al., *Crystal structures of a Formin Homology-2 domain reveal a tethered dimer architecture.* Cell, 2004. **116**(5): p. 711-23.
62. Paunola, E., P.K. Mattila, and P. Lappalainen, *WH2 domain: a small, versatile adapter for actin monomers.* FEBS Lett, 2002. **513**(1): p. 92-7.
63. Bravo-Cordero, J.J., et al., *Functions of cofilin in cell locomotion and invasion.* Nat Rev Mol Cell Biol, 2013. **14**(7): p. 405-15.

64. Rayment, I., et al., *Three-dimensional structure of myosin subfragment-1: a molecular motor.* Science, 1993. **261**(5117): p. 50-8.
65. Vignjevic, D., et al., *Role of fascin in filopodial protrusion.* J Cell Biol, 2006. **174**(6): p. 863-75.
66. Paavilainen, V.O., et al., *Regulation of cytoskeletal dynamics by actin-monomer-binding proteins.* Trends Cell Biol, 2004. **14**(7): p. 386-94.
67. Insall, R.H. and L.M. Machesky, *Actin dynamics at the leading edge: from simple machinery to complex networks.* Dev Cell, 2009. **17**(3): p. 310-22.
68. Tseng, Y., et al., *How actin crosslinking and bundling proteins cooperate to generate an enhanced cell mechanical response.* Biochem Biophys Res Commun, 2005. **334**(1): p. 183-92.
69. Carlier, M.F. and D. Pantaloni, *Control of actin dynamics in cell motility.* J Mol Biol, 1997. **269**(4): p. 459-67.
70. Sun, H.Q., et al., *Gelsolin, a multifunctional actin regulatory protein.* J Biol Chem, 1999. **274**(47): p. 33179-82.
71. Fowler, V.M. and R. Dominguez, *Tropomodulins and Leiomodins: Actin Pointed End Caps and Nucleators in Muscles.* Biophys J, 2017. **112**(9): p. 1742-1760.
72. Tsukada, T., et al., *Leiomodin-2 is an antagonist of tropomodulin-1 at the pointed end of the thin filaments in cardiac muscle.* J Cell Sci, 2010. **123**(Pt 18): p. 3136-45.
73. Onji, T., M. Takagi, and N. Shibata, *Gelsolin is Ca2+-sensitive regulator of actomyosin system in platelet.* Biochem Biophys Res Commun, 1988. **155**(1): p. 91-9.
74. Chen, X., et al., *Mechanisms of leiomodin 2-mediated regulation of actin filament in muscle cells.* Proc Natl Acad Sci U S A, 2015. **112**(41): p. 12687-92.
75. Unger, A. and H. Hinssen, *Electron-microscopical localization of gelsolin in various crustacean muscles.* Cell Tissue Res, 2010. **341**(2): p. 313-23.
76. Nyakern-Meazza, M., et al., *Tropomyosin and gelsolin cooperate in controlling the microfilament system.* J Biol Chem, 2002. **277**(32): p. 28774-9.
77. Boczkowska, M., et al., *How Leiomodin and Tropomodulin use a common fold for different actin assembly functions.* Nat Commun, 2015. **6**: p. 8314.
78. Skwarek-Maruszewska, A., et al., *Different localizations and cellular behaviors of leiomodin and tropomodulin in mature cardiomyocyte sarcomeres.* Mol Biol Cell, 2010. **21**(19): p. 3352-61.
79. Chereau, D., et al., *Leiomodin is an actin filament nucleator in muscle cells.* Science, 2008. **320**(5873): p. 239-43.
80. Kostyukova, A.S., *Leiomodin/tropomyosin interactions are isoform specific.* Arch Biochem Biophys, 2007. **465**(1): p. 227-30.
81. Colpan, M., et al., *Localization of the binding interface between leiomodin-2 and alpha-tropomyosin.* Biochim Biophys Acta, 2016. **1864**(5): p. 523-30.
82. Ly, T., et al., *The N-terminal tropomyosin- and actin-binding sites are important for leiomodin 2's function.* Mol Biol Cell, 2016. **27**(16): p. 2565-75.
83. McLaughlin, P.J., et al., *Structure of gelsolin segment 1-actin complex and the mechanism of filament severing.* Nature, 1993. **364**(6439): p. 685-92.
84. Burtnick, L.D., et al., *The crystal structure of plasma gelsolin: implications for actin severing, capping, and nucleation.* Cell, 1997. **90**(4): p. 661-70.
85. Silacci, P., et al., *Gelsolin superfamily proteins: key regulators of cellular functions.* Cell Mol Life Sci, 2004. **61**(19-20): p. 2614-23.
86. Schleicher, M., et al., *Actin-binding proteins are conserved from slime molds to man.* Dev Genet, 1988. **9**(4-5): p. 521-30.

87. Sklyarova, T., et al., *Fragmin60 encodes an actin-binding protein with a C2 domain and controls actin Thr-203 phosphorylation in Physarum plasmodia and sclerotia.* J Biol Chem, 2002. **277**(42): p. 39840-9.
88. Kwiatkowski, D.J., et al., *Plasma and cytoplasmic gelsolins are encoded by a single gene and contain a duplicated actin-binding domain.* Nature, 1986. **323**(6087): p. 455-8.
89. Way, M. and A. Weeds, *Nucleotide sequence of pig plasma gelsolin. Comparison of protein sequence with human gelsolin and other actin-severing proteins shows strong homologies and evidence for large internal repeats.* J Mol Biol, 1988. **203**(4): p. 1127-33.
90. Mishra, V.S., et al., *The human actin-regulatory protein cap G: gene structure and chromosome location.* Genomics, 1994. **23**(3): p. 560-5.
91. Stocker, S., M. Hiery, and G. Marriott, *Phototactic migration of Dictyostelium cells is linked to a new type of gelsolin-related protein.* Mol Biol Cell, 1999. **10**(1): p. 161-78.
92. Kawamoto, S., et al., *Der f 16: a novel gelsolin-related molecule identified as an allergen from the house dust mite, Dermatophagoides farinae.* FEBS Lett, 2002. **516**(1-3): p. 234-8.
93. Gloss, A., et al., *Villidin, a novel WD-repeat and villin-related protein from Dictyostelium, is associated with membranes and the cytoskeleton.* Mol Biol Cell, 2003. **14**(7): p. 2716-27.
94. Klaavuniemi, T., S. Yamashiro, and S. Ono, *Caenorhabditis elegans gelsolin-like protein 1 is a novel actin filament-severing protein with four gelsolin-like repeats.* J Biol Chem, 2008. **283**(38): p. 26071-80.
95. Hatanaka, H., et al., *Tertiary structure of destrin and structural similarity between two actin-regulating protein families.* Cell, 1996. **85**(7): p. 1047-55.
96. Choe, H., et al., *The calcium activation of gelsolin: insights from the 3A structure of the G4-G6/actin complex.* J Mol Biol, 2002. **324**(4): p. 691-702.
97. Nag, S., et al., *Ca2+ binding by domain 2 plays a critical role in the activation and stabilization of gelsolin.* Proc Natl Acad Sci U S A, 2009. **106**(33): p. 13713-8.
98. Wang, H., et al., *Helix straightening as an activation mechanism in the gelsolin superfamily of actin regulatory proteins.* J Biol Chem, 2009. **284**(32): p. 21265-9.
99. Kazmirski, S.L., et al., *Loss of a metal-binding site in gelsolin leads to familial amyloidosis-Finnish type.* Nat Struct Biol, 2002. **9**(2): p. 112-6.
100. Burtnick, L.D., et al., *Structure of the N-terminal half of gelsolin bound to actin: roles in severing, apoptosis and FAF.* EMBO J, 2004. **23**(14): p. 2713-22.
101. Zapun, A., et al., *Calcium-dependent conformational stability of modules 1 and 2 of human gelsolin.* Biochem J, 2000. **350 Pt 3**: p. 873-81.
102. Chen, C.D., et al., *Furin initiates gelsolin familial amyloidosis in the Golgi through a defect in Ca(2+) stabilization.* EMBO J, 2001. **20**(22): p. 6277-87.
103. Pope, B., S. Maciver, and A. Weeds, *Localization of the calcium-sensitive actin monomer binding site in gelsolin to segment 4 and identification of calcium binding sites.* Biochemistry, 1995. **34**(5): p. 1583-8.
104. Khaitlina, S., M. Walloscheck, and H. Hinssen, *Calcium-induced conformational changes in the C-terminal half of gelsolin stabilize its interaction with the actin monomer.* Biochemistry, 2004. **43**(40): p. 12838-45.
105. Chumnarnsilpa, S., et al., *Calcium ion exchange in crystalline gelsolin.* J Mol Biol, 2006. **357**(3): p. 773-82.
106. Roustan, C., et al., *Calcium-induced conformational changes in the amino-terminal half of gelsolin.* FEBS Lett, 2007. **581**(4): p. 681-6.

107. Bryan, J. and S. Hwo, *Definition of an N-terminal actin-binding domain and a C-terminal Ca2+ regulatory domain in human brevin.* J Cell Biol, 1986. **102**(4): p. 1439-46.
108. Kwiatkowski, D.J. and H.L. Yin, *Molecular biology of gelsolin, a calcium-regulated actin filament severing protein.* Biorheology, 1987. **24**(6): p. 643-7.
109. Hellweg, T., H. Hinssen, and W. Eimer, *The Ca(2+)-induced conformational change of gelsolin is located in the carboxyl-terminal half of the molecule.* Biophys J, 1993. **65**(2): p. 799-805.
110. Allen, P.G. and P.A. Janmey, *Gelsolin displaces phalloidin from actin filaments. A new fluorescence method shows that both Ca2+ and Mg2+ affect the rate at which gelsolin severs F-actin.* J Biol Chem, 1994. **269**(52): p. 32916-23.
111. Selden, L.A., et al., *Severing of F-actin by the amino-terminal half of gelsolin suggests internal cooperativity in gelsolin.* Biophys J, 1998. **75**(6): p. 3092-100.
112. Way, M., B. Pope, and A.G. Weeds, *Are the conserved sequences in segment 1 of gelsolin important for binding actin?* J Cell Biol, 1992. **116**(5): p. 1135-43.
113. Way, M., B. Pope, and A.G. Weeds, *Evidence for functional homology in the F-actin binding domains of gelsolin and alpha-actinin: implications for the requirements of severing and capping.* J Cell Biol, 1992. **119**(4): p. 835-42.
114. Kinosian, H.J., et al., *Kinetics of gelsolin interaction with phalloidin-stabilized F-actin. Rate constants for binding and severing.* Biochemistry, 1996. **35**(51): p. 16550-6.
115. Gremm, D. and A. Wegner, *Gelsolin as a calcium-regulated actin filament-capping protein.* Eur J Biochem, 2000. **267**(14): p. 4339-45.
116. Kinosian, H.J., et al., *Ca2+ regulation of gelsolin activity: binding and severing of F-actin.* Biophys J, 1998. **75**(6): p. 3101-9.
117. Lin, K.M., M. Mejillano, and H.L. Yin, *Ca2+ regulation of gelsolin by its C-terminal tail.* J Biol Chem, 2000. **275**(36): p. 27746-52.
118. Kwiatkowski, D.J., P.A. Janmey, and H.L. Yin, *Identification of critical functional and regulatory domains in gelsolin.* J Cell Biol, 1989. **108**(5): p. 1717-26.
119. Pope, B.J., J.T. Gooch, and A.G. Weeds, *Probing the effects of calcium on gelsolin.* Biochemistry, 1997. **36**(50): p. 15848-55.
120. Lueck, A., et al., *Calcium regulation of gelsolin and adseverin: a natural test of the helix latch hypothesis.* Biochemistry, 2000. **39**(18): p. 5274-9.
121. Kolappan, S., et al., *Gelsolin domains 4-6 in active, actin-free conformation identifies sites of regulatory calcium ions.* J Mol Biol, 2003. **329**(1): p. 85-92.
122. Lagarrigue, E., et al., *Co-operation of domain-binding and calcium-binding sites in the activation of gelsolin.* Eur J Biochem, 2003. **270**(10): p. 2236-43.
123. Lagarrigue, E., et al., *The activation of gelsolin by low pH: the calcium latch is sensitive to calcium but not pH.* Eur J Biochem, 2003. **270**(20): p. 4105-12.
124. Ditsch, A. and A. Wegner, *Two low-affinity Ca(2+)-binding sites of gelsolin that regulate association with actin.* Eur J Biochem, 1995. **229**(2): p. 512-6.
125. Kiselar, J.G., et al., *Structural analysis of gelsolin using synchrotron protein footprinting.* Mol Cell Proteomics, 2003. **2**(10): p. 1120-32.
126. Kiselar, J.G., et al., *Visualizing the Ca2+-dependent activation of gelsolin by using synchrotron footprinting.* Proc Natl Acad Sci U S A, 2003. **100**(7): p. 3942-7.
127. Ashish, et al., *Global structure changes associated with Ca2+ activation of full-length human plasma gelsolin.* J Biol Chem, 2007. **282**(35): p. 25884-92.
128. Weeds, A.G., et al., *Identification of the trapped calcium in the gelsolin segment 1-actin complex: implications for the role of calcium in the control of gelsolin activity.* FEBS Lett, 1995. **360**(3): p. 227-30.

129. Lamb, J.A., et al., *Modulation of gelsolin function. Activation at low pH overrides Ca2+ requirement.* J Biol Chem, 1993. **268**(12): p. 8999-9004.
130. Garg, R., et al., *Visual insight into how low pH alone can induce actin-severing ability in gelsolin under calcium-free conditions.* J Biol Chem, 2011. **286**(23): p. 20387-97.
131. Solomon, J.P., et al., *Gelsolin amyloidosis: genetics, biochemistry, pathology and possible strategies for therapeutic intervention.* Crit Rev Biochem Mol Biol, 2012. **47**(3): p. 282-96.
132. Ratnaswamy, G., et al., *Destabilization of Ca2+-free gelsolin may not be responsible for proteolysis in Familial Amyloidosis of Finnish Type.* Proc Natl Acad Sci U S A, 2001. **98**(5): p. 2334-9.
133. Robinson, R.C., S. Choe, and L.D. Burtnick, *The disintegration of a molecule: the role of gelsolin in FAF, familial amyloidosis (Finnish type).* Proc Natl Acad Sci U S A, 2001. **98**(5): p. 2117-8.
134. Pope, B., M. Way, and A.G. Weeds, *Two of the three actin-binding domains of gelsolin bind to the same subdomain of actin. Implications of capping and severing mechanisms.* FEBS Lett, 1991. **280**(1): p. 70-4.
135. Van Troys, M., et al., *Evidence for an actin binding helix in gelsolin segment 2; have homologous sequences in segments 1 and 2 of gelsolin evolved to divergent actin binding functions?* FEBS Lett, 1996. **397**(2-3): p. 191-6.
136. Robinson, R.C., et al., *Domain movement in gelsolin: a calcium-activated switch.* Science, 1999. **286**(5446): p. 1939-42.
137. Irobi, E., et al., *From the first to the second domain of gelsolin: a common path on the surface of actin?* FEBS Lett, 2003. **552**(2-3): p. 86-90.
138. Nag, A., et al., *Aggregation of membrane proteins by cytosolic cross-linkers: theory and simulation of the LAT-Grb2-SOS1 system.* Biophys J, 2009. **96**(7): p. 2604-23.
139. Southwick, F.S., *Gain-of-function mutations conferring actin-severing activity to human macrophage cap G.* J Biol Chem, 1995. **270**(1): p. 45-8.
140. Bearer, E.L., *Direct observation of actin filament severing by gelsolin and binding by gCap39 and CapZ.* J Cell Biol, 1991. **115**(6): p. 1629-38.
141. Prochniewicz, E., et al., *Cooperativity in F-actin: binding of gelsolin at the barbed end affects structure and dynamics of the whole filament.* J Mol Biol, 1996. **260**(5): p. 756-66.
142. McGough, A., W. Chiu, and M. Way, *Determination of the gelsolin binding site on F-actin: implications for severing and capping.* Biophys J, 1998. **74**(2 Pt 1): p. 764-72.
143. Hild, G., B. Bugyi, and M. Nyitrai, *Conformational dynamics of actin: effectors and implications for biological function.* Cytoskeleton (Hoboken), 2010. **67**(10): p. 609-29.
144. Hayakawa, K., H. Tatsumi, and M. Sokabe, *Actin filaments function as a tension sensor by tension-dependent binding of cofilin to the filament.* J Cell Biol, 2011. **195**(5): p. 721-7.
145. Risca, V.I., et al., *Actin filament curvature biases branching direction.* Proc Natl Acad Sci U S A, 2012. **109**(8): p. 2913-8.
146. Kang, H., et al., *Identification of cation-binding sites on actin that drive polymerization and modulate bending stiffness.* Proc Natl Acad Sci U S A, 2012. **109**(42): p. 16923-7.
147. Nag, S., et al., *Gelsolin: The tail of a molecular gymnast.* Cytoskeleton, 2013. **70**(7): p. 360-84.
148. Hartwig, J.H., K.A. Chambers, and T.P. Stossel, *Association of gelsolin with actin filaments and cell membranes of macrophages and platelets.* The Journal of cell biology, 1989. **108**(2): p. 467-79.

149. Allen, P.G., *Actin filament uncapping localizes to ruffling lamellae and rocketing vesicles.* Nature Cell Biology, 2003. **5**(11): p. 972-9.
150. Yin, H.L. and P.A. Janmey, *Phosphoinositide regulation of the actin cytoskeleton.* Annual review of physiology, 2003. **65**: p. 761-89.
151. Janmey, P.A., *Phosphoinositides and calcium as regulators of cellular actin assembly and disassembly.* Annual review of physiology, 1994. **56**: p. 169-91.
152. Schafer, D.A. and J.A. Cooper, *Control of actin assembly at filament ends.* Annual review of cell and developmental biology, 1995. **11**: p. 497-518.
153. Hilpela, P., M.K. Vartiainen, and P. Lappalainen, *Regulation of the actin cytoskeleton by PI(4,5)P2 and PI(3,4,5)P3.* Current Topics in Microbiology and Immunology, 2004. **282**: p. 117-63.
154. Janmey, P.A. and T.P. Stossel, *Modulation of gelsolin function by phosphatidylinositol 4,5-bisphosphate.* Nature, 1987. **325**(6102): p. 362-4.
155. Yu, F.X., et al., *gCap39, a calcium ion- and polyphosphoinositide-regulated actin capping protein.* Science, 1990. **250**(4986): p. 1413-5.
156. Schafer, D.A., P.B. Jennings, and J.A. Cooper, *Dynamics of capping protein and actin assembly in vitro: uncapping barbed ends by polyphosphoinositides.* The Journal of cell biology, 1996. **135**(1): p. 169-79.
157. Lassing, I. and U. Lindberg, *Specific interaction between phosphatidylinositol 4,5-bisphosphate and profilactin.* Nature, 1985. **314**(6010): p. 472-4.
158. Yonezawa, N., et al., *Inhibition of the interactions of cofilin, destrin, and deoxyribonuclease I with actin by phosphoinositides.* The Journal of biological chemistry, 1990. **265**(15): p. 8382-6.
159. Palmgren, S., et al., *Interactions with PIP2, ADP-actin monomers, and capping protein regulate the activity and localization of yeast twinfilin.* The Journal of cell biology, 2001. **155**(2): p. 251-60.
160. Higgs, H.N. and T.D. Pollard, *Activation by Cdc42 and PIP(2) of Wiskott-Aldrich syndrome protein (WASp) stimulates actin nucleation by Arp2/3 complex.* The Journal of cell biology, 2000. **150**(6): p. 1311-20.
161. Miki, H., K. Miura, and T. Takenawa, *N-WASP, a novel actin-depolymerizing protein, regulates the cortical cytoskeletal rearrangement in a PIP2-dependent manner downstream of tyrosine kinases.* The EMBO journal, 1996. **15**(19): p. 5326-35.
162. Schafer, D.A., et al., *Dynamin2 and cortactin regulate actin assembly and filament organization.* Current biology : CB, 2002. **12**(21): p. 1852-7.
163. Fukami, K., et al., *Requirement of phosphatidylinositol 4,5-bisphosphate for alpha-actinin function.* Nature, 1992. **359**(6391): p. 150-2.
164. Furuhashi, K., et al., *Inositol phospholipid-induced suppression of F-actin-gelating activity of smooth muscle filamin.* Biochemical and Biophysical Research Communications, 1992. **184**(3): p. 1261-5.
165. Stock, A., et al., *Domain analysis of cortexillin I: actin-bundling, PIP(2)-binding and the rescue of cytokinesis.* The EMBO journal, 1999. **18**(19): p. 5274-84.
166. Gilmore, A.P. and K. Burridge, *Regulation of vinculin binding to talin and actin by phosphatidyl-inositol-4-5-bisphosphate.* Nature, 1996. **381**(6582): p. 531-5.
167. Hirao, M., et al., *Regulation mechanism of ERM (ezrin/radixin/moesin) protein/plasma membrane association: possible involvement of phosphatidylinositol turnover and Rho-dependent signaling pathway.* The Journal of cell biology, 1996. **135**(1): p. 37-51.

168. Chou, J., et al., *Distribution of gelsolin and phosphoinositol 4,5-bisphosphate in lamellipodia during EGF-induced motility.* The international journal of biochemistry & cell biology, 2002. **34**(7): p. 776-90.
169. Janmey, P.A. and P.T. Matsudaira, *Functional comparison of villin and gelsolin. Effects of Ca2+, KCl, and polyphosphoinositides.* The Journal of biological chemistry, 1988. **263**(32): p. 16738-43.
170. Maekawa, S. and H. Sakai, *Inhibition of actin regulatory activity of the 74-kDa protein from bovine adrenal medulla (adseverin) by some phospholipids.* The Journal of biological chemistry, 1990. **265**(19): p. 10940-2.
171. Janmey, P.A., et al., *Phosphoinositide-binding peptides derived from the sequences of gelsolin and villin.* The Journal of biological chemistry, 1992. **267**(17): p. 11818-23.
172. Feng, L., et al., *Full-contact domain labeling: identification of a novel phosphoinositide binding site on gelsolin that requires the complete protein.* Biochemistry, 2001. **40**(4): p. 904-13.
173. Hartwig, J.H., et al., *Thrombin receptor ligation and activated Rac uncap actin filament barbed ends through phosphoinositide synthesis in permeabilized human platelets.* Cell, 1995. **82**(4): p. 643-53.
174. Tuominen, E.K., et al., *Fluorescent phosphoinositide derivatives reveal specific binding of gelsolin and other actin regulatory proteins to mixed lipid bilayers.* European journal of biochemistry / FEBS, 1999. **263**(1): p. 85-92.
175. Banno, Y., et al., *Effects of gelsolin on human platelet cytosolic phosphoinositide-phospholipase C isozymes.* The Journal of biological chemistry, 1992. **267**(10): p. 6488-94.
176. Urosev, D., et al., *The structure of gelsolin bound to ATP.* Journal of molecular biology, 2006. **357**(3): p. 765-72.
177. Liepina, I., et al., *Molecular dynamics study of a gelsolin-derived peptide binding to a lipid bilayer containing phosphatidylinositol 4,5-bisphosphate.* Biopolymers, 2003. **71**(1): p. 49-70.
178. Lin, K.M., et al., *Gelsolin binding to phosphatidylinositol 4,5-bisphosphate is modulated by calcium and pH.* The Journal of biological chemistry, 1997. **272**(33): p. 20443-50.
179. Ito, H., et al., *Affinity chromatography of human plasma gelsolin with polyphosphate compounds on immobilized Cibacron Blue F3GA.* Journal of chromatography, 1990. **526**(2): p. 397-406.
180. Yamamoto, H., et al., *Affinity separation of human plasma gelsolin on Affi-Gel Blue.* Journal of biochemistry, 1989. **105**(5): p. 799-802.
181. Kambe, H., et al., *Human plasma gelsolin reversibly binds Mg-ATP in Ca(2+)-sensitive manner.* Journal of biochemistry, 1992. **111**(6): p. 722-5.
182. Gremm, D. and A. Wegner, *Co-operative binding of Ca2+ ions to the regulatory binding sites of gelsolin.* European journal of biochemistry / FEBS, 1999. **262**(2): p. 330-4.
183. Yamamoto, H., et al., *Human plasma gelsolin binds adenosine triphosphate.* Journal of Biochemistry, 1990. **108**(4): p. 505-6.
184. Burtnick, L.D., et al., *Structure of the N-terminal half of gelsolin bound to actin: roles in severing, apoptosis and FAF.* EMBO journal, 2004. **23**(14): p. 2713-22.
185. Choe, H., et al., *The calcium activation of gelsolin: insights from the 3A structure of the G4-G6/actin complex.* Journal of molecular biology, 2002. **324**(4): p. 691-702.
186. Nag, S., et al., *Ca2+ binding by domain 2 plays a critical role in the activation and stabilization of gelsolin.* Proceedings of the National Academy of Sciences of the United States of America, 2009. **106**(33): p. 13713-8.

187. Narayan, K., et al., *Activation in isolation: exposure of the actin-binding site in the C-terminal half of gelsolin does not require actin.* FEBS letters, 2003. **552**(2-3): p. 82-5.
188. Wang, H., et al., *Helix straightening as an activation mechanism in the gelsolin superfamily of actin regulatory proteins.* The Journal of biological chemistry, 2009. **284**(32): p. 21265-9.
189. Allen, P.G., et al., *Binding of phosphate, aluminum fluoride, or beryllium fluoride to F-actin inhibits severing by gelsolin.* The Journal of biological chemistry, 1996. **271**(9): p. 4665-70.
190. Laham, L.E., et al., *Identification of two sites in gelsolin with different sensitivities to adenine nucleotides.* European journal of biochemistry / FEBS, 1995. **234**(1): p. 1-7.
191. Maravall, M., et al., *Estimating intracellular calcium concentrations and buffering without wavelength ratioing.* Biophysical journal, 2000. **78**(5): p. 2655-67.
192. Baffy, G., et al., *Disturbed intracellular calcium-related processes of hepatocytes and neutrophils in human alcoholic liver disease.* Clinical biochemistry, 1990. **23**(3): p. 241-5.
193. Saqr, H.E., et al., *Mechanisms through which PDGF alters intracellular calcium levels in U-1242 MG human glioma cells.* Neurochemistry international, 1999. **35**(6): p. 411-22.
194. Nohutcu, R.M., et al., *Effects of hormones and cytokines on stimulation of adenylate cyclase and intracellular calcium concentration in human and canine periodontal-ligament fibroblasts.* Archives of oral biology, 1993. **38**(10): p. 871-9.
195. Shi, Y., et al., *Regulation of intracellular free calcium concentration during heterocyst differentiation by HetR and NtcA in Anabaena sp. PCC 7120.* Proceedings of the National Academy of Sciences of the United States of America, 2006. **103**(30): p. 11334-9.
196. Dvorak, M.M., et al., *Physiological changes in extracellular calcium concentration directly control osteoblast function in the absence of calciotropic hormones.* Proceedings of the National Academy of Sciences of the United States of America, 2004. **101**(14): p. 5140-5.
197. McCarthy, J. and R. Kumar, *Divalent cation metabolism: calcium*, in *Atlas of Diseases of the Kidney* R. Schrier and T. Berl, Editors. 1999, Current Medicine. p. 4.1-4.8.
198. Murphy, E., *Mysteries of magnesium homeostasis.* Circulation Research, 2000. **86**(3): p. 245-8.
199. Imamura, H., et al., *Visualization of ATP levels inside single living cells with fluorescence resonance energy transfer-based genetically encoded indicators.* Proceedings of the National Academy of Sciences of the United States of America, 2009. **106**(37): p. 15651-6.
200. Gribble, F.M., et al., *A novel method for measurement of submembrane ATP concentration.* The Journal of biological chemistry, 2000. **275**(39): p. 30046-9.
201. Ataullakhanov, F.I. and V.M. Vitvitsky, *What determines the intracellular ATP concentration.* Bioscience reports, 2002. **22**(5-6): p. 501-11.
202. Niki, I., F.M. Ashcroft, and S.J. Ashcroft, *The dependence on intracellular ATP concentration of ATP-sensitive K-channels and of Na,K-ATPase in intact HIT-T15 beta-cells.* FEBS letters, 1989. **257**(2): p. 361-4.
203. Ahern, G.P. and D.R. Laver, *ATP inhibition and rectification of a Ca2+-activated anion channel in sarcoplasmic reticulum of skeletal muscle.* Biophysical journal, 1998. **74**(5): p. 2335-51.

204. Ballarin, C. and M.C. Sorgato, *An electrophysiological study of yeast mitochondria. Evidence for two inner membrane anion channels sensitive to ATP.* The Journal of biological chemistry, 1995. **270**(33): p. 19262-8.
205. Bennetts, B., et al., *Cytoplasmic ATP-sensing domains regulate gating of skeletal muscle ClC-1 chloride channels.* The Journal of biological chemistry, 2005. **280**(37): p. 32452-8.
206. Zhang, X.D., P.Y. Tseng, and T.Y. Chen, *ATP inhibition of CLC-1 is controlled by oxidation and reduction.* The Journal of general physiology, 2008. **132**(4): p. 421-8.
207. MacGregor, G.G., et al., *Nucleotides and phospholipids compete for binding to the C terminus of KATP channels.* Proceedings of the National Academy of Sciences of the United States of America, 2002. **99**(5): p. 2726-31.
208. Conley, C.A., et al., *Leiomodins: larger members of the tropomodulin (Tmod) gene family.* Genomics, 2001. **73**(2): p. 127-39.
209. Conley, C.A., *Leiomodin and tropomodulin in smooth muscle.* Am J Physiol Cell Physiol, 2001. **280**(6): p. C1645-56.
210. Nanda, V. and J.M. Miano, *Leiomodin 1, a new serum response factor-dependent target gene expressed preferentially in differentiated smooth muscle cells.* J Biol Chem, 2012. **287**(4): p. 2459-67.
211. Halim, D., et al., *Loss of LMOD1 impairs smooth muscle cytocontractility and causes megacystis microcolon intestinal hypoperistalsis syndrome in humans and mice.* Proc Natl Acad Sci U S A, 2017.
212. Pappas, C.T., et al., *Knockout of Lmod2 results in shorter thin filaments followed by dilated cardiomyopathy and juvenile lethality.* Proc Natl Acad Sci U S A, 2015. **112**(44): p. 13573-8.
213. Nworu, C.U., et al., *Leiomodin 3 and tropomodulin 4 have overlapping functions during skeletal myofibrillogenesis.* J Cell Sci, 2015. **128**(2): p. 239-50.
214. Yuen, M., et al., *Leiomodin-3 dysfunction results in thin filament disorganization and nemaline myopathy.* J Clin Invest, 2014. **124**(11): p. 4693-708.
215. Cenik, B.K., et al., *Severe myopathy in mice lacking the MEF2/SRF-dependent gene leiomodin-3.* J Clin Invest, 2015. **125**(4): p. 1569-78.
216. Li, S.S., *Specificity and versatility of SH3 and other proline-recognition domains: structural basis and implications for cellular signal transduction.* Biochem J, 2005. **390**(Pt 3): p. 641-53.
217. Almenar-Queralt, A., C.C. Gregorio, and V.M. Fowler, *Tropomodulin assembles early in myofibrillogenesis in chick skeletal muscle: evidence that thin filaments rearrange to form striated myofibrils.* J Cell Sci, 1999. **112 (Pt 8)**: p. 1111-23.
218. Li, S., et al., *Lmod2 piggyBac mutant mice exhibit dilated cardiomyopathy.* Cell Biosci, 2016. **6**: p. 38.
219. Gokhin, D.S. and V.M. Fowler, *Tropomodulin capping of actin filaments in striated muscle development and physiology.* J Biomed Biotechnol, 2011. **2011**: p. 103069.
220. Tsukada, T., et al., *Identification of residues within tropomodulin-1 responsible for its localization at the pointed ends of the actin filaments in cardiac myocytes.* J Biol Chem, 2011. **286**(3): p. 2194-204.
221. Weber, A., et al., *Tropomodulin caps the pointed ends of actin filaments.* J Cell Biol, 1994. **127**(6 Pt 1): p. 1627-35.
222. Rao, J.N., Y. Madasu, and R. Dominguez, *Mechanism of actin filament pointed-end capping by tropomodulin.* Science, 2014. **345**(6195): p. 463-7.

223. Dominguez, R., *The WH2 Domain and Actin Nucleation: Necessary but Insufficient.* Trends Biochem Sci, 2016. **41**(6): p. 478-90.
224. Toth, M.A., et al., *Biochemical Activities of the Wiskott-Aldrich Syndrome Homology Region 2 Domains of Sarcomere Length Short (SALS) Protein.* J Biol Chem, 2016. **291**(2): p. 667-80.
225. Fuxreiter, M., *Fuzziness: linking regulation to protein dynamics.* Mol Biosyst, 2012. **8**(1): p. 168-77.
226. Bai, J., J.H. Hartwig, and N. Perrimon, *SALS, a WH2-domain-containing protein, promotes sarcomeric actin filament elongation from pointed ends during Drosophila muscle growth.* Dev Cell, 2007. **13**(6): p. 828-42.
227. Sussman, M.A., et al., *Altered expression of tropomodulin in cardiomyocytes disrupts the sarcomeric structure of myofibrils.* Circ Res, 1998. **82**(1): p. 94-105.
228. Sussman, M.A., et al., *Pathogenesis of dilated cardiomyopathy: molecular, structural, and population analyses in tropomodulin-overexpressing transgenic mice.* Am J Pathol, 1999. **155**(6): p. 2101-13.
229. Rosado, M., et al., *Critical roles for multiple formins during cardiac myofibril development and repair.* Mol Biol Cell, 2014. **25**(6): p. 811-27.
230. Taniguchi, K., et al., *Mammalian formin fhod3 regulates actin assembly and sarcomere organization in striated muscles.* J Biol Chem, 2009. **284**(43): p. 29873-81.
231. Mossakowska, M., J. Belagyi, and H. Strzelecka-Golaszewska, *An EPR study of the rotational dynamics of actins from striated and smooth muscle and their complexes with heavy meromyosin.* Eur J Biochem, 1988. **175**(3): p. 557-64.
232. Spudich, J.A. and S. Watt, *The regulation of rabbit skeletal muscle contraction. I. Biochemical studies of the interaction of the tropomyosin-troponin complex with actin and the proteolytic fragments of myosin.* J Biol Chem, 1971. **246**(15): p. 4866-71.
233. Houk, T.W., Jr. and K. Ue, *The measurement of actin concentration in solution: a comparison of methods.* Anal Biochem, 1974. **62**(1): p. 66-74.
234. Elzinga, M., et al., *Complete amino-acid sequence of actin of rabbit skeletal muscle.* Proc Natl Acad Sci U S A, 1973. **70**(9): p. 2687-91.
235. Geeves, M.A., S.E. Hitchcock-DeGregori, and P.W. Gunning, *A systematic nomenclature for mammalian tropomyosin isoforms.* J Muscle Res Cell Motil, 2015. **36**(2): p. 147-53.
236. Smillie, L.B., *Preparation and identification of alpha- and beta-tropomyosins.* Methods Enzymol, 1982. **85 Pt B**: p. 234-41.
237. Kis-Bicskei, N., et al., *Purification of tropomyosin Br-3 and 5NM1 and characterization of their interactions with actin.* Cytoskeleton (Hoboken), 2013. **70**(11): p. 755-65.
238. Bugyi, B., et al., *Formins regulate actin filament flexibility through long range allosteric interactions.* J Biol Chem, 2006. **281**(16): p. 10727-36.
239. Papp, G., et al., *Conformational changes in actin filaments induced by formin binding to the barbed end.* Biophys J, 2006. **91**(7): p. 2564-72.
240. Ujfalusi, Z., et al., *Myosin and tropomyosin stabilize the conformation of formin-nucleated actin filaments.* J Biol Chem, 2012. **287**(38): p. 31894-904.
241. Criddle, A.H., M.A. Geeves, and T. Jeffries, *The use of actin labelled with N-(1-pyrenyl)iodoacetamide to study the interaction of actin with myosin subfragments and troponin/tropomyosin.* Biochem J, 1985. **232**(2): p. 343-9.
242. Lakowicz, J.R. and SpringerLink (Online service), *Principles of Fluorescence Spectroscopy*. 2006, Springer Science+Business Media, LLC,: Boston, MA.
243. Vinson, V.K., et al., *Interactions of Acanthamoeba profilin with actin and nucleotides bound to actin.* Biochemistry, 1998. **37**(31): p. 10871-80.

244. Nyitrai, M., et al., *The flexibility of actin filaments as revealed by fluorescence resonance energy transfer. The influence of divalent cations.* J Biol Chem, 1999. **274**(19): p. 12996-3001.
245. Somogyi, B., et al., *Forster-type energy transfer as a probe for changes in local fluctuations of the protein matrix.* Biochemistry, 1984. **23**(15): p. 3403-11.
246. Nyitrai, M., et al., *Effect of Ca2+-Mg2+ exchange on the flexibility and/or conformation of the small domain in monomeric actin.* Biophys J, 1998. **74**(5): p. 2474-81.
247. Huang, W., et al., *Kinetic Analysis of PI3K Reactions with Fluorescent PIP2 Derivatives.* Analytical and Bioanalytical Chemistry, 2011. **401**(6): p. 1881-1888.
248. Spudich, J.A. and S. Watt, *The regulation of rabbit skeletal muscle contraction. I. Biochemical studies of the interaction of the tropomyosin-troponin complex with actin and the proteolytic fragments of myosin.* Journal of biological chemistry, 1971. **246**(15): p. 4866-71.
249. Kubala, M., J. Plasek, and E. Amler, *Fluorescence competition assay for the assessment of ATP binding to an isolated domain of Na+, K(+)-ATPase.* Physiol Res, 2004. **53**(1): p. 109-13.
250. Flanagan, L.A., et al., *The structure of divalent cation-induced aggregates of PIP2 and their alteration by gelsolin and tau.* Biophysical Journal, 1997. **73**(3): p. 1440-1447.
251. Levental, I., et al., *Calcium-dependent lateral organization in phosphatidylinositol 4,5-bisphosphate (PIP2)- and cholesterol-containing monolayers.* Biochemistry, 2009. **48**(34): p. 8241-8248.
252. DeForte, S. and V.N. Uversky, *Order, Disorder, and Everything in Between.* Molecules, 2016. **21**(8).
253. Dunker, A.K., et al., *Function and structure of inherently disordered proteins.* Curr Opin Struct Biol, 2008. **18**(6): p. 756-64.
254. Tompa, P., et al., *Intrinsically disordered proteins: emerging interaction specialists.* Curr Opin Struct Biol, 2015. **35**: p. 49-59.
255. Dosztanyi, Z., et al., *IUPred: web server for the prediction of intrinsically unstructured regions of proteins based on estimated energy content.* Bioinformatics, 2005. **21**(16): p. 3433-4.
256. Dosztanyi, Z., et al., *The pairwise energy content estimated from amino acid composition discriminates between folded and intrinsically unstructured proteins.* J Mol Biol, 2005. **347**(4): p. 827-39.
257. Hild, G., et al., *The influence of divalent cations on the dynamic properties of actin filaments: a spectroscopic study.* Biophys J, 1998. **75**(6): p. 3015-22.
258. Hild, G., M. Nyitrai, and B. Somogyi, *Intermonomer flexibility of Ca- and Mg-actin filaments at different pH values.* Eur J Biochem, 2002. **269**(3): p. 842-9.
259. Ujfalusi, Z., et al., *Effect of tropomyosin on formin-bound actin filaments.* Biophys J, 2009. **96**(1): p. 162-8.
260. Pollard, T.D., *Regulation of actin filament assembly by Arp2/3 complex and formins.* Annu Rev Biophys Biomol Struct, 2007. **36**: p. 451-77.
261. Ono, S., *Dynamic regulation of sarcomeric actin filaments in striated muscle.* Cytoskeleton (Hoboken), 2010. **67**(11): p. 677-92.
262. Sanger, J.W., et al., *Assembly and Maintenance of Myofibrils in Striated Muscle.* Handb Exp Pharmacol, 2017. **235**: p. 39-75.
263. Gunning, P., G. O'Neill, and E. Hardeman, *Tropomyosin-based regulation of the actin cytoskeleton in time and space.* Physiol Rev, 2008. **88**(1): p. 1-35.

264. Gunning, P.W., et al., *Tropomyosin isoforms: divining rods for actin cytoskeleton function.* Trends Cell Biol, 2005. **15**(6): p. 333-41.
265. Orlova, A., E. Prochniewicz, and E.H. Egelman, *Structural dynamics of F-actin: II. Cooperativity in structural transitions.* J Mol Biol, 1995. **245**(5): p. 598-607.
266. Somogyi, B., et al., *Protein flexibility as revealed by fluorescence resonance energy transfer: An extension of the method for systems with multiple labels.* Journal of Photochemistry and Photobiology B: Biology, 2000. **59**(1-3): p. 26-32.
267. Higuchi, H. and S. Takemori, *Butanedione monoxime suppresses contraction and ATPase activity of rabbit skeletal muscle.* J Biochem, 1989. **105**(4): p. 638-43.
268. Umeki, N., K. Hirose, and T.Q. Uyeda, *Cofilin-induced cooperative conformational changes of actin subunits revealed using cofilin-actin fusion protein.* Sci Rep, 2016. **6**: p. 20406.
269. Loscalzo, J., G.H. Reed, and A. Weber, *Conformational change and cooperativity in actin filaments free of tropomyosin.* Proc Natl Acad Sci U S A, 1975. **72**(9): p. 3412-5.
270. Oosawa, F., *Dynamic properties of F-actin and the thin filament.* Nihon Seirigaku Zasshi, 1972. **34**(2): p. 96-7.
271. Ngo, K.X., et al., *Allosteric regulation by cooperative conformational changes of actin filaments drives mutually exclusive binding with cofilin and myosin.* Sci Rep, 2016. **6**: p. 35449.
272. Koldsø, H., et al., *Lipid clustering correlates with membrane curvature as revealed by molecular simulations of complex lipid bilayers.* PLoS computational biology, 2014. **10**(10): p. e1003911.
273. Kovacs, M., et al., *Mechanism of blebbistatin inhibition of myosin II.* J Biol Chem, 2004. **279**(34): p. 35557-63.

VI. List of Abbreviations

ABP: actin binding proteins

ADF: actin depolymerising factor

ADP: adenosine diphosphate

Arp2/3 complex: actin related protein 2/3 complex

ATP: adenosine triphosphate

FITC: fluorescein isothiocyanate

FRET: fluorescence resonance energy transfer

GSN: gelsolin

IAEDANS: 5-[2-[(2-Iodo-1-oxoethyl)amino]ethylamino]-1-naphthalenesulfonic acid

Kd: dissociation equilibrium constant

$Lmod^{FL}$*:* full-length cardiac leiomodin2

MOPS: 3-(N-morpholino) propanesulfonic acid

P_i: inorganic phosphate

PIP_2: phosphatidylinositol 4,5-bisphosphate

PIP_3: phosphatidylinositol (3,4,5)-triphosphate

TRIS: tris(hydroxymethyl)aminomethane

VASP: vasodilatator-stimulated phosphoprotein

VII. Publications

VII.1. Publications related to this thesis

Dávid Szatmári, Beáta Bugyi, Zoltán Ujfalusi, László Grama, Réka Dudás and Miklós Nyitrai

Cardiac leiomodin2 binds to the sides of actin filaments and regulate the ATPase activity of myosin

***PLOS ONE* 12:**(10) Paper 186288. 21 p. (2017)

IF: 2.806

David Szatmari, Bo Xue, Balakrishnan Kannan, Leslie D. Burtnick, Beáta Bugyi, Miklós Nyitrai, Robert C. Robinson

ATP competes with PIP_2 for binding to gelsolin

submitted (2017)

Szilvia Barkó*, **Dávid Szatmári***, Emőke Bódis, Katalin Türmer, Zoltán Ujfalusi, David Popp, Robert C Robinson, Miklós Nyitrai

Large-scale purification and in vitro characterization of the assembly of MreB from Leptospira interrogans

BIOCHIMICA ET BIOPHYSICA ACTA-GENERAL SUBJECTS 1860:*(9) pp. 1942-1952. (2016)*

***equal contributors**

IF: 4.702

Kollar V, **Szatmari D**, Grama L, Kellermayer MSZ

Dynamic Strength of Titin's Z-Disk End

***JOURNAL OF BIOMEDICINE AND BIOTECHNOLOGY* 2010:** *Paper 838530. 8 p.* (2010)

IF: 1.230

Kellermayer MSZ, Bianco P, Martonfalvi Z, Nagy A, Kengyel A, **Szatmari D**, Huber T, Linari M, Caremani M, Lombardi V

Muscle thixotropy: More than just cross-bridges? Response to comment by Campbell and Lakie

BIOPHYSICAL JOURNAL **94:**(1) *pp. 329-330.* (2008)

IF: 4.683

Bianco P, Nagy A, Kengyel A, **Szatmari D**, Martonfalvi Z, Huber T, Kellermayer MSZ

Interaction forces between F-Actin and titin PEVK domain measured with optical tweezers

BIOPHYSICAL JOURNAL **93:**(6) *pp. 2102-2109.* (2007)

IF: 4.627

VII.3. Book chapter not related to this thesis

Varga S, Varga D, Hoffmann G, Németh Z, **Szatmári D**, Mátics R, Rauch T, Varga M

Fejlődésbiológia és természettudományok. Fejlődési mintázatképzés (pattern formation)

In: Rauch Tibor, Varga Máté, Hoffmann Gyula (szerk.)

Fejlődésbiológia II: Epigenetika és fejlődési mintázatképzés.

Pécs: Kronosz (2014). *pp.255-310.*

(ISBN:9786155339998)

VII.4. Posters related to this thesis

Szatmári Dávid, Bugyi Beáta, Ujfalusi Zoltán, Grama László, Dudás Réka és Nyitrai Miklós

A szívizom leiomodin2 képes az aktin filamentumok oldalához kötni és szabályozza a miozin ATPáz aktivitását

Sümeg, Hungary, 16-19 May 2017.

47. Membrán-Transzport Konferencia

David Szatmari, Wei Lin Lee, Shi Min Jiang, Jonathan Hobley, Miklós Nyitrai, Robert C. Robinson
STRUCTURAL DYNAMICS OF HUMAN GELSOLIN
Melbourne, Australia, 24-27 November 2013.
The 37th Annual Conference of the Australian Society for Biophysics

Szatmari D, Dudas R, Nyitrai M
Expression and biophysical characterization of cardiac leiomodin 2
Budapest, Hungary, 23-27 August 2011.
8th European Biophysics Congress
***Published abstract: EUROPEAN BIOPHYSICS JOURNAL* 40:**(Suppl 1) *p. 61*. (2011)

VII.5. Other posters

Dávid Szatmári, Péter Sárkány, Béla Kocsis, Tamás Nagy, Attila Miseta, Robert C. Robinson and Miklós Nyitrai
Intracellular ion concentration dependent remodelling of bacterial MreB assemblies
Helsinki, Finnland, 4-8 June 2017.
European Cytoskeletal Forum Meeting 2017

David Szatmari, Reka Dudas, Attila Nagy, Gabor Hild and Miklos Nyitrai
Expression and biophysical characterization of exportin6
Palermo, Italy, 28 August – 2 September 2009.
13th European Conference on the Spectroscopy of Biological Molecules 2009

Szatmári D, Huber T, Németh V, Kollár V, Grama L, Kellermayer MSZ
A titin mechanoszenzor vizsgálata.
Sümeg, Hungary, 20-23 May 2008.

38. Membrán-Transzport Konferencia

Huber T, **Szatmári D**, Mártonfalvi Zs, Kellermayer MSZ
A titin PEVK domén szekvenciamotivumainak szerkezete és mechanikája
37. Membrán-transzport Konferencia Sümeg Hungary május 22-25 (2007)

Huber T, **Szatmári D**, Mártonfalvi Zs, Kellermayer MSZ
The stucture and mechanics of the titin's PEVK domain sequence motifs
IV. International Conference on Molecular Recognition Pécs Hungary 2007 August 15-18 (2007)

VII.6. Lectures not related to this thesis

Huber T, **Szatmári D**, Mártonfalvi Zs, Murvai Ü, Kiss B, Karsai Á, Grama L, Kellermayer MSZ
Imaging and manipulation of cells and molecules with atomic force microscopy and fluorescence-AFM combinations
25 th Congress for European Society for Microcirculation Budapest, August 26-29 (2008)

Kellermayer MSZ, Bianco P, Nagy A, Karsai Á, Kengyel A, Huber T, Kiss B, Mártonfalvi Zs, **Szatmári D**, Grama L
Nanomechanhanics of of single biomolecules
Joint meeting of Hungarian and German Biophysicists May 17-20 Hünfeld Germany (2007)